UNIVERSIDADE FEDERAL DE SANTA CATARINA
CAMPUS FLORIANÓPOLIS
PROGRAMA DE PÓS-GRADUAÇÃO EM CIÊNCIA E ENGENHARIA DE MATERIAIS

Francesca Tatiana Albino

DEVELOPMENT OF 3D-PRINTED METALLIC AND BIMETALLIC CATALYSTS SUPPORTED ON GEOPOLYMERS

Florianópolis
2023
Francesca Tatiana Albino

DEVELOPMENT OF 3D-PRINTED METALLIC AND BIMETALLIC CATALYSTS SUPPORTED ON GEOPOLYMERS

Dissertação submetida ao Programa de Pós-Graduação em Ciência e Engenharia de Materiais da Universidade Federal de Santa Catarina como requisito parcial para a obtenção do título de Mestra em Cerâmicas.

Orientador(a): Prof.Dr. Luiano Senff
Coorientador(a): Prof. Dr. Dachamir Hotza
Prof. Dr. Marcus Mandolesi Sá

Florianópolis

2023

Ficha de identificação da obra elaborada pelo autor,
através do Programa de Geração Automática da Biblioteca Universitária da UFSC.

Albino, Francesca Tatiana
DEVELOPMENT OF 3D-PRINTED METALLIC AND BIMETALLIC CATALYSTS SUPPORTED ON GEOPOLYMERS / Francesca Tatiana Albino ; orientador, Luciano Senff, coorientador, Dachamir Hotza, coorientador, Marcus Mandolesi Sá, 2023.
112 p.

Dissertação (mestrado) - Universidade Federal de Santa Catarina, Centro Tecnológico, Programa de Pós-Graduação em Ciência e Engenharia de Materiais, Florianópolis, 2023.

Inclui referências.

1. Ciência e Engenharia de Materiais. 2. manufatura aditiva. 3. geopolimero. 4. catalisador. 5. reação organica. I. Senff, Luciano . II. Hotza, Dachamir. III. Mandolesi Sá, Marcus IV. Universidade Federal de Santa Catarina. Programa de Pós-Graduação em Ciência e Engenharia de Materiais. V. Título.

Francesca Tatiana Albino

DEVELOPMENT OF 3D-PRINTED METALLIC AND BIMETALLIC CATALYSTS SUPPORTED ON GEOPOLYMERS

como

O presente trabalho em nível de Mestrado foi avaliado e aprovado, em 15 de dezembro de 2023, pela banca examinadora composta pelos seguintes membros:

Dra. Emanoelle Diz Acosta

Instituição UFSC

Dra. Karine Goulart de Oliveira

Instituição UFSC

Certificamos que esta é a versão original e final do trabalho de conclusão que foi julgado adequado para obtenção do título de Mestre em Ciência e Engenharia de Materiais.

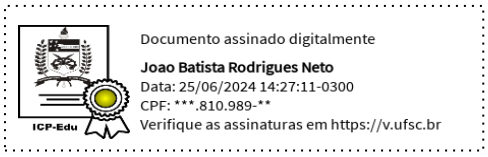

Coordenação do Programa de Pós-Graduação

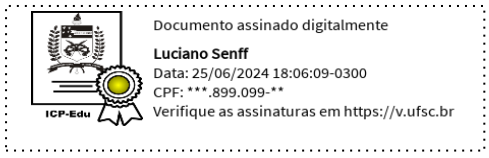

Prof. Dr. Luciano Senff

Orientador

Florianópolis, 2023

“That's what I do.
I drink, and I know things”
— Tyrion Lannister

AGRADECIMENTOS

Gostaria de agradecer primeiramente aos meus pais, Vanderlei e Cristina, por todo apoio e carinho durante todos esses anos de caminhada dentro da pesquisa acadêmica. Aos meus irmãos Anderson e Gian e minha cunhada Larini, por estarem do meu lado e me fazerem sempre buscar o meu melhor.

Ao prof. Luciano por ter acreditado nesse trabalho e ter me dado todo suporte necessário. Ao prof. Dacha por esses longos e maravilhosos 10 anos de orientação, por me dar liberdade e amparo em todos os projetos que fui inserida e por toda afeição durante o processo. Ao prof. Marcus que foi imprescindível para que a pesquisa se realizasse e ter dado a oportunidade de voltar as raízes da química.

A Pietra por ter me convidado, de forma quase despretensiosa a fazer parte da pesquisa, sem ela com certeza eu não teria descoberto esse mundo que para mim hoje é tão importante. Ao Vini, Maisa, Vavo, Kevin, Thiago, Josy e Thaiane, pelas conversas, abrações, acolhimento e sempre acreditarem que esse trabalho fosse possível e pela confiança em minhas capacidades, mesmo quando eu subestimava o meu potencial.

Aos meus amigos do laboratório Vivian, Fabi, Mattos, Rafa, Júlia, Thamy, Ste, Vidal e Zé, por estarem do meu lado principalmente nesses últimos meses, sendo companheiros não só de pesquisa, mas também de bar e fofoca.

Ao Pedro, do MESOLab, sem ele essa pesquisa não teria acontecido e muito menos tomado os rumos que tomou.

A todos os amigos que construí nessa jornada dentro da engenharia de materiais: Isa, Marcela, Manu, Duda, Ana, Sarah, Marcelo, Gabi, Ricardinho, Doug, Maria, Leícia.

A todas as manas e PosGraduManas: Gui, Luan, Jucão, Bea, Rafa, Giulia, Bernardo, Rovaris, Denize, Maria, Sara, Tonho, Paulo, Fernando, Jeka, Willian, Mari, Betina, Rodolfo, Moises, Larissa, Murilo, Dani.

Aos novos amigos que construí na cozinha e que foram indispensáveis para minha alegria nos últimos meses: Ana, Dinha, Erika, Gustavo, Tayia, Rosangela, Rozi.

Ao CNPQ e a UFSC pelo fomento e oportunidade de realizar esse trabalho na maior adversidade possível que é ser pesquisador no Brasil.

RESUMO

A catalisa heterogênea baseada em metais de transição oferece notáveis oportunidades na química. Além da facilidade de recuperação, reciclabilidade e redução de resíduos metálicos, os suportes sólidos proporcionam a vantagem adicional de acomodar múltiplos metais. O avanço de sistemas catalíticos com propriedades ativas, seletivas e mecanicamente estáveis, incorporando metais de baixa toxicidade e custo acessível, como cobre e níquel, em substratos sólidos, apresenta promissoras aplicações em catálise. Os geopolímeros, compostos por sílica e alumina, são suportes de catalisadores ecologicamente corretos. Eles curam à temperatura ambiente, possuem uma área superficial elevada, porosidade inerente e estabilidade robusta. O uso da tecnologia de impressão tridimensional (3D) possibilita a deposição precisa de materiais catalíticos, abrindo novas oportunidades para o design e otimização de desempenho de catalisadores. Neste contexto, o estudo apresentou catalisadores suportados em material geopolimérico fabricado por impressão 3D. Nitrato de níquel (Ni(NO3)2) e nitrato de cobre (Cu(NO3)2) foram empregados como precursores metálicos para a síntese dos catalisadores. Essa abordagem facilitou a distribuição uniforme das espécies metálicas dentro da matriz geopolimérica. A caracterização abrangente dos catalisadores foi realizada por meio de diversas técnicas analíticas. Difração de raios X (XRD), fluorescência de raios X (XRF), espectroscopia de raios X por dispersão de energia (EDX), redução termoprogramada (TPR), Brunauer-Emmett-Teller (BET), microscopia eletrônica de varredura (SEM) foram conduzidas para visualizar a morfologia e microestrutura dos catalisadores impressos. Os catalisadores serão testados em diferentes reações orgânicas, como condensação de Knoevenagel, síntese de diazóis, cicloadição e reações click, e analisados por Ressonância Magnética Nuclear (RMN). Os resultados indicam que os catalisadores sintetizados apresentam área superficial elevada, porosidade substancial e atributos térmicos e morfológicos propícios para aplicações versáteis em diversos processos catalíticos, especialmente na química orgânica.

Palavra Chave: impressão 3D, catalisadores metálicos e bimetálicos, geopolímero.

ABSTRACT

Transition metal-based heterogeneous catalysis offers notable opportunities in chemistry. Besides ease of workup, recyclability, and reduced metallic waste, solid supports offer the added advantage of accommodating multiple metals. Advancing catalytic systems with active, selective, and mechanically stable properties, incorporating low-toxicity, cost-effective metals, like copper and nickel onto solid substrates, holds promise in catalysis. Geopolymers, comprising silica and alumina, are eco-friendly catalyst supports. They cure at room temperature, possess a high surface area, inherent porosity, and robust stability. The use of three dimensional (3D) printing technology enables the precise deposition of catalyst materials and offers new opportunities for catalyst design and performance optimization. In this context, the study presented catalysts supported on geopolymer material made from 3D printing. Nickel nitrate ($Ni(NO_3)_2$) and copper nitrate ($Cu(NO_3)_2$) were employed as metal precursors for the synthesis of the catalysts. This approach facilitated the uniform distribution of the metal species within the geopolymer matrix. Comprehensive characterization of the catalysts was performed using various analytical techniques. X-ray diffraction (XRD), X-ray fluorescent (XRF), energy-dispersive X-ray spectroscopy (EDX), thermoprogrammed reduction (TPR), Brunauer-Emmett-Teller (BET), scanning electron microscopy (SEM), examination was conducted to visualize the morphology and microstructure of the printed catalysts. The catalysts will be tested for different organic reactions, such as Knoevenagel condensation, diazole synthesis cycloaddition and click reactions and analyzed by Nuclear Magnetic Resonance (NMR). The findings indicate that the synthesized catalysts exhibit elevated surface area, substantial porosity, and possess thermal and morphological attributes conducive to versatile applications in various catalytic processes, particularly within the organic chemistry.

Keywords: 3D printing, metallic and bimetallic catalysts, geopolymer.

RESUMO EXPANDIDO

A catalise heterogênea baseada em metais de transição apresenta oportunidades convincentes na química. Além das vantagens comumente enfatizadas, como facilidade de trabalho, reciclabilidade e redução de resíduos metálicos, os suportes sólidos trazem outra vantagem significativa - eles têm o potencial de acomodar mais de um metal. Consequentemente, esses sistemas catalíticos podem facilitar múltiplos tipos de construções de ligações, expandindo ainda mais sua versatilidade e utilidade em processos químicos sustentáveis [1].

Essa capacidade de hospedar metais em suportes sólidos, muitas vezes referida como catálise monometálica e bimetálica, permite que químicos e pesquisadores projetem catalisadores com reatividade sob medida para uma ampla gama de transformações químicas [2]. Ao selecionar e combinar cuidadosamente diferentes metais de transição, é possível promover várias reações de formação de ligações, tornando esses catalisadores ferramentas excepcionalmente versáteis na busca por processos químicos mais verdes e eficientes.

O avanço de sistemas catalíticos que não apenas são ativos e seletivos, mas também possuem estabilidade mecânica e química, enquanto incorporam múltiplos metais conhecidos por sua baixa toxicidade em comparação com outros catalisadores metálicos, acessibilidade e facilidade de manuseio em substratos sólidos, tem grande promessa em catálise. Portanto, cobre e níquel, metais que atendem a esses critérios, foram escolhidos [3]. Além disso, considerando a importância da sustentabilidade ambiental, um material foi diligentemente procurado para atender a todos esses pré-requisitos, garantindo assim que potenciais preocupações ambientais sejam minimizadas.

Nesse sentido, geopolímeros são uma classe de materiais ativados por álcalis que demonstram uma escolha economicamente viável para reduzir o impacto ambiental dos catalisadores [4]. Seu material bruto consiste principalmente de sílica e alumina e já foi utilizado como suportes de catalisadores para diferentes fins. Entre suas principais características estão o endurecimento à temperatura ambiente, alta superfície de contato, porosidade intrínseca, estabilidade térmica e química [5].

Considerando uma maneira sustentável, segura e barata de obter catalisadores, além de escolher um material apropriado, o processo deve ser o mais verde possível. A fabricação aditiva ou impressão 3D tem sido usada para substituir

outros métodos de produção, principalmente devido à possibilidade de gerar peças com geometrias complexas a partir de um modelo computacional [6].

Considerando esses aspectos, torna-se possível vislumbrar um catalisador capaz de facilitar uma ampla gama de reações químicas, que vão desde a produção farmacêutica, alimentícia e cosmética até a geração de energia baseada em hidrogênio. Os suportes de catalisadores foram fabricados usando materiais geopoliméricos por meio de fabricação aditiva, com níquel e cobre servindo como componentes ativos, seja em configurações monometálicas ou bimetálicas. Esses metais foram incorporados às formulações geopoliméricas por meio de dois métodos distintos: impregnação úmida ou integração durante o processo de impressão. Essa técnica inovadora, relativamente pouco explorada na literatura existente, busca aumentar significativamente a atividade catalítica.

Em resumo, o desenvolvimento de catalisadores metálicos e bimetálicos impressos em 3D suportados em geopolímeros demonstra uma abordagem sustentável e eficiente em catálise, destacando o potencial para avanços na síntese de compostos orgânicos valiosos com aplicações em diversas indústrias.

SUMMARY

1 INTRODUCTION

Transition metal-based heterogeneous catalysis indeed presents compelling opportunities in chemistry. In addition to the commonly emphasized advantages such as ease of workup, recyclability, and reduced metallic waste, solid supports bring forth another significant advantage—they have the potential to accommodate more than one metal. Consequently, these catalytic systems can facilitate multiple types of bond constructions, further expanding their versatility and usefulness in sustainable chemical processes.

This capability to host metals on solid supports, often referred to as monometallic and bimetallic catalysis, enables chemists and researchers to design catalysts with tailored reactivity for a wide range of chemical transformations. By carefully selecting and combining different transition metals, it is possible to promote various bond-forming reactions, making these catalysts exceptionally versatile tools in the pursuit of greener and more efficient chemical processes.

The advancement of catalytic systems that are not only active, selective, but also possess mechanical and chemical stability, while incorporating multiple metals known for their low toxicity when compared to other metal catalysts, affordability, and ease of handling onto solid substrates, holds great promise in catalysis. Therefore, copper and nickel, metals that align with these criteria, were chosen. Moreover, considering the importance of environmental sustainability, a material was diligently sought after to fulfill all these prerequisites, thus ensuring that potential environmental concerns are minimized.

In this regard, geopolymers are a class of alkali-activated materials that demonstrate an economically viable choice to reduce the environmental impact of catalysts. Their raw material consists mainly of silica and alumina and has already been used as catalyst supports for different purposes. Among their main features are hardening at room temperature, high contact surface, intrinsic porosity, thermal and chemical stability.

Considering a sustainable, safe, and cheap way to obtain catalysts, in addition to choosing an appropriate material, the process must be as green as possible. Additive manufacturing or 3D printing has been used to replace other production methods, mainly due to the possibility of generating parts with complex geometries from a computational model.

Considering these aspects, it becomes possible to envision a catalyst capable of facilitating a wide range of chemical reactions, spanning from pharmaceutical, food, and cosmetic production to hydrogen-based energy generation. The catalyst supports were fabricated using geopolymeric materials through additive manufacturing, with nickel and copper serving as the active components, either in monometallic or bimetallic configurations. These metals were incorporated into the geopolymeric formulations through two distinct methods: wet impregnation or integration during the printing process. This novel technique, relatively unexplored in existing literature, seeks to enhance catalytic activity significantly.

2 OBJECTIVE OF THE RESEARCH

2.1 GENERAL OBJECTIVES

The aim objective of this work is to develop metal-supported geopolymeric materials through additive manufacturing catalysts for organic reaction. The catalysts will incorporate nickel and/or copper as the active phase. The study aims to investigate and compare various methods for introducing the metal components into the geopolymeric support.

2.2 SPECIFIC OBJECTIVES

The primary goals of this work are as follows:

1. Modify geopolymeric formulations to achieve optimal properties for additive manufacturing by considering their rheological properties;

2. Explore and employ techniques for incorporating nickel and copper on the geopolymeric support. This may involve methods such as impregnation or direct synthesis;

3. Develop bimetallic catalysts, with the combination of nickel and copper as active phases;

4. Evaluate the performance between catalysts prepared via impregnation and those produced through addition techniques. This analysis aims to assess the impact of the different preparation methods on the resulting catalyst's performance;

5. Utilize catalysts across diverse organic reactions while examining their reusability and structural integrity;

6. Characterize the synthesized catalysts using various analytical techniques, including X-ray diffraction (XRD), X-ray fluorescent (XRF),

energy-dispersive X-ray spectroscopy (EDX), thermoprogrammed reduction (TPR), Brunauer-Emmett-Teller (BET), scanning electron microscopy (SEM). These techniques provide valuable insights into the catalyst's crystal structure, morphology, and catalyst behavior.

3 LITERATURE REVIEW

Catalysis, whether in its homogeneous or heterogeneous forms, has played a pivotal role in advancing the principles of green chemistry and sustainable synthesis. Catalytic processes render traditional, nonrenewable, low atom economy, and wasteful protocols obsolete, offering eco-friendly alternatives to well-established but often century-old practices.

The utilization of catalysis aligns with the fundamental tenets of Green Chemistry in several ways, contributing to various key principles, succinctly summarized here: 1 (waste prevention), 2 (maximization of atom economy), 5 (restriction of auxiliary substances), 6 (enhanced energy efficiency), 8 (reduction of derivatives), 9 (promotion of catalytic reactions), and 12 (promotion of safer chemistry) from the comprehensive twelve-point framework of Green Chemistry [7], [8].

Heterogeneous catalysis, as per its definition, involves a catalytic process where the catalyst and the reaction mixture exist in distinct phases. A prevalent instance of this occurs in laboratory settings, where the catalyst is typically in a solid state, while the reaction mixture is immersed in a solvent, leading to what is known as solid/liquid (S/L) reactions [1].

This characteristic enables straightforward separation of the catalyst from the reaction medium, whether it exists in a liquid or gas phase. Such separability greatly simplifies the task of removing the catalyst from the final product, easing its recovery and potential reactivation when necessary. This, in turn, promotes catalyst recycling, potentially reducing the environmental footprint and enhancing the sustainability of the overall process.

Solid catalysts, particularly those derived from metals, are commonly referred to as "metal catalysts." However, it is crucial to emphasize that this category encompasses not only the elemental forms of metals but also includes the ionic forms of transition metals. This broader classification encompasses salts, oxides, or hydroxides [3]. Toxicity remains a concern regardless of whether the catalyst exists as a soluble complex or a solid material. However, the generally limited solubility of solid forms helps minimize leaching into the solution, mitigating potential environmental impacts.

The chosen metal (active sites) needs to be supported on some material for catalysis in a more efficient way. When in structured objects, it can be carried out by

impregnation in the case of microporous structures [9]. Another method that can be used is to introduce the metal into the support structure during its processing, thus generating a material that would not require so many production steps. The preparation method influences textural properties such as specific area, structural characteristics, and the activity, stability, and lifetime of catalysts [10].

The support must keep the active sites in direct contact with the compound to be catalyzed. For this, it needs to be stable, resistant and have a high contact surface. Materials that have these characteristics are found in the class of geopolymers. They are inorganic polymers obtained by mixing a dry aluminosilicate with an alkaline solution and other constituents, if necessary. The main constituent is the source material, which must be rich in silicon (Si) and aluminum (Al). The alkaline solution is usually based on sodium (hydroxide or silicate) or potassium (hydroxide or silicate) [4]. The result of the process is a nanocomposite that looks like an artificial rock.

Thus, a method where it is possible to generate a complex design to produce catalysts is necessary. Among the currently known manufacturing modes, additive manufacturing, known as 3D printing, can be used. The choice of a 3D graphic model and a material system are enough to build a part. Consequently, it is possible to generate parts with arbitrary geometries without the need for adaptations and with a reduction in manufacturing steps.

Due to reasonable production time, less skilled labor, the ability to build complicated structural designs and the reduction of work steps, 3D printing has been considered a sustainable technology in recent years [11].

The following sections will explore the broad aspects of heterogeneous catalysis, encompassing the production of catalysts, the selection of metals, the choice of support materials, the manufacturing techniques involved, and the diverse applications of the resulting samples.

3.1 ADDITIVE MANUFACTURING

Additive manufacturing (AM) or 3D printing is one of the fastest growing automated manufacturing technologies, with the ability to go directly from CAD models to finished components. In this manufacturing model, three-dimensional parts of arbitrary complex geometries are built layer by layer [12].

Presently, three-dimensional (3D) printing represents a robust technology that is continuously progressing, with an increasing number of emerging application domains and promising prospects across various markets, including electrochemical devices[13], [14], automotive industry [15], [16] biomaterials [17], [18], chemical synthesis [19], [20], microfluidic devices [21], [22], medical applications [23], pharmaceutical field [24]materials science [25], [26], and catalysis [27], [28], [29], [30], [31], [32], [33]

In the 3D printing process, parts are made by accumulating layers shaped in a precisely two-dimensional (x-y) plane. The third (z) dimension occurs because of single layers being built on top of each other, show in Figure 1, but not as a continuous z coordinate [34].

Figure 1 Demonstration of the printing syringe and its coordinates: x; y and z.

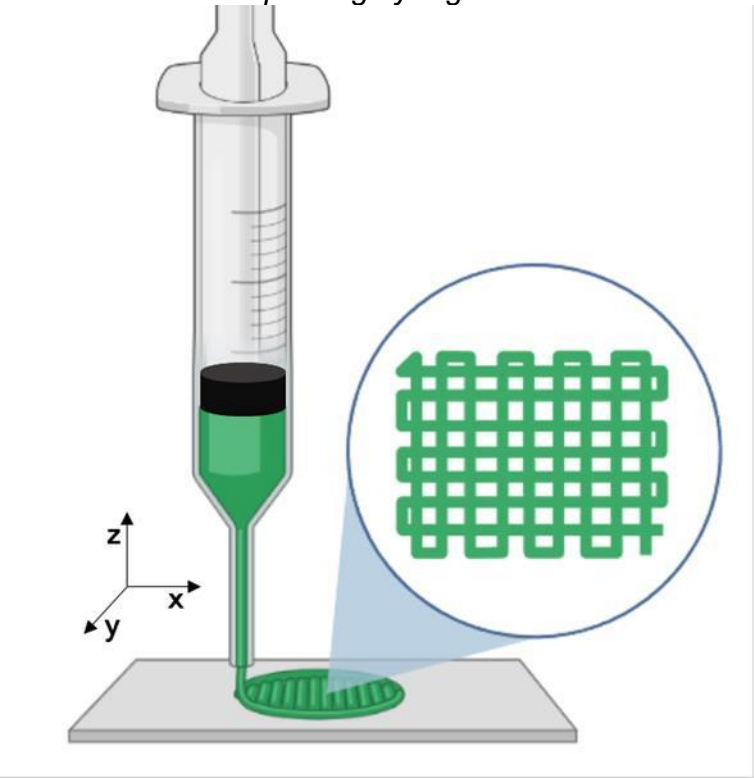

Source: author (2023).

This process consists of four steps: model design, slicing, printing and post-treatment. The desired design is transformed into data that is divided into several thin layers through a slicing process. The transformed data is transmitted to a 3D printer, and a three-dimensional body is created through the process of stacking materials

layer by layer [35]. The post-treatment of the molded part can be done by cleaning, polishing, heat treatment and/or functionalization.

Based on the printing principle, there are various basic of forming methods in 3D printing, including extrusion, powder-based, lamination, and other forms. Each of these basic forms encompasses different specific printing methods, each with its own distinctive features, operational characteristics, and scope of application[27].

Extrusion-based printing offers several advantages, including its simplicity of operation and low cost. This technique allows for the direct incorporation of different active or chemical components into the printing slurry/ink or wire. Consequently, materials with specific structures can be achieved through the extrusion process, offering a broad range of applications. Additionally, this method provides flexibility in designing slurry components and structures [36]. The processes involved: include inkjet printing (IJP) [37], direct ink writing (DIW) [38], [39], stereolithography (SLA) [40] , selective laser sintering (SLS) [41], [42], fused deposition ceramics (FDC) [43], laminated object manufacturing (LOM) [44] fused deposition modeling (FDM) [45], digital light processing (DLP) [46], selective laser melting (SLM) [47], electron beam melting (EBM) [48].

Direct ink writing (DIW) technology was initially developed for printing ceramic materials but has since been extended to a wide range of materials including ceramics, plastics, gels, carbon materials, and more. The DIW process involves using a shear dilute fluid slurry as the printing material, allowing for direct extrusion of the masterbatch without the need for melting or curing processes [25].

In the manufacturing process itself, it is then used to construct the designed object and is simultaneously transferred to a state that has its final physical properties, or at least sufficient mechanical strength to transfer the constructed object to further processing steps [35], [49].

The AM process time varies greatly depending on the configuration, such as: the layer thickness, material output speed and pressure, final part height, nozzle thickness and complexity of the chosen design [50]. Even though the process is relatively fast when compared to other manufacturing modes.

Additive manufacturing techniques impose constraints on the dimensions of fine aggregates. Specifically, these methods utilize fine sand particles with a median particle size (d50) ranging between 170–250 μm. The significance of adhering to these particle size specifications lies in two critical aspects. Firstly, it facilitates enhanced

homogeneity of the powder bed, which is crucial for powder-based 3D printing processes. Secondly, it aligns with the requirement for a diminutive nozzle diameter in extrusion-based 3D printing setups. Ensuring these particle size parameters enables more efficient and consistent additive manufacturing outcomes [51].

For an ideal 3D printable material, it is desirable to have a low initial static yield stress to facilitate the initiation of flow and a low dynamic viscosity to enable smooth transportation during the printing process. However, once the material is extruded, it should rapidly increase its yield stress. This ensures that it can withstand the load from subsequent layers without excessive deformation, maintaining the structural integrity of the printed object [52].

Additive manufacturing (AM) can be employed in the production of monoliths, which are systems consisting of functional microchannels with a regular three-dimensional structure. These monoliths have the potential to replace conventional catalysts and chemical reactors, addressing several challenges posed by traditional systems. Products created through AM techniques, like Figure 2, can be precisely designed, allowing for meticulous attention to detail and customization tailored to specific processes [30].

Figure 2 Design and structure of 3D Geopolymer.

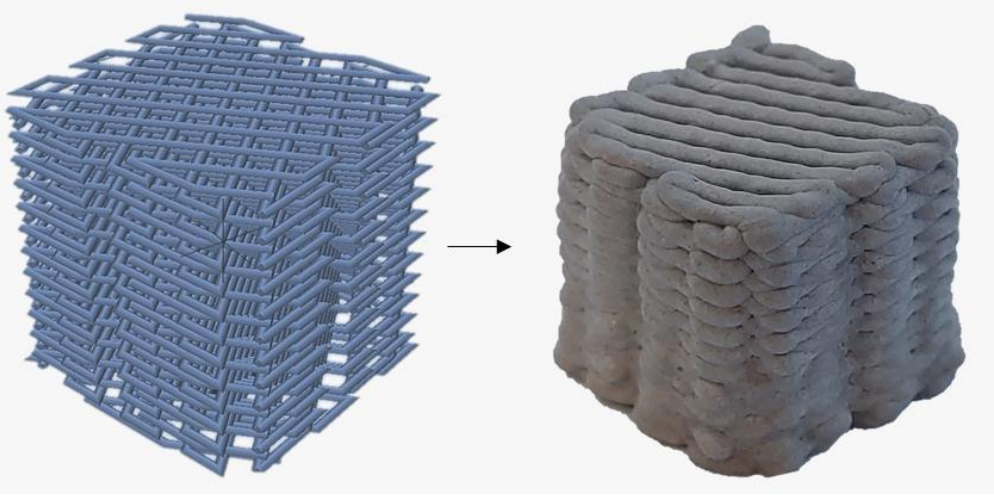

Source: author (2023).

The utilization of 3D printing in catalyst fabrication is considered a groundbreaking process with a wide range of distinctive possibilities. This approach enables the construction of customized architectures with advantageous catalytic

surface characteristics, promoting enhanced interaction with the reactant media. The design of these architectures can be based on theoretical models, considering specific requirements such as size, geometry, and cross-sectional types when applied to reactor design. Regarding catalyst fabrication, 3D printing provides control over wall thicknesses, pore sizes, and shapes. The primary objective typically revolves around increasing surface areas to maximize the accessibility of active sites involved in the reaction to the reactant molecules [53].

When it comes to active phases and supports in catalysis, it is crucial to consider the integrity, availability, and regeneration capability of the active centers throughout the catalytic bed. Furthermore, AM enables precise tuning of other significant properties, including the porous, mechanical properties, thermal conductivity, dielectric constant, specific surface area, chemical resistance, hardness, and channel tortuosity.

Ceramics have proven to be highly suitable materials for catalyst manufacturing, offering a wide range of desirable properties. These properties encompass mechanical strength, specific surface area, thermal shock resistance, corrosion resistance, pore size, pore distribution, shape (open or closed; spherical, elongated, or random), and interconnectivity. These characteristics make ceramics well-suited for applications in catalysis [29]. To achieve the desired material properties, the successful fabrication of functional components using ceramics may necessitate efficient coating techniques, ensure that the final ceramic catalyst exhibits the desired performance characteristics required for its intended application.

The earliest examples of porous material catalysts structures, produced using 3D printing technology were ceramic support structures made of aluminum oxide, created through a direct fabrication method [54]. After that, is an increasing demand for raw materials used in the production of catalysts. As the field of catalysis continues to expand and new applications emerge, the need for diverse and specialized catalyst materials grows.

In a study conducted by *Tubio et al.* [32], a Cu/Al_2O_3 catalyst was prepared using an ink was formulated by dispersing Al_2O_3 powder into a $Cu(NO_3)_2$ solution. To adjust the rheology of the ink, hydroxypropyl methyl cellulose was incorporated as a viscosity modifier. After extrusion, a sintering process was employed at a temperature of 1400 °C to eliminate the organic components and decompose the copper species.

Lucentini et al. [55] employed 3D printing technology to fabricate Ce/Ni catalysts in their study. Specifically, binderless CeO_2 monoliths were printed, incorporating NiO for catalytic ammonia decomposition. The result of the reaction runs indicated that structuring the powdered nanoparticles through 3D printing resulted in improved catalytic stability compared to the catalyst in powder form.

Zeolites have shown great potential as materials for 3D printing of catalysts. A notable method was reported by *Thakkar et al.*[56], where zeolite powders were mixed with bentonite clay as a binder, methyl cellulose, and poly(vinyl) alcohol (PVA). The resulting mixture was extruded, subsequently, the printed structures were dried and calcined to remove the binders. The printed zeolite structures were found to be effective for CO_2 removal, showcasing the potential of 3D-printed zeolite catalysts in addressing environmental challenges.

The research conducted by *Innocentini et al.* [57] a metakaolin-based geopolymer with a lattice component was prepared using a 3D printer. The catalytic activity of geopolymers was evaluated through the transesterification reaction of refined soybean oil into biodiesel. This research aimed to investigate the potential of MG as a catalyst for biodiesel production, focusing on its catalytic performance and efficiency in the transesterification process.

Indeed, in many studies focusing on ceramic material catalysts using an AM technique, a post-processing step is commonly employed. This step typically involves the impregnation of the active phase onto the printed porous material and/or subsequent thermal treatment [58], [59], [60], [61].

Scaling the additive manufacturing (AM) process remains a significant advantage as it simplifies the process and reduces costs while adhering to the same fundamental design principles. This scalability, combined with the potential to minimize waste generation, lower energy consumption, and decrease production time by eliminating the need for component assembly, positions AM as a critical player in constructing a sustainable future. By leveraging these advantages, AM can contribute to sustainable manufacturing practices and enable the development of environmentally friendly and efficient production processes.

3.2 HETEROGENOUS CATALYSIS

Catalysis, as a phenomenon, has been present for thousands of years in the form of fermentation, also known as bio-catalysis. The earliest documented record of a catalytic reaction can be traced back to 1552 when Cordus conducted the dehydration of alcohol to ether. The foundations of modern catalysis can be traced back over two centuries ago to Elizabeth Fulhame's 1794 essay, where she introduced the concept of catalysis through her experiments on oxidation-reduction, she suggested that a small amount of water was necessary for the reaction to take place, laying the groundwork for understanding catalytic processes [62].

The practical advancements in catalysis have spurred extensive research into understanding the underlying mechanisms that govern catalytic reactions. This led to the emergence of heterogeneous catalysis as a multidisciplinary field encompassing chemistry, chemical engineering, surface science, and more recently, materials science. The incorporation of materials science has opened up new avenues for catalyst development, with the synthesis of novel materials such as carbon nanostructures (nanotubes, graphene, graphene oxide), metal-organic frameworks, covalent organic frameworks, synthetic zeolites, and clays [1], [3], [63], [64], [65].

A including applications in the automotive industry [66]. One of the key advantages of catalytic processes is their ability to replace the use of nonrenewable reagents with high atom economy, resulting in a significant reduction in the environmental impact associated with the production of pharmaceuticals and fine chemicals.

Catalysis finds classification into two main types: homogeneous catalysis, involving a single phase, and heterogeneous catalysis, occurring at or near an interface between phases. Autocatalysis refers to catalysis induced by one of the reaction products, while intramolecular catalysis pertains to catalysis initiated by a group within the reactant molecule itself. It's noteworthy that the term "catalysis" is sometimes employed even when the catalytic substance is consumed in the reaction, in such cases, the catalytic substance should be referred to as an activator [67].

In homogeneous catalysis, the catalyst is soluble in the reaction medium. This means that the catalyst exists in the same phase as the reactants and products, allowing for intimate interaction and efficient catalytic activity within the solution.

Heterogeneous catalysis, on the other hand, involves catalysts that are insoluble or immiscible with the reaction medium. In this case, the catalyst typically exists as a solid or supported species, while the reactants and products remain in a different phase (usually gas or liquid). The catalytic reaction occurs at the interface between the catalyst and the reaction medium [1].

Each type of catalysis possesses distinct characteristics and applications. The choice of the appropriate catalytic system depends on factors such as reaction conditions, reactant solubility, desired selectivity, and the overall objectives of the process.

In the context of this work, the catalyst produced from the solid material will be employed in a heterogeneous catalytic system. The solid catalyst will provide active sites on its surface where the desired reactions can take place. The reactants, which may be in a liquid or gas phase, will encounter the solid catalyst, and the catalytic process will occur at the interface between the catalyst and the reactants.

The ability of solid surfaces to make and break bonds with molecules is the basis for the phenomenon of heterogeneous catalysis, where the catalyst is in a different physical state from its reactants and products, as show in Figure 3 [68].

Figure 3 Heterogeneous catalysis: A - External diffusion of reagents; B- Adsorption, C- Surface reaction; D- desorption and diffusion of the product.

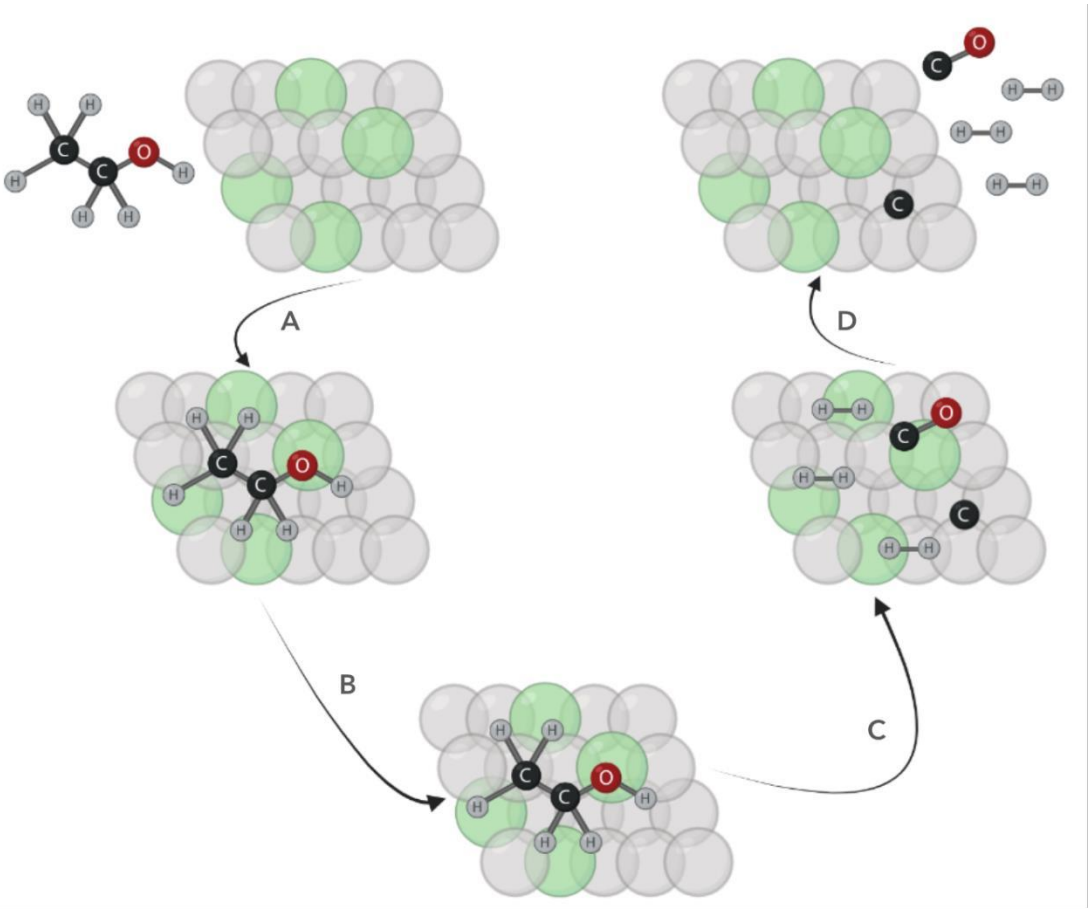

Source: author (2023).

A solid surface has three closely coupled functions when acting as a catalyst for a chemical reaction. First, it adsorbs the reagents (Fig. 3-A) and cleaves the necessary bonds. It then holds the reactants in proximity so they can react (Fig. 3-B), and finally the surface allows the products (Fig. 3-C) and them desorb back into the surrounding phase (Fig. 3-D) [65].

In the chemical adsorption step, there is an exchange of chemical bonds with the active site, causing specific bonds to be activated, and these species can form an activated complex that serves as a precursor of the reaction products [69]. When all the reaction electrons are rearranged, the products that are on the solid surface move, releasing the catalyst sites again for the adsorption of the reagents. This is the last step of the catalytic process.

During a chemical reaction, the breaking and formation of chemical bonds occur. All chemical bonds possess energy to keep the atoms together, and this energy

must be supplied to break a bond and initiate a reaction. The energy required to initiate a reaction is known as the activation energy. In noncatalytic reactions, the activation energy is typically higher compared to catalytic reactions [1].

A catalyst plays a significant role in a chemical process by altering the reaction mechanism, which involves breaking down the overall reaction into elementary steps that have significantly lower activation energies. It is important to note that the presence of a catalyst does not modify the basic thermodynamic features of the process. The overall energy of the reactants and the final products remains the same in the presence of a catalyst. Therefore, catalysis is primarily a kinetic phenomenon [1].

In summary, a catalyst facilitates a chemical reaction by reducing the activation energy required to initiate the reaction. It does not alter the overall energy of the reactants and products and acts as a kinetic facilitator rather than a thermodynamic modifier [70].

One significant benefit of heterogeneous catalysis is the ease of separating the solid catalyst from the reaction medium. This is particularly advantageous in laboratory applications and industrial processes. After the reaction is completed, the solid catalyst can be conveniently separated from the liquid or gas phase. This facilitates the removal of the catalyst from the product and allows for its recovery and potential reactivation if necessary. The ability to recycle and reuse the catalyst promotes sustainability, reduces the need for additional catalyst synthesis, and minimizes waste generation, ultimately decreasing the environmental impact of the process [70].

The solid nature of the catalyst also enables its utilization in various reactor configurations. It can be employed as a fixed-bed catalyst, a fluidized bed catalyst, or in other forms, depending on the specific process requirements. This flexibility in catalyst design and implementation further contributes to the efficiency and sustainability of the overall process.

Heterogeneous catalysts do indeed come with their own set of limitations and challenges. Unlike in homogeneous catalysis where every dissolved catalytic species is considered an active center, in heterogeneous catalysis a significant portion of the catalyst material is buried beneath the surface where the reactions take place. This reduces the number of available active centers, resulting in lower activity per unit

weight of catalyst. This limitation can impact the overall efficiency of the catalytic process [1].

Another common issue encountered in heterogeneous catalysis is mass-transport limitation. This refers to the need for substrates and reacting partners to be effectively transported to the surface of the catalyst for the reaction to occur. This becomes particularly challenging in three-phase systems, such as hydrogenations, where liquid, gas, and solid phases are involved. Diffusion limitations and restricted accessibility of reactants to the active sites can hinder the overall reaction rate and efficiency [1].

Furthermore, the preparation of industrial heterogeneous catalysts often involves specialized techniques. Each step of the catalyst's synthesis and preparation process is crucial, and even minor alterations can lead to notable changes in the catalyst's performance. The preparation conditions strongly influence the characteristics of the catalyst, including its surface area, pore structure, active site distribution, and stability. Achieving the desired catalyst properties requires careful optimization and understanding of the synthesis process, often considered as both science and art.

In heterogeneous catalysis, the surfaces of the catalyst materials play a crucial role as the primary sites where reactions take place. These surfaces can include the outer surface of the catalyst particles as well as the internal surfaces within porous materials. The chemical and physical properties of these surfaces have a significant impact on the mechanism of surface interactions, which in turn influences the formation of products in catalytic reactions [71].

3.2.1 Active phase

The concept of the active phase of catalysts was introduced by Taylor in the 1920s, highlighting the existence of specific sites on the surface that catalyze chemical reactions. These active sites consist of a group of atoms or functional groups that possess the ability to facilitate the desired reaction. Taylor proposed that these active sites are present in relatively small numbers compared to the total number of atoms in the bulk of the catalyst material [72].

Taylor's hypothesis regarding the limited presence of active sites on the catalyst surface has been supported and confirmed by modern surface science

measurements. These measurements have provided evidence that a catalyst is predominantly composed of an inactive surface with only a small fraction of active sites responsible for catalytic activity. The active sites are strategically positioned on the surface and possess unique chemical and structural properties that enable them to interact with the reactants and lower the activation energy of the desired chemical transformations [73].

The active sites must possess suitable adsorption capabilities, adhering to the principles of the Sabatier principle. This principle dictates that substrate molecules should be able to effectively bind and subsequently release from the active site. The adsorption process should strike a balance, neither being too weak nor too strong. Optimal adsorption ensures the formation of reactive intermediates and facilitates the progression of the catalytic reaction. Equally important is the desorption of product molecules from the active site, allowing for the regeneration of the site and the continuation of the catalytic cycle. The compatibility between substrate adsorption and desorption is pivotal in achieving high catalytic activity and selectivity [65].

In many cases, these active sites are composed of metals or metal nanoparticles, which possess unique catalytic properties. When these metal species are supported on a solid material, such as an oxide or carbon-based support, they form what is referred to as the active phase. These active phases include single or multiatom sites, surface clusters, kinks, terraces, steps, and defects, which can arise from the presence of vacant or missing atoms within the catalyst material [1].

3.2.1.1 Monometallic

Metals, in their various forms, hold a crucial position in diverse catalytic processes. When referring to metal catalysts, it commonly encompasses elemental metals, but ionic forms of transition metals also hold significance. Salts, oxides, and hydroxides of transition metals are frequently employed and can undergo in situ reduction to the zero-valence form. Therefore, the scope of metal catalysts encompasses a wide range of forms, including elemental metals, ionic species, and organometallic complexes, all contributing significantly to catalytic processes.

Transition metals, often referred to as heavy metal catalysts, exhibit excellent catalytic properties. However, they are associated with a significant drawback—

pronounced toxicity. This toxicity applies irrespective of whether the catalyst is in the form of a soluble complex or a solid material. Nonetheless, the low solubility of solid metal catalysts limits their leaching into the reaction solution, thereby minimizing potential toxicity risks. Among the elements in the periodic table, only a relatively small group of transition metals are considered catalytically active in heterogeneous catalysis, whereas a broader range of metals demonstrate catalytic activity in their metal complex forms, primarily in homogeneous catalysis. The periodic table in Figure 5 provides a visual representation, highlighting the transition metals that are commonly employed in heterogeneous catalytic processes [1].

Figure 4 A periodic table of elements that focuses on the metals most employed in heterogeneous catalysis.

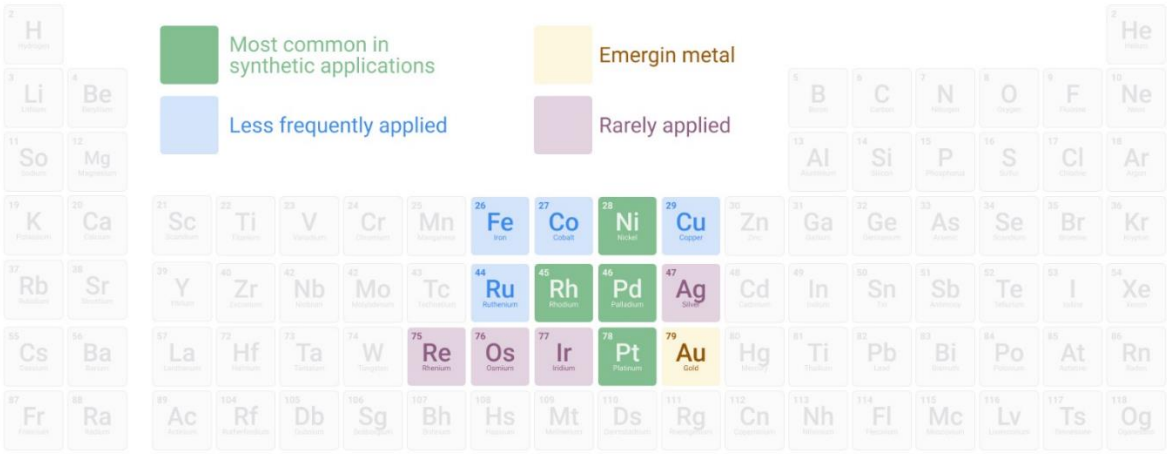

Source: adapted of TÖRÖK; SCHÄFER; KOKEL, 2021 [1].

Figure 2 illustrates that nickel (Ni), palladium (Pd), platinum (Pt), and rhodium (Rh) are the transition metals frequently employed in synthetic processes. Among these metals, nickel stands out as the most cost-effective option, making it a popular choice in both laboratory and industrial applications [74].

The second major group of metals comprises non-noble metal catalysts that were not extensively utilized in the past. However, several factors, including cost, availability, abundance, and favorable toxicology profiles (moderate to low toxicity), have prompted increased exploration of the catalytic properties of these metals. Metals such as iron (Fe) [75], cobalt (Co) [76], and copper (Cu) [77] have gained significant attention due to their desirable characteristics and potential applications in catalysis.

In the context of this investigative inquiry, our primary emphasis will be directed towards an examination of the intrinsic attributes and catalytic behaviors of nickel (Ni) and copper (Cu) metals. This exclusive focus is predicated upon the salient and pertinent aspects alluded to earlier, which render these specific metal species highly compelling subjects of the scope of this study.

The metals, together with their respective catalysts and prevalent applications, have been succinctly encapsulated in Table 1. It is pertinent to underscore that the prime focus of this work lies inherently within the domain of our laboratory's available precursors, specifically the nitrates of both metals. This emphasis aligns seamlessly with the overarching theme of synthesis and the preparatory techniques heretofore employed in our antecedent research endeavors, all while maintaining due consideration for the ceramic support materials.

Table 1 Metallic precursors, with their applications, preparation methods and material used for support.

Metal	Precursor form	Support	Preparation method	Applications	Reference
Nickel	$NiCl_2 \cdot 6H_2O$	Geopolymer	Impregnation	CO_2 methanation	[78]
	$Ni(NO_3)_2 \cdot 6H2O$	Al_2O_3	Impregnation	Alcohol amination	[76]
	$Ni(NO_3)_2 \cdot 6H_2O$	SiO_2	Deposition–precipitation	CO_2 hydrogenation	[79]
	$Ni(NO_3)_2 \cdot 6H_2O$		Impregnation	Hydrocarboxylation	[80]
	$Ni_3Si_4O_{12}H_2$	SiO_2	Suspensions	Hydrogenolysis	[81]
	Ni	SiO_2	Deposition	Hydrogenolysis of Phenol	[82]
	$Ni(NO_3)_2 \cdot 6H_2O$	SiO_2	Impregnation	Hydrogenation of Furfural	[83]
	$Ni(NO_3)_2 \cdot 6H_2O$	Silica gel	Impregnation	Dry reforming of methane	[84]
	$Ni(NO_3)_2 \cdot 6H_2O$	SiO_2	Impregnation	CO_2 reforming and partial oxidation of methane	[85]
	$Ni(NO_3)_2 \cdot 6H_2O$	TiO2	Solvothermal treatment	Photocatalytic hydrogen	[86]
	$Ni(NO_3)_2 \cdot 6H_2O$	Al_2O_3	Impregnation/3d printed	CO_2 methanation	[58]
	$Ni(NO_3)_2 \cdot 6H_2O$	$MgAl_2O_4$	Sol-gel	Steam reforming of acetone	[87]
	$Ni(NO_3)_2 \cdot 6H_2O$	$Ce_xTi_{1-x}O_2$	Impregnation	Steam reforming of ethanol	[88]
	$Ni(NO_3)_2 \cdot 6H_2O$	Al_2O_3	Impregnation	Ethanol steam reforming	[89], [90], [91], [92], [93], [94], [95], [96]
	$Ni(NO_3)_2 \cdot 6H_2O$	TiO_2	Wet synthesis	Steam reforming of methanol	[97]
	$Ni(NO_3)_2 \cdot 6H_2O$	Al_2O_3	Impregnation	Steam reforming of methanol	[98], [99], [100], [101]

	$Ni(NO_3)_2 \cdot 6H_2O$	CeO_2	Impregnation	Steam reforming of methanol	[102]
	$Ni(NO_3)_2 \cdot 6H_2O$	Al_2O_3	Impregnation	Steam reforming of glycerol	[103], [104], [105], [106]
	$Ni(NO_3)_2 \cdot 6H_2O$	CeO_2–SiO_2	Impregnation	Steam reforming of LPG	[107]
	$Ni(H_2BDP\text{-}SO_3)_2$		Impregnation	Suzuki–Miyaura reaction	[108]
	$Ni(NO_3)_2 \cdot 6H_2O$	Activated carbon	Impregnation	Carbonylation of methanol	[109]
	$Ni(AOC)_2 \cdot 4H_2O$	CeO2	Aqueous solution	Carbonylation of ethanol	[110]
	Various	Various	Various	Sonogashira coupling	[111]
	$Ni(NO_3)_2 \cdot 6H_2O$	SBA-15	Impregnation	Carbonylative Coupling	[112]
	$Ni(OAc)0.4H_2O$	Al_2O_3	Impregnation	Carbonylative Homocoupling	[113]
	Ni metallic	Fe_3O_4	Heat	Phenoxy carbonylation	[114]
Copper	$Cu(NO_3)_2 \cdot 2.5H_2O$	Al_2O_3	3D print	Ullmann reaction	[32]
	Cu-exchanged zeolite	Geopolymer	3D print	NO_x removal	[115]
	$Cu(NO_3)_2.2.5H_2O$	Al_2O_3	Various	Steam reforming of methanol	[116], [117], [118], [119], [120], [121]
	$Cu(NO_3)_2 \cdot 3H_2O$	Silica	Impregnation	Steam reforming of methanol	[122]
	$Cu(NO_3)_2.2.5H_2O$	$CeO_2 \cdot Al_2O_3$	Impregnation	Steam reforming of methanol	[123]
	$Cu(NO_3)_2.2.5H_2O$	MCM-41	Impregnation	Steam reforming of methanol	[124]
	$Cu(NO_3)_3.3H_2O)$	Co/MgO	Co-precipitation	Steam reforming of glycerol	[125]
	$CuSO_4$	Chitosan	Aqueous solution	Cycloaddition	[126]
	$CuCl_2 \cdot 2H_2O$	Silica	Solution reaction	Click Synthesis	[127]
	$Cu(CH_3COO)_2$	Silica	Impregnation	Cycloaddition reactions	[128], [129]
	$Cu(CH_3COO)_2$	Silica	Sol–gel process	Huisgen and Ullmann reaction	[130]
	$CuSO_4.5H_2O$	Cellulose	Solution reaction	Coupling reactions	[131]
	$Cu(NO_3)_2 \cdot 3H_2O$	MOFs	Green Synthesis	CO_2 Fixation Reaction	[132]
	$Cu(NO_3)_2.2.5H_2O$	Mordenite	Ion-exchange	Methanol carbonylation	[133]
	$CuCl_2.2H_2O$	Ce- MOF	Solvothermal reaction	Oxidation to Acetic Acid	[134]
	Cu nanoparticles	COF	Condensation	Gaser–Hay heterocoupling	[135]
	$Cu(NO_3)_2 \cdot 4H_2O$	Al_2O_3	Chemisorption-hydrolysis	Epoxidation	[136]
	$Cu(NO_3)_2 \bullet 3H_2O$	Activated Carbon	Solution reaction	Sonogashira Reaction	[137]
	$Cu(AOC)_2 \cdot 3H_2O$	Graphite	Refluxing reaction	Suzuki cross coupling reaction	[138]

$Cu(OAc)_2$	$Fe_3O_4.SiO_2$	Solution reaction	Suzuki–Miyaura reaction	[139]
$Cu(OTf)_2$	Silica	Refluxing reaction	Multicomponent Click Reaction	[140]
$Cu(OH)_2$	Cellulose	Schweizer's reagent	Click reaction	[141]

Source: author (2023).

As evident from the tabulated data, it becomes apparent that both nickel (Ni) and copper (Cu) exhibit the capacity to serve as catalysts for a diverse array of chemical reactions. These catalytic processes manifest with distinctive preparation methodologies, encompassing various precursor materials, and engage in a wide spectrum of chemical transformations. In essence, the catalytic potential of these metals transcends numerous reaction types, underscoring the versatility and applicability of nickel and copper-based catalysts in heterogeneous catalysis.

3.2.1.2 Bimetallic

Bimetallic catalysts have indeed proven to be a valuable tool in our quest to understand the intricate relationship between a metal's catalytic activity and its underlying electronic structure. Initially, the investigations were rooted in the electronic structure of an entire metal crystal, treating it as a unified entity, rather than delving into the localized electronic attributes of individual surface atoms. However, as a wealth of experimental data on chemisorption and catalytic processes on alloy surfaces has accumulated, it has become increasingly apparent that the localized properties of surface atoms play a pivotal role in catalytic phenomena [142].

The fundamental inquiry into the synthesis, catalytic behavior, surface chemistry, and structural attributes of bimetallic catalysts has evolved into a rapidly advancing and exhilarating domain within the heterogeneous catalysis landscape. This area of research not only holds profound implications for energy conversion but also serves as an enabler for transformative chemical processes [143].

In catalysis, the introduction of a second metal, referred to as the "guest metal," to an initial metal, known as the "host metal," presents a means to finely adjust catalytic performance parameters such as activity, selectivity, and durability. This tuning is achieved by modifying electronic and/or structural factors within the catalyst system. A

catalyst composed of two distinct metal components is broadly termed a "bimetallic catalyst" [144].

A bimetallic catalyst is conventionally defined as a catalytic crystallite comprising two distinct metal constituents. These constituent metals may take on various structural arrangements, including alloy formation, intermetallic phases, or nanocomposite structures. Alloy catalysts may manifest as bulk alloys, surface alloys, or near-surface alloys. In parallel, nanocomposite structures encompass core–shell configurations of bimetallic nanoparticles, intricate nanodendritic morphologies, and other structurally intricate arrangements. This diverse landscape of bimetallic catalyst architectures provides a versatile toolkit for fine-tuning catalytic responses to meet specific application requirements [143].

In the case of a Ni-Cu alloy, even within this combined state, the atoms of the two distinct metals retain their inherent chemical differences. While the bonding properties of these atoms may undergo some modifications, their individual characteristics remain discernible [144].

Substantiating the existence of divergent surface and bulk compositions within Ni-Cu alloys, compelling evidence is derived from the observation that robust hydrogen (H_2) chemisorption does not manifest on copper (Cu) surfaces. Remarkably, the mere inclusion of a small proportion of Cu into a Ni-based alloy leads to a dramatic reduction in the quantity of strongly chemisorbed hydrogen, an indication that the surface of the catalyst harbors a significantly higher concentration of Cu atoms compared to the bulk [145], [146].

Heterogeneous catalysis finds one of its most prominent and advantageous applications in facilitating hydrogen production. Among the various reactions employed for this purpose, methanol reforming stands out as a noteworthy example, serving as a means to generate hydrogen fuel. Nickel and Copper-based catalysts are widely studied, the synergistic interplay between these two metals within a bimetallic system yields significant enhancements in catalytic efficiency and physicochemical attributes. Importantly, this enhancement surpasses the performance of their monometallic catalyst counterparts. This cooperative interaction between the metal constituents not only amplifies catalytic reactivity but also contributes to the overall effectiveness of hydrogen production processes. [98], [146], [147].

Indeed, aside from methanol reforming, several other mechanisms for hydrogen production have been extensively studied, particularly involving the steam

reforming of various compounds like ethanol [148], [149], [150], glycerol [151], and methane [145].

Nickel and copper bimetallic catalysts have indeed showcased their remarkable versatility and efficacy in a broad spectrum of chemical reactions, particularly within the domain of organic chemistry. These catalysts have become popular choices for various organic transformations due to their efficiency and recyclability.

This type of bimetallic catalyst are widely employed in hydrogenation processes, where they facilitate the addition of hydrogen to unsaturated organic compounds. This includes the hydrogenation of alkenes[152], [153], alkynes [154], these two groups of organic molecules have been extensively studied with copper and nickel bimetallic catalysts since the 1950s [155], [156].

Examples of other organic compounds amenable to hydrogenation with copper and nickel bimetallic catalysts include oleic acid[157], furfural [158], [159], and carbon dioxide[160], [161], particularly when supported on ceramic materials.

Indeed, advancements in equipment for observing and characterizing chemical reactions, coupled with a growing awareness of environmental concerns and the principles of green chemistry, have led to increased research and innovation in the use of bimetallic catalysts. These catalysts have garnered significant attention for their potential to facilitate sustainable and efficient chemical processes.

Some organic reactions such as Sonogashira coupling reaction has been carried out using homogeneous palladium (Pd) catalysts. While Pd catalysts are known for their high performance and stereoselectivity, they come with certain limitations, including the use of toxic ligands, the high cost of palladium, and challenges associated with separating Pd residues from the reaction products. Consequently, there has been a preference among researchers for Pd-free systems [162].

This reaction is essential for generating valuable intermediates employed in the synthesis of biologically active compounds, agrochemicals, pharmaceuticals, polymers, and engineered materials, numerous studies have been conducted with a focus on developing catalysts that do not contain heavy metals and are reusable, mainly with nickel and copper [163], [164].

The efficiency and reusability of these catalysts make them particularly appealing for organic chemists. Their ability to promote a variety of organic reactions with high selectivity and under mild conditions contributes to the development of

greener and more sustainable synthetic methodologies in organic chemistry. Additionally, their recyclability aligns with the principles of green chemistry, reducing waste and environmental impact in chemical processes.

3.2.2 Support

The concept of supported metal catalysts is relatively straightforward. Small particles of the active metal component are dispersed onto the surface of a support material. Additionally, self-supported catalysts can be used, where the metal component itself serves as the support material [165], [166].

The physical characteristics of the catalyst surface, such as surface area, morphology, and porosity, also play a critical role. A higher surface area provides more active sites for the reactants to interact, increasing the likelihood of successful catalytic reactions. The surface morphology, including the presence of steps, edges, and defects, can influence the binding energies and diffusion of reactants and intermediates, influencing the reaction kinetics and selectivity [1].

The preparation of supported metal catalysts offers two significant advantages: efficacy and cost-effectiveness. By dispersing the metal as small particles on the support material, a larger portion of the metal becomes accessible for catalytic reactions. This means that less metal is required for achieving the desired catalytic activity. Supported metal catalysts are commonly prepared by reducing commercially available metal salts in the presence of the support material [167].

The support plays a vital role in determining the catalytic performance, as it enables the supported catalyst to function as an active center for the desired reaction. The support material's properties can range from inert to possessing acidic, basic, or unique electronic characteristics (such as being an insulator or conductor) [168], [169]. Anchoring the catalyst to the support can be achieved through diverse interactions, including acid-base interactions, hydrogen bonding, or simple van der Waals forces.

Common materials used as catalyst supports include alumina, titania, graphite, activated carbon, and silica [71], [170], [171], [172]. These materials possess desirable characteristics such as a high surface area, chemical and mechanical stability, and the ability to effectively disperse catalyst particles across their surfaces.

Porous ceramics have attractive potential as a catalytic support due to their high chemical, thermal and mechanical stability, low density, excellent reliability and

easy customization of microchannels of different formats. One of the most studied ceramic materials as a support for catalysts is alumina, due to the geometric effect and its high surface area, allowing greater dispersion of the active phase, in addition to being stable at high temperatures and relatively inexpensive [170], [173], [174].

Among the different ceramic supports used, in addition to alumina, zirconium oxides stand out, because they have a mesoporous structure and even a high surface area [175], [176], [177]. The following can also be mentioned, among other studied ceramic materials: silicon carbide [178], [179], cerium oxide[10], [180], MCM-41 (Mobil Composition of Matter No. 41) [124], [181] which have catalytic activity. A common point among the ceramic materials studied is that they normally undergo a sintering heat treatment at high temperatures to acquire mechanical resistance.

In a study conducted by *Zhang et al.* in 2012, a Ni.Ca-cementitious material was successfully synthesized at a low temperature of 60 °C, with a alkali-activated steel slag polymerization followed by ion exchange as the method of catalyst preparation. This innovative technique facilitated the efficient incorporation of nickel (Ni) and calcium (Ca) into the cementitious matrix, resulting in a material with improved properties, particularly in the field of photocatalysis [182].

The reduced number of stages and energy in its production, especially the firing stage, a thermal stability, a large contact surface and mechanical resistance, would be an ideal support, in addition to guaranteeing the sustainability of the entire process to be followed [183]. In this regard, geopolymers become interesting materials for use as alternative catalysts and are discussed in the subsequent topic.

3.3 GEOPOLYMERIC MATERIALS

A geopolymer (GPs) is defined as a stable, solid aluminum silicate formed by alkaline activation at room temperature [184]. Materials referred to as 'geopolymers' have also been described in the literature as 'mineral polymers', 'inorganic polymers', 'inorganic polymer glasses', 'alkali-bonded ceramics', 'alkali ash', 'soil cements', 'hydro pottery' and a variety of other names [185], [186], [187].

Geopolymers are a subset of the broader class of alkali-activated binders or alkali-activated materials [188], which also includes materials formed by carbonates or activation of calcium-rich metallurgical slags, giving rise to other products such as hydrated calcium silicate.

The general representation of a typical geopolymer composition is expressed as $nM_2O \cdot Al_2O_3 \cdot xSiO_2 \cdot yH_2O$, where M represents the alkali metal [189]. The activity of geopolymer is generally influenced by various characteristics of the source materials. These include the chemical components, soluble silicon-aluminum content, particle size, and the presence of inert particles. These factors play a significant role in determining the activity and performance of the geopolymer material [190].

Indeed, the glass phase in geopolymer materials is typically inert in water and does not exhibit cementitious properties on its own. It is only through alkaline activation that the glass phase becomes reactive and develops cementitious properties. When an alkaline solution is introduced to the geopolymer system, it triggers a chemical reaction that leads to the dissolution and recombination of the glass phase, resulting in the formation of a cementitious matrix [191]. The alkaline solution commonly used in geopolymer synthesis consists of NaOH (sodium hydroxide), Na_2SiO_3 (sodium silicate), KOH (potassium hydroxide), and K_2SiO_3 (potassium silicate).

The geopolymerization process (Figure 6) involves a rapid mixture reaction where Silica-Aluminum source materials are dissolved using an alkaline solution. This reaction generates heat and forms a gel, which binds aggregates and unreacted source materials, resulting in the formation of geopolymer bonds. The dissolution of Si and Al atoms occurs through the action of OH ions, causing the precursor ions to condense and form monomers known as Silate. This, representing silicon-oxo-aluminate, contributes to the construction of chains and rings within a three-dimensional polymeric network, often in the form of (Na,K)-(Si-O-Al-O-Si-O) [192], [193].

Figure 5 Geopolymerization process.

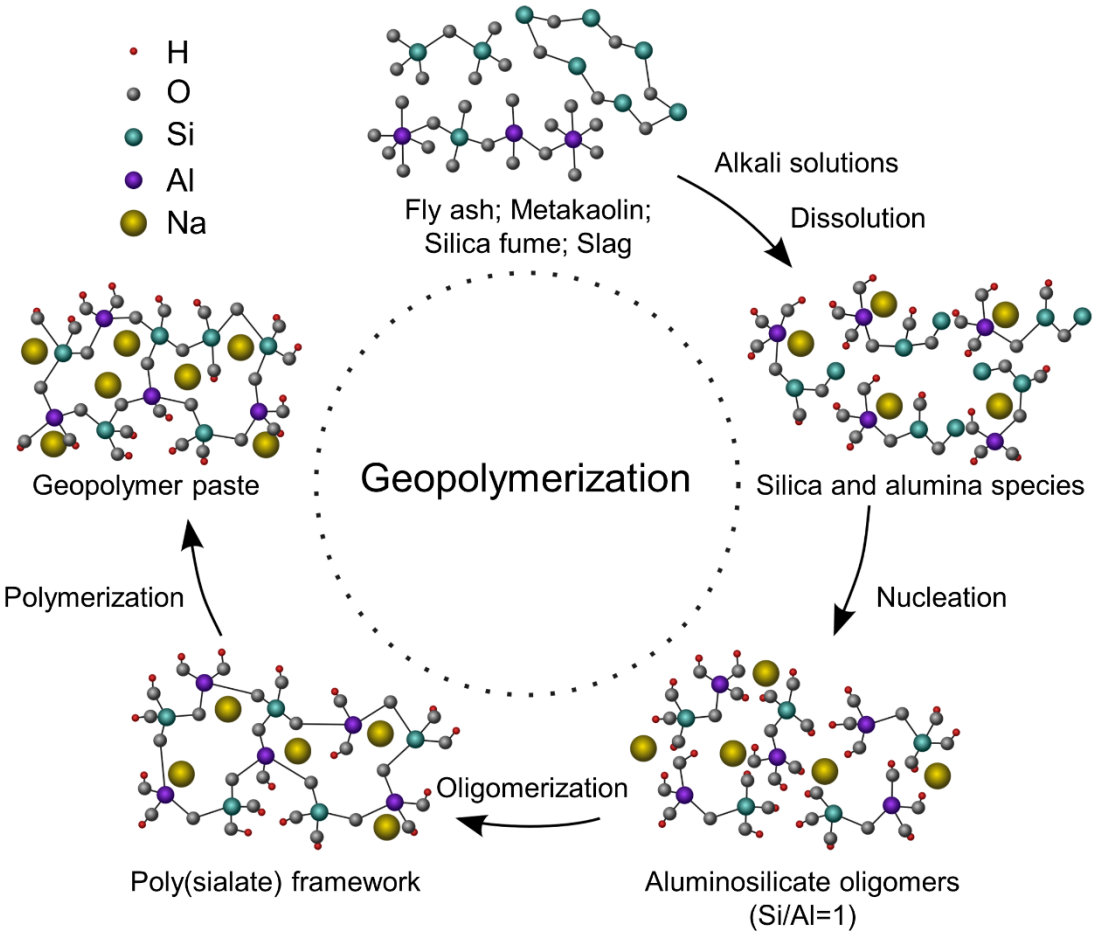

Source: author (2023).

The intrinsic characteristic of a geopolymer is that the binding phase comprises an alkaline aluminum silicate gel, with aluminum and silicon bonded in a tetrahedral gel structure, being relatively resistant to dissolution in water [194]. This set of Si–O–Al and alkaline activator is normally bound alternately by oxygens in the presence of positive ions (Na^{+}, K^{+}, Li^{+}, Ca^{+2}, Ba^{+2}, NH^{4+}, H_3O^{+}). These positive ions have the purpose of balancing the negative charge of Al^{+3} in the fourth coordination [184], [195].

In geopolymers, the SiO_2/Al_2O_3 ratio plays a crucial role as the most important parameter in controlling both the microstructure and mechanical properties. A low SiO_2/Al_2O_3 molar ratio leads to a larger specific surface area [196] while an increase in the $SiO_2/Al2O_3$ molar ratio fosters the development of mechanical properties [197]. This highlights the significance of carefully adjusting this ratio to achieve desired material characteristics during the geopolymerization process. The water/solid ratio also plays a significant role in determining the properties of geopolymers. This ratio

influences not only the mechanical properties but also the density, porosity, and microstructure of the resulting geopolymers [196].

Efflorescence in geopolymers results from a chemical reaction between the alkalis present in the material and atmospheric carbon dioxide. This reaction is a dominant cause of deterioration in geopolymer materials [198]. The occurrence of efflorescence is influenced by the conditions during the activation process, such as temperature and humidity. The main contributing factors for efflorescence formation are the availability of Na^+ and OH^- ions, which are closely related to the porous structure of the geopolymer.

By carefully addressing these parameters, it is possible to optimize the material, especially when considering the application of geopolymers in catalysts, factors such as efflorescence control, chemical composition, and microstructure become crucial in ensuring the catalyst's effectiveness and stability.

A novel class of heterogeneous catalysts has been developed based on geopolymer materials, showcasing their catalytic prowess in industrially significant reactions, they exhibit several characteristics that make them attractive catalysts. A high surface area, allows for more active sites available for catalytic reactions, promoting efficient contact between the catalyst and reactants [5]. Geopolymers have flexible chemical compositions that can be adjusted by incorporating different elements or modifying the ratio of silicon (Si) to aluminum (Al) atoms and capabilities to incorporate various metal ions as active centers [199]. Besides often possessing a mesoporous structure, characterized by the presence of interconnected pores in the nanometer range, enhances mass transfer. The combination of these properties and the low-cost preparation promising choice for catalysts in various catalytic processes, ranging from environmental remediation to industrial synthesis.

The primary objective of employing geopolymers as catalysts is to eliminate contaminants and impurities. In certain scenarios, geopolymer modification can create active sites within its structure, thus enabling it to function as a catalyst [200], [201]However, in most cases, the addition of an active phase as metal oxides, metals, alloys, nitrates, and sulphides to the geopolymer structure, typically in the form of coatings, yields the catalyst, these additional components augment the catalytic properties of the geopolymer [202].

Photocatalysts based on geopolymers have emerged as a promising solution for addressing environmental challenges [182], [203], [204]. Geopolymers, with their

unique structure and composition, exhibit excellent photocatalytic properties that enable them to efficiently absorb and degrade harmful gases. By simply incorporating oxides into the slurry, it is possible to achieve oxides/composites with a porosity ranging from 34% to 40% by volume. These resulting composites, characterized by their substantial porosity, can be utilized as cost-effective catalysts for syngas purification [205].

Geopolymeric catalysts find additional applications in the production of biodiesel. One key benefit is their thermal stability, enabling them to withstand the high temperatures required for transesterification reactions. They can also be tailored to have specific acidic or basic properties, allowing them to function as solid acid or base catalysts, respectively, in the transesterification process [57], [206], [207], [208].

Other studies have demonstrated that geopolymer exhibits catalytic properties for the liquid-phase Beckmann rearrangement of cyclohexanone oxime to ε-caprolactam [209]. A fly-ash based geopolymers have been synthesized as highly reactive porous aluminosilicate heterogeneous catalysts, with a focus on their potential applications in Friedel-Crafts benzylation reactions involving benzene and various substituted aromatics [210].

In addition to the high specific surface area and the presence of strong alkaline sites for the catalytic action, geopolymers also show good workability as aqueous pastes and have cementitious properties, that is, they can consolidate at room temperature, allowing their conformation by methods based on additive manufacturing [57].

3D printing using geopolymers represents a burgeoning frontier within of additive manufacturing (AM) technologies. One notable advantage of this technology is the potential utilization of municipal and industrial solid waste as viable precursors for GPs. These waste materials encompass a diverse range of sources, including slag, fly ash, silica fume, red mud, waste glass, and mine tailings, among others [193], [211], [212], [213]. By harnessing these waste materials as feedstocks for GPs, it offers a promising avenue for sustainable and eco-friendly construction practices, while simultaneously addressing waste management challenges.

Pumpability assumes critical significance as it defines the fresh geopolymer mixture's ability to transform under pressure within the printing system. This property is closely interlinked with the rheological characteristics, especially the yield stress and plastic viscosity of the material. Generally, higher values of these properties tend to

hinder pumpability, making it more challenging to extrude the mixture effectively. However, it is important to note that these high values also contribute to enhancing buildability, which refers to the capacity of the printed material to retain its shape and form during the construction process [214] .

Hence, achieving the desired rheological properties in geopolymer mixtures necessitates striking a delicate balance between pumpability and buildability. This equilibrium is essential to ensure the production of high-quality geopolymer 3D printing material.

Another important rheological property is the extrudability, it plays a crucial role in determining the geopolymer mixture's ability to flow smoothly through the printing head nozzle, forming a continuous filament during 3D printing. To ensure seamless extrusion, the mixture should possess an optimal yield stress and a low plastic viscosity. Incorrectly proportioned mixtures or inadequate mixing can result in particle segregation, nozzle clogging, or filament tearing [51].

The latest trends in sustainable materials and sustainable technologies make geopolymer 3D printing a promising technology in the industrial and research sector, although there are still some challenges to be overcome in the manufacture of this type of material, mainly regarding workability. Workability is the ease of transporting the material from the syringe to the printer's nozzle, since the behavior of the material is time-dependent, the variation in its properties can lead to segregation or clogging in the processing nozzle, caused by hardening of the material in the printing syringe, as the geopolymer cures at room temperature [215].

To mitigate clogging issues and enhance workability in geopolymer mixtures for 3D printing, selecting appropriate aluminosilicate source materials and alkali silicate/hydroxide activating agents is crucial. Incorporating supplementary components, such as plasticizers, accelerators or retarders, thixotropic thickeners, proves beneficial in enhancing workability [216].

Of particular significance are plasticizing additives, which play a pivotal role in this process. The introduction of finely dispersed fillers possessing a high specific surface area and surface-active functional groups exerts a discernible impact on the viscosity of the geopolymer mortar. These modifications enable precise manipulation of the mixture's flow behavior, facilitating improved printability and workability during the 3D printing process [51].

Indeed, buildability is another crucial parameter in the context of a fresh geopolymer mixture during the extrusion-based 3D printing process. It primarily pertains to the ability of the laminated extruded filament to maintain its intended form without experiencing significant deformations or collapsing. Several factors contribute to the buildability of a geopolymer mixture [214], [216], [217]:

A) Setting Rate: The rate at which the geopolymer mixture sets and solidifies plays a crucial role in determining how well the printed object retains its shape and form during the printing process.
B) Time Gap Between Extrusions: The time interval between successive extrusions also impacts buildability. Sufficient curing time between layers is essential to ensure proper bonding and structural integrity of the printed object.
C) Rigidity of Fresh Material: The inherent rigidity of the fresh geopolymer material influences its ability to hold its shape and resist deformation during the printing process.
D) Binding Capacity between Filament Layers: The capability of the geopolymer material to effectively bind between the layers of the extruded filament significantly influences buildability. A strong and cohesive bond ensures the stability and structural integrity of the printed object.

Furthermore, monitoring and adjusting the extrusion parameters in real-time are essential for maintaining the desired rheological behavior throughout the printing process and minimize the possible defects. These heterogeneities that arise during the extrusion-based 3D printing process can result in the formation of voids, they act as weak points, reducing the overall structural integrity and more susceptible to fractures and failure under mechanical [216].

In addition to its significant impact in the construction industry, additive manufacturing technologies present promising opportunities for various advanced energy and environmental applications of 3D printed geopolymers. These applications include their use as catalysts, water purification filters, adsorvents, construction, conductive materials, as shows in Figure 7.

Figure 6 3D-printed geopolymers. A- [218]*, B-* [219]*, C-* [220]*, D-* [221]*, E-* [222]*, F-* [223]*, G-* [224]*, H-* [57] *and I-* [225].

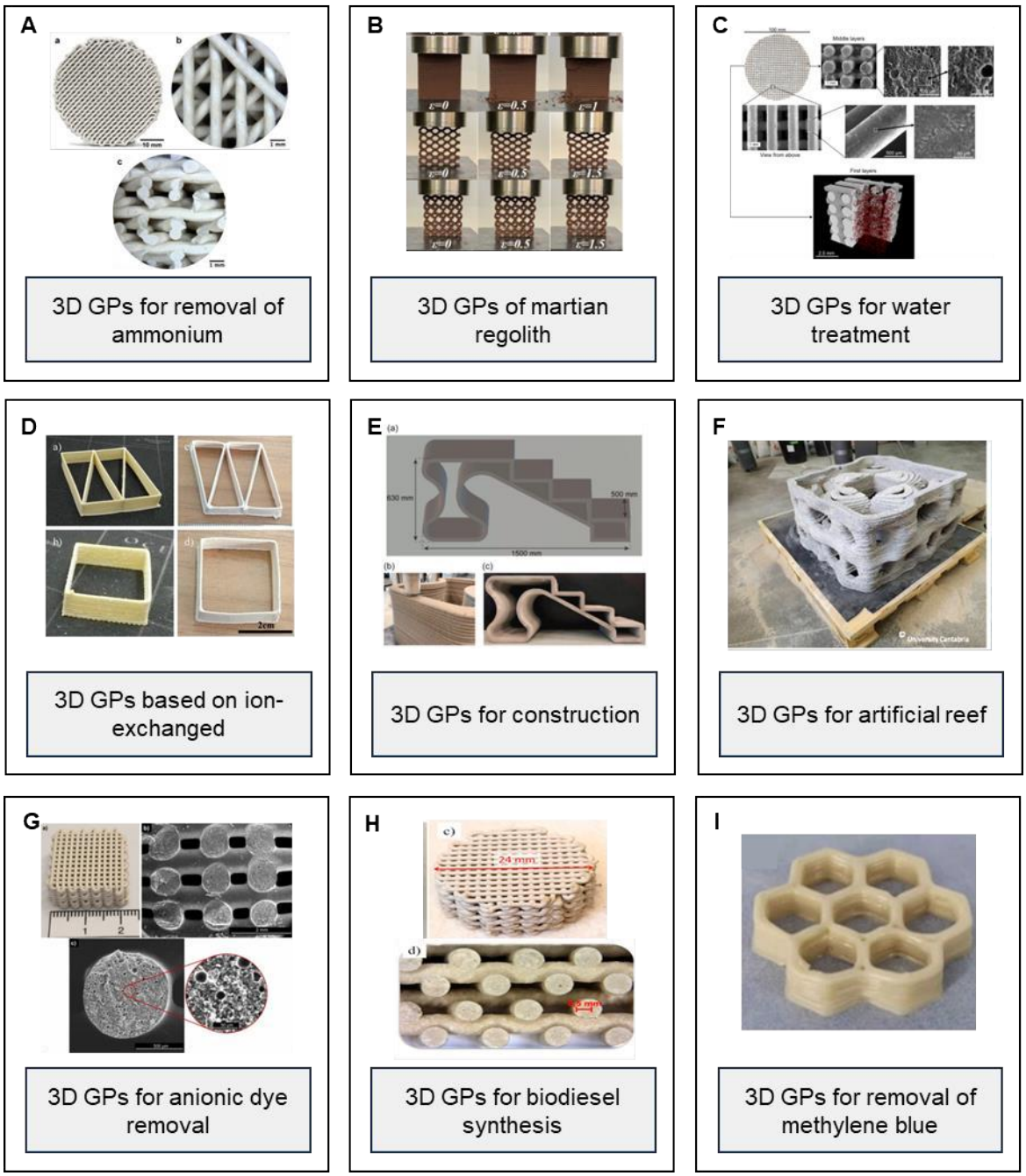

Source: author (2023).

Looking forward, the potential for practical applications of AM technologies using geopolymers is expected to expand into new and diverse areas. Researchers are likely to explore and discover novel uses for 3D printed geopolymers in various fields, thanks to their versatile properties and customizable characteristics. As the technology and understanding of geopolymers continue to advance, we can anticipate exciting developments and innovative applications, making significant contributions to

the advancement of energy-efficient and sustainable solutions in different industries and environmental applications.

4 MATERIALS AND METHODS

4.1 OVERVIEW

In the studied catalysts, there are two main components: the support and the active phase. The support was crafted using geopolymer, comprising metakaolin, sodium silicate, sodium hydroxide, and PEG. For effective catalysis to occur, the support must possess a high surface area to allow interaction with the substrate. One approach to functionalize the catalyst is through the impregnation of the active phase into the support material.

The impregnation method involves three stages, shows in the Figure 8. First, the support is contacted with a solution of nickel nitrate or copper nitrate to monometallic catalysts, and for both metals for de bimetallic catalysts, and water, ensuring thorough mixing. In the second stage, the system is dried to remove solvents.

Alternatively, another method to make the support suitable for catalytic reforming of ethanol is to include the active phase during the preparation and manufacturing of the support. This approach offers practical advantages by reducing subsequent steps and risks of compromising the support's structure, shows in Figure 6 in addition method.

Figure 7 Steps of the two methods of preparation of catalysts in this study.

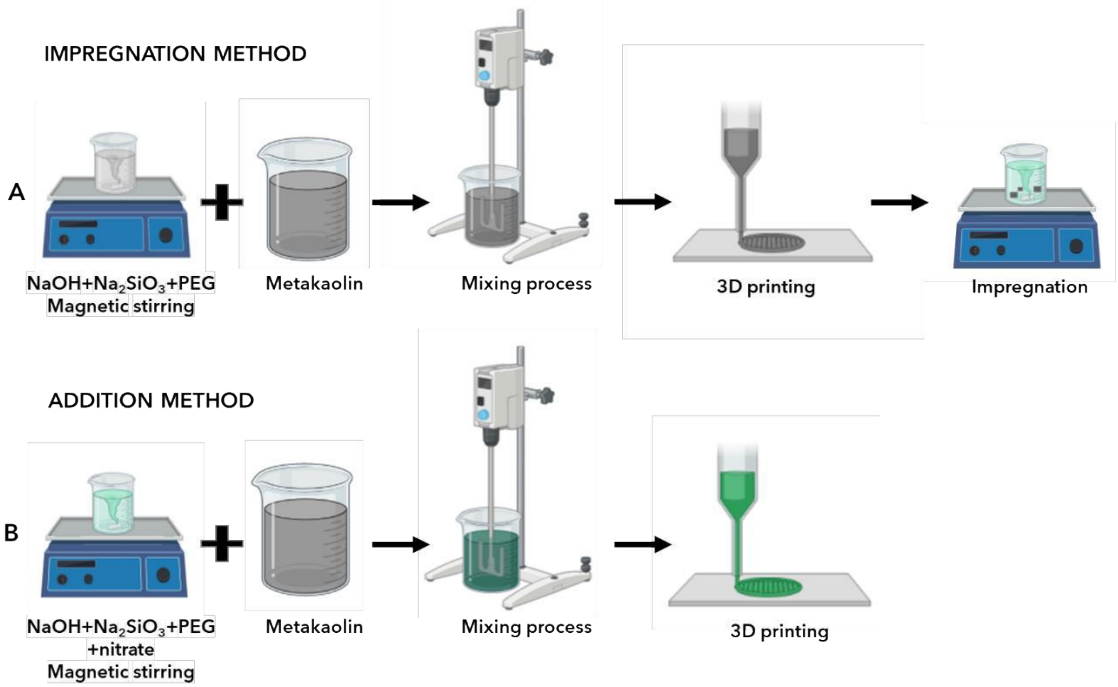

Source: author (2023).

The developed samples were categorized into three groups: without metal, metal incorporated into the support, and the metal via wet impregnation. These samples are solely comprised of the geopolymer support described in Section 4.2 and are identified according to the nomenclature outlined in Table 2.

Table 2 Description of the samples.

	Name	Description	Method
1	GEO	Geopolymer	
2	Ni10_IMP	Sample with 10 w.t% of $Ni(NO_3)_2.6H_2O$	IMPREGNATION
3	Ni10Cu2_IMP	Sample with 10 w.t% of $Ni(NO_3)_2.6H_2O$ and 2 w.t% of $Cu(NO_3)_2.3H_2O$	IMPREGNATION
4	Cu10_IMP	Sample with 10 w.t% $Cu(NO_3)_2.3H_2O$	IMPREGNATION
5	Ni10_ADD	Sample with 10 w.t% of $Ni(NO_3)_2.6H_2O$	ADDITION
6	Ni10Cu2_ADD	Sample with 10 w.t% of $Ni(NO_3)_2.6H_2O$ and 2 w.t% of $Cu(NO_3)_2.3H_2O$	ADDITION
7	Cu10_ADD	Sample with 10 w.t% $Cu(NO_3)_2.3H_2O$	ADDITION

Source: author (2023).

The experimental procedure of this work was performed at the Laboratório de Processamento Cerâmico (ProCer – EQA – UFSC) and the Nucleo de Pesquisa em Materiais Cerâmicos e Compósitos (CERMAT - EMC – UFSC).

4.2 MATERIALS

In this study, metakaolin from two different suppliers was utilized as a source of silica and alumina. The metakaolin from HP Ultra, supplied by Metacaulim do Brasil®, was referred to as MK-B. The metakaolin from Imerys SA® was referred to as MK-I. Commercial materials were also employed in the research. Sodium hydroxide (NaOH) from Commercial Neon® with a purity of 99% was used as an alkaline activation source. Sodium silicate (10.8 wt. % Na_2O, 34.20 wt. % SiO_2 and 55.0 wt. % H_2O) from Quimidrol® was also utilized as an alkaline activation source. Polyethylene

glycol (PEG-400) from Neon Comercial® with a purity of 98% was incorporated as an additive in the additive manufacturing process. It served to reduce the formation of bubbles and increase the working time during the printing of supports. For the active phase, a nickel nitrate ($Ni(NO_3)_2.6H_2O$) and copper nitrate ($Cu(NO_3)_2.3H_2O$) from Commercial Neon® with a purity of 99% was employed as the metals precursor.

4.3 OBTAINING GEOPOLYMER SUPPORTS

To produce the supports, a geopolymeric paste was utilized. The formulations of the paste, as outlined in Table 3, were adjusted to achieve geopolymers with suitable rheological properties for printing and sufficient mechanical strength for catalytic applications. In terms of mass quantities, the maximum amount that can be accommodated in a 55 cm³ printing syringe includes the following proportions: 60 g of metakaolin, 50 g of alkaline activators (NaOH/Sodium silicate ratio = 1), and 3.3 g of PEG-400 (equivalent to 3% of the total mass of 110 g).

Table 3 Mass of reagents to produce geopolymer paste.

Reagents	Mass (w.t%)
Metakaolin Brasil (MK-B)	26.5
Metakaolin Imerys (MK-I)	26.5
Sodium silicate	25.5
Sodium hydroxide solution 10M	18.5
Polyethylene glycol	3

Source: author (2023).

The chemical composition analysis of the metakaolins was conducted using X-ray fluorescence (XRF; Shimadzu EDX-7000 HS). XRF in is a quantitative analytical technique commonly employed particularly useful in identifying the levels of various oxides and rarer elements that constitute the metakaolin samples, the chemical composition of MK-B and MK-I are displayed in Table 3. XRF analysis is widely used in various industries and scientific research fields to characterize the chemical composition of materials, including rocks, minerals, ceramics, and other solid samples. Its quantitative nature and ability to detect a broad range of elements make it a valuable tool in chemical analysis and material characterization.

Table 4 Chemical composition (XRF, w.t%)

Oxides	MK-B	MK-I
SiO_2	56.12	52.84
Al_2O_3	36.00	43.31
Fe_2O_3	2.27	0.85
TiO_2	1.64	1.13
K_2O	1.62	0.04
ZrO_2	0.07	0.02
Other oxides	2.28	1.81

Source: author (2023).

The preparation of the mixture involves several steps as follows:

1. The liquid reagents, including a 10M NaOH solution, sodium silicate (Na_2SiO_3), and polyethylene glycol (PEG), are added in a beaker. These reagents are carefully measured and combined for 10 min under magnetic stirring.
2. The metakaolin is dried in an oven at a temperature of 100 °C for 12 hours to remove any moisture. Once dried, the metakaolin is transferred to a separate beaker.
3. The mixture containing the alkaline activator (from Step 1) is poured over the metakaolin in the beaker. The metakaolin is then subjected to mechanical mixing using a mechanical mixer, specifically an IKA RW20 model with a propeller equipped with four blades. The mixing process is carried out for 6 min at a speed of around 500 RPM.

These steps ensure the proper combination and homogenization of the metakaolin, alkaline activators, and PEG to form the geopolymeric paste. The mechanical mixing step is crucial in achieving a uniform and well-mixed paste with suitable rheological properties for subsequent 3D printing applications.

Once the geopolymeric paste is thoroughly mixed, it is transferred to the printing syringe for further processing using additive manufacturing techniques. In this case, a Dura Printer® E-03 model with pneumatic injection is utilized for 3D printing of the geopolymers.

The design of the printed structures is created initially in Solidworks2017® software, allowing the customization of different designs to achieve desired porosity and specific surface area. The design file is then converted into a compatible format

(STL) for the printer. Slic3r® software is employed to slice the design into parallel lines, generating the contours of each layer and determining the printing path coordinates.

During the 3D printing process, specific parameters are set to ensure optimal printing results. These parameters include:

i) Maximum height: Up to 110 mm, indicating the maximum height of the printed structure.

ii) Layer thickness: Up to 3 mm, determining the thickness of each printed layer.

iii) Printer nozzles: 0.8 mm in size, indicating the diameter of the printer nozzles used for extrusion.

iv) Printing speed: Up to 120 mm/s, controlling the speed at which the material is deposited during printing.

v) Temperature of the printing table: Maintained at 25 °C to provide a stable printing environment.

By adjusting these printing parameters, the desired characteristics such as porosity and specific surface area can be achieved in the printed geopolymeric structures.

Figure 8 Geopolymeric support obtained by 3D printing.

Source: author (2023).

After the 3D printing process, the curing of the geopolymeric pieces is conducted at room temperature for a duration of 7 days.

4.4 IMPREGNATION METHOD

To impregnate the geopolymeric support (Fig. 6-A) with nickel or copper, after 28 days, the dry supports were weighed, and different mass percentages were used for the monometallic catalysts. For the monometallic nickel catalysts, the supports were impregnated with a solution containing 10% by weight of $Ni(NO_3)_2.6H_2O$. Similarly, for the monometallic copper catalysts, a solution containing 10% by weight of $Cu(NO_3)_2.3H_2O$ was used. For the bimetallic catalysts, a combination of nickel and copper was used. The supports were immersed in a solution containing 10% by weight of $Ni(NO_3)_2.6H_2O$ and 2% by weight of $Cu(NO_3)_2.3H_2O$.

The nitrates were dissolved in a total volume of 50 ml of distilled water. The support was then immersed in the solution and subjected to agitation for approximately 8 h at a temperature of 60 ºC. This step allowed the impregnation of the metals into the geopolymeric support.

After the impregnation process, the catalyst was removed from the solution, and any remaining water was evaporated. A portion of the catalyst was further dried in an oven at a temperature of 80 ºC for 1 h. This drying process ensured the removal of any residual moisture from the catalyst before further characterization and testing.

By following this impregnation method, the desired metal precursors (nickel or copper) were incorporated into the geopolymeric support, forming the monometallic and bimetallic catalysts for subsequent analysis and evaluation.

4.5 ADDITION METHOD

In the process of introducing the active phase into the geopolymer paste, a physical mixture is created by adding the solid nitrate during the mixing step of the liquid reagents (Fig. 6-B). The liquid reagents, including NaOH (10 M), sodium silicate (Na_2SiO_3), and polyethylene glycol (PEG), are added to a beaker and stirred magnetically for 10 min until homogenization, the materials employed maintain equivalent mass percentages to those found in the pure geopolymer showed in Table 2. Then, the solid nitrate is added to the same beaker and stirred for another 20 min.

The process continues similarly to the obtention of the geopolymer support. The liquid reagent mixture is poured over the metakaolin, and the geopolymeric paste

is formed using a mechanical mixer at approximately 500 RPM for 6 min. The resulting geopolymer paste contains the metallic precursor incorporated into it.

The geopolymer paste, now containing the metallic precursor, is transferred to the syringe for 3D printing of the catalysts. In this method, the nitrates are added to the geopolymer mass during the mixing process, eliminating the need for a separate wet impregnation step after printing.

After 3D printing, the printed catalyst pieces undergo a curing process at room temperature for 7 days.

4.6 CHARACTERIZATION

The characterization of catalysts is imperative for evaluating the feasibility and efficacy of materials within the reaction medium. Accordingly, the justification for employing a diverse set of characterization techniques is rooted in the necessity to comprehensively analyze the prepared catalysts. Through the application of these techniques contribute to a deeper understanding of the catalyst's performance and unlock its inherent potential in the given application.

4.6.1 X-Ray Diffraction (XRD)

X-ray Diffraction (XRD) analysis is a widely used technique in materials science that enables the determination of a material's composition and crystallographic structure. It involves irradiating a material with X-rays and measuring the intensities and scattering angles of the X-rays that emerge from the material.

The primary purpose of XRD analysis is to identify materials based on their unique diffraction patterns. Additionally, it can provide insights into deviations from the ideal crystal structure, such as internal stresses and defects within the material.

In crystalline materials, atoms are arranged in a regular and repetitive pattern throughout the crystal, extending in all three dimensions of space. As atoms contain electrons capable of absorbing and re-emitting electromagnetic radiation, they act as scatterers of light. The interference of scattered light results in diffraction phenomena [226] .

To determine the crystalline structures of the metal oxides, powder X-ray diffraction was performed using the Rigaku® MiniFlex600 DRX equipment at the Linden Laboratory of UFSC (Universidade Federal de Santa Catarina).

For analysis, the catalysts were finely ground using an agate mortar, sieved through a Retsch® granulometric sieve with a 125 μm mesh, and then transferred to 2 ml Eppendorf tubes. The samples in powder form were placed in an aluminum sample holder and compacted.

During the XRD analysis, a Cu-Kα copper tube was utilized, with a wavelength (λ) of 1.5420 Å. The measurement was conducted in the 2θ range between 10 and 100°, with a sweep speed of $0.01°\cdot s^{-1}$.

4.6.2 X-ray fluorescent (XRF)

X-ray Fluorescence (XRF) spectrometers represent potent analytical tools crafted for the elucidation of the elemental composition inherent in diverse materials. Through the assessment of the energies and intensities associated with emitted X-rays, these instruments discern the presence and concentrations of individual elements.

For X-ray Fluorescence (XRF) analysis, the catalysts were prepared in two different ways: powder and small pieces. For powder analysis the catalysts were randomly fractured using an agate mortar and subsequently transformed into a powder. This powder underwent sieving through a 125 μm particle size sieve and was then transferred to 2 mL Eppendorf tubes. Samples prepared using the impregnation method were randomly fractured into small pieces, approximately measuring 3 mm. These fragments were affixed to the sample holder to facilitate the analysis of the thickness of the impregnated layer.

The analysis was conducted using the Shimadzu EDX-7200 equipment at the Shimadzu Analytical Division (São Paulo – SP). The procedure was executed in an air atmosphere, employing a 5mm collimator for powder samples, and 1- and 3-mm collimators for broken samples. The sample cup, constructed from polypropylene, was subjected to an X-ray beam for a duration of 30 seconds at a maximum energy of 40 keV.

4.6.3 Scanning Electron Microscopy (SEM)

Scanning Electron Microscopy (SEM) is a technique used to produce high-resolution images of a sample's surface by scanning it with a focused electron beam. It is commonly employed for the analysis of material morphology. Additionally, SEM can provide information about the chemical composition of the samples using Energy-Dispersive X-ray Spectroscopy (EDS).

For SEM analysis, the catalyst samples were randomly broken using an agate mortar, and small pieces measuring approximately 3 mm were affixed to the sample holder using double-sided tape. Gold coating was not necessary for these samples.

The SEM images were acquired using the Hitachi® TM3030 (CERMAT – EMC – UFSC) and JEOL® JSM-6390LV Scanning Electron Microscope (LCME – UFSC) instruments. The SEM was operated at low vacuum, and the voltage was set at 5KeV with a tungsten filament. The magnification levels used for imaging were 30x, 150x, 200x, and 400x. Additionally, complementary analyses were conducted using EDS, which is integrated into the SEM vacuum chamber. EDS detects the energy associated with each electron and provides information about the chemical composition of the samples. The selected magnitude for the EDS analysis was 100 μm.

4.6.4 Thermoprogrammed Reduction (TPR)

Thermoprogrammed Reduction (TPR) is a thermoanalytical technique used to characterize the internal and surface structure of a material, particularly for assessing the reducing power of a catalyst. It provides valuable information regarding the ease of reducing metal oxides, which is crucial for catalyst design and application.

In TPR analysis, a mixture of a reducing gas, typically 5% H_2 in N_2, is passed over the catalyst oxide while the temperature is gradually increased using a linear heating ramp. As the temperature rises, reduction of the oxide occurs, and the consumption of hydrogen is measured. The resulting signal represents the reaction rate and exhibits a peak at a characteristic temperature, which is influenced by both the oxide material and the heating rate [227].

The TPR analyses were conducted at the Laboratorio de Combustão e catálise Aplicada - UFSC Joinville, using the ChemBET® equipment with BET, pulse titration,

TPD, TPR, TPO. The experimental conditions included a ramp temperature up to 800 °C and a gas flow rate of 75 ml/min (composed of 95% nitrogen and 5% hydrogen).

To ensure accurate measurements and eliminate interference from moisture, the samples underwent a gas purge process in a nitrogen atmosphere. The purge involved passing a nitrogen flow of 75 ml/min over the samples at a temperature of 300 °C for a duration of 3 h. This step helps remove any residual moisture before initiating the TPR analysis, allowing for a clean signal that primarily reflects the change in hydrogen concentration during the reduction process.

4.6.5 Brunauer-Emmett-Teller (BET)

The Brunauer-Emmett-Teller (BET) theory is formulated to elucidate the physical adsorption of gas molecules onto a solid surface. This theory serves as the foundation for a crucial analytical technique employed in determining the specific surface area of materials. The BET theory is particularly applicable to systems involving multilayer adsorption. In practice, this theory commonly employs probing gases that do not undergo chemical reactions with the material surfaces, serving as adsorbates for the quantification of specific surface area [228]

The catalysts were prepared through two distinct methodologies: powder and small pieces. In the case of powder analysis, the catalysts were randomly fractured using an agate mortar, leading to their transformation into a fine powder. Subsequently, this powder underwent sieving through a 125 μm particle size sieve and was subsequently transferred to 2 mL Eppendorf tubes for further processing.

On the other hand, for small pieces analysis, the catalysts were randomly fractured into small pieces, each measuring approximately 3 mm in dimensions. The samples were prepared using varied methods to investigate the pores formed within the solid because of the additive manufacturing process.

The analysis was conducted in two distinct manners using different equipment. Samples in powder form were acquired employing the single-point ChemBET Pulsar TPR/TPD Automated Chemisorption Flow Analyzer, (LAC - UFSC – Joinville). Meanwhile, samples in pieces were analyzed in the Nanotec laboratory (UFSC - Florianopolis) equipament model Nova 2200e, both of Quantachrome Instruments, utilizing same techniques. The analysis was carried out under a nitrogen atmosphere with a flow rate of 75 mL/min, utilizing a mass of 100 mg for each sample. Prior to

analysis, a degassing step at 300°C for 3 hours in N2 5.0 was performed to ensure the removal of any residual gases or contaminants.

4.6.6 Nuclear Magnetic Resonance (NMR)

Nuclear Magnetic Resonance (NMR) spectroscopy stands as an advanced characterization technique employed to discern the molecular structure at the atomic level within a given sample. Beyond elucidating molecular structures, NMR spectroscopy can identify phase changes, conformational and configurational alterations [229].

This spectroscopy method serves as a valuable tool for elucidating the structures of organic compounds. Within the ^{1}H spectra, three key features—chemical shift, signal intensity, and multiplicity—contribute distinct and informative details, collectively enhancing our understanding of the molecular composition and arrangement in the analyzed compounds.

The 1H NMR and 13C NMR spectra were acquired using Varian AS-400 spectrometers (400 and 100 MHz, respectively) and Bruker AC-200F (200 and 50 MHz, respectively) (QMC-UFSC-Florianópolis). CDCl3 served as the solvent. Chemical shifts were recorded in parts per million (ppm), referenced to TMS at 0.00 ppm or to solvents (CDCl3 at 7.26 ppm or DMSO-d6 at 2.48 ppm for 1H NMR and CDCl3 at 77.16 ppm or DMSO-d6 at 39.52 ppm for 13C NMR) as standard internal references.

The coupling constants (J) were measured in Hertz (Hz), and coupling patterns were designated as follows: s (simple), d (doublet), dd (double doublet), t (triplet), q (quartet), dq (double quartet), m (multiplet), and br s (broad singlet).

5 RESULTS AND DISCUSSION

5.1 STRUCTURAL AND MICROSTRUCTURAL CHARACTERIZATION

The aluminosilicate source materials, namely Metakaolin do Brasil (MK-B) and Metacaulim Imerys (MK-I), underwent XRD analysis, as depicted in Figure 11, with the results for all samples presented in Figure 12.

Figure 9 XRD of Metakaolin samples (MK-B and MK-I) highlighting the quartz and kaolinite areas.

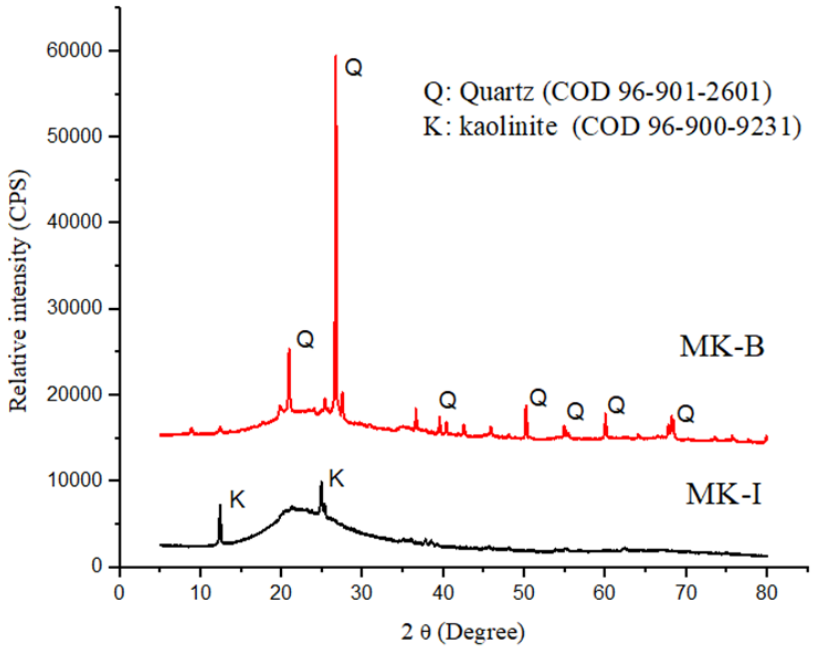

Source: author (2023).

The match peaks of the XRD data was performed by using the program and the graphical interface HighScore Plus®. All the samples exhibited peaks corresponding to quartz, which is present in the utilized metakaolin. The shift of the amorphous metakaolin peak (at 23° in 2θ) to 25 to 35° indicates the formation of geopolymers [186]. The crystalline phases identified in the samples include kaolinite-1 Md ($Al_2Si_2O_5(OH)_4$), Ref. Pattern 01-088-0893), sodium aluminum silicate ($Na_2Al_2Si_3O_{10}$, Ref. Pattern 00-046-0740), and a presence of quartz (SiO_2, Ref. Pattern 01-070-3755).

Figure 10 Presents the X-ray diffraction (XRD) analysis of the samples generated in this study. It illustrates the graphical representation of the obtained data (Q = quartz; M = mullite; C = copper; N = nickel; K = kaolinite; S = sodium carbonates, Z = zeolite).

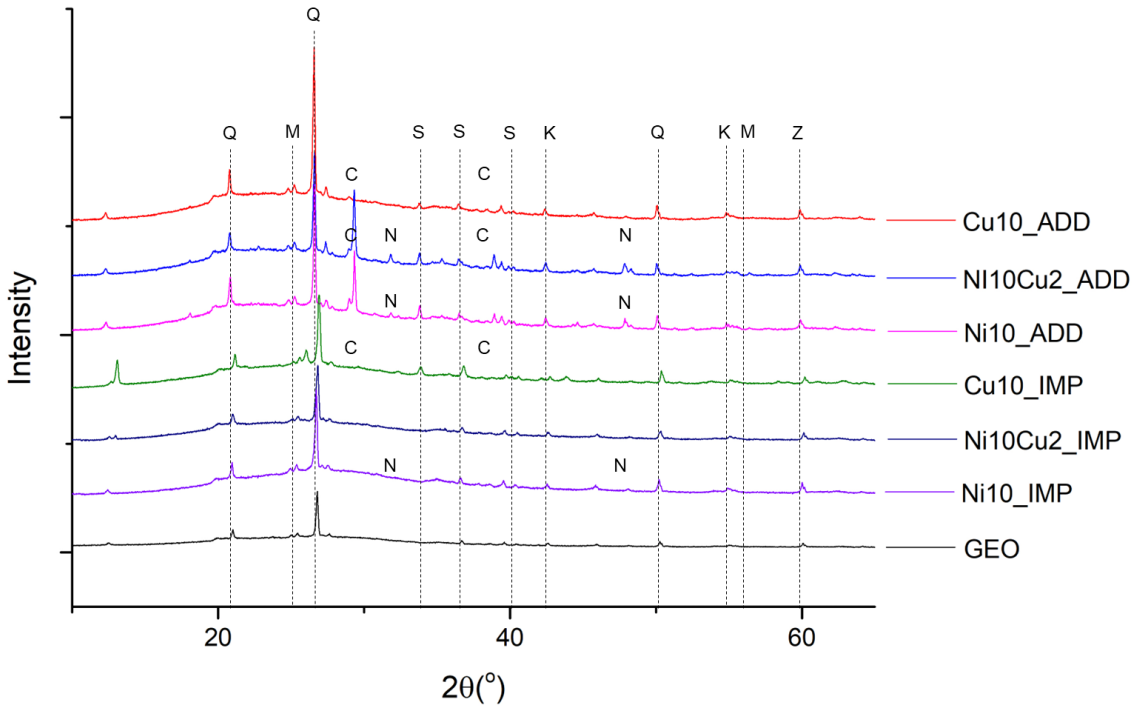

Source: author (2023).

The X-ray diffraction (XRD) patterns of geopolymers typically display humps around 29° 2θ, indicating the formation of an N-A-S-H type gel [230], [231] The peaks observed at approximately 32.1°, 37.9°and 40.2° in the patterns can be attributed to sodium carbonates (Na_2CO_3, Ref. Pattern 01-075-6816) [232]. These peaks may arise from carbonation that occurred during the sample preparation process.

The peak at 59.9° 2θ is present in all samples, this suggests the formation of new crystalline phases during the curing process. These crystals are likely to be associated with zeolites, which has been observed by other researchers in geopolymers as well[233], [234].

The methods used for sample preparation did not lead to any substantial alteration in the nature of the geopolymer present in the support material, as indicated by the position of the diffraction peaks.

The samples containing 10% copper nitrate, produced using both methods, and the bimetallic sample generated through the addition method exhibited discernible

CuO peaks (CuO Ref. Pattern 00-002-1067). Conversely, the sample crafted through both addition and impregnation methods, which incorporates nickel, showcased the formation of aluminum and nickel phases ($Al_{0.42}Ni_{0.58}$ Ref. Pattern 00-044-1267) alongside pure nickel (Ni Ref. Pattern 00-003-1043).

Furthermore, the presence of diffraction peaks at 2θ = 37.4° and 43.5° in the metallic samples by both methods and in the bimetallic sample preparate by the addition, indicates the existence of a crystalline phase of pure nickel (Ni Ref. Pattern 00-003-1043). The weak peaks observed at 2θ = 36.5° and 38.9°, can be attributed to the monoclinic phase of CuO (CuO Ref. Pattern 00-002-1067).

In the XRD patterns of the bimetallic sample prepared using the impregnation method, no peaks were observed that could be attributed to the presence of metal or metal oxides. There are possible reasons for this observation, including the non-crystalline nature of the particles, uniform dispersion of the particles, preferential orientation of particles, and very small particle sizes, or non-impregnation of the material.

Peaks originating from mixed phases such as aluminates, from nickel, were detected in the samples. This finding is significant as it suggests that there were reactions between the geopolymer and the oxides during the synthesis, indicating that the presence of the nitrate could compromise the support.

The lack of observable peaks and the small intensity related to metal or metal oxides in the XRD patterns could be attributed to the sensitivity limitations of the equipment used. The methods employed for catalyst development introduce only a minute quantity of nickel and copper into the samples, theoretically amounting to 2.14 w.t% in samples containing 10 w.t% of nickel nitrate, 2.65 w.t% in the samples with 10w.t% of copper nitrate and 0.55 w.t% of copper in the bimetallic samples. This low concentration of the metals may fall below the detection threshold of the XRD equipment, thereby explaining the absence of corresponding peaks.

Table 5 Theoretical and Experimental weight of the metals in the catalysts.

Sample	Theoretical weight (w.t%)		Experimental weight XRD (w.t%)		Experimental weight XRF (w.t%)	
	Ni	Cu	Ni	Cu	NiO	CuO
Ni10_IMP	2.14	-	1.09	-	3.27	0.04
Ni10Cu2_IMP	2.14	0.55	-	-	3.02	1.60
Cu10_IMP	-	2.76	-	0.79	0.02	5.58
Ni10_ADD	2.14	-	1.46	-	2.97	0.02
Ni10Cu2_ADD	2.14	0.55	1.62	0.49	3.12	0.93
Cu10_ADD	-	2.76	-	1.56	0.01	3.64

Source: author (2023).

The samples prepared using the impregnation method exhibited the most noticeable discrepancies in XRD analysis, indicating clear differences among the samples. One potential error lies in the control of impregnation parameters, including the concentration and volume of the impregnation solution, as well as the impregnation time and temperature. Inaccurate measurements or deviations from the intended parameters can result in uneven distribution of the impregnated species or inadequate coverage on the substrate, leading to inconsistent or suboptimal performance.

Another significant source of error is related to the interaction between the substrate and the impregnation solution. Surface properties, such as roughness, porosity, and chemical composition, can influence the adsorption and diffusion behavior of the impregnating species. Inadequate surface preparation or incomplete wetting of the substrate can cause incomplete impregnation, resulting in reduced effectiveness or loss of desired functionalities.

Quantifying the active phase in geopolymers via X-ray diffraction (XRD) analysis may have been challenging, leading to some disagreements between theory and experimental results, as indicated in Table 5, although the results are plausible given the method used to produce the samples.

The quantification of geopolymer presents complexities compared to the quantification of other materials due to the unique characteristics mainly from the geopolymer ceramic matrix. These challenges arise from the following factors [235], [236], [237]:

i) Amorphous content: Geopolymers often contain amorphous phases, which do not produce distinct diffraction peaks in XRD patterns. As a result, the quantification of crystalline phases may be affected, leading to underestimation or overestimation of their relative abundance.

ii) Preferred orientation: Geopolymeric samples can exhibit preferred orientation, where the crystal planes of certain phases align preferentially in a particular direction. This can lead to an overestimation of the abundance of these phases in the XRD analysis.

iii) Peak overlapping: In complex geopolymeric systems, different phases may have similar diffraction patterns, resulting in overlapping peaks. This can make it challenging to accurately separate and quantify individual phases.

iv) Calibration standards: The use of appropriate calibration standards is crucial for accurate quantification. However, finding suitable standards that closely match the composition and crystal structure of the geopolymeric samples can be challenging, leading to potential errors in the quantification process.

To minimize these errors, it is important to carefully consider the limitations and assumptions associated with XRD analysis of geopolymeric samples. For this purpose, a supplementary X-ray Fluorescence (XRF) analysis was conducted to showcase and quantify the concentration of each metal present in the produced samples.

Moreover, in comparison to commonly employed methods like Energy Dispersive X-ray Spectroscopy (EDX) and X-ray Photoelectron Spectroscopy (XPS), X-ray Fluorescence (XRF), as show in Table 5, offers the advantage of providing information about the elemental content of a sample from a larger volume. The fundamental principle of the XRF analytical method is rooted in the interaction of a material with high-energy X-ray radiation, resulting in X-ray absorption. This absorption/excitation phenomenon and subsequent relaxation processes induce the emission of fluorescence photons by atoms, each possessing specific energy characteristics [238].

Thought it's crucial to note that the intensity of the analytical lines in X-ray Fluorescence (XRF) is influenced not solely by the elemental content but also by factors such as particle size, chemical composition, and various experimental parameters specific to the sample.

The observation of metal concentrations in the samples exceeding the expected percentages may be attributed to various factors, several studies have demonstrated that the intensity from a sample exhibited an increase as the particle

size decreased [239], [240], [241], [242]. This phenomenon arises due to the diminution in size and the decrease in the extent of voids within the sample. Following the same rationale, reducing the particle size of one of two sample components results in a higher intensity relative to the component with a fixed particle size. Additionally, if the particle size of both components is reduced, their respective intensities may either increase or decrease based on their relative absorption coefficients. Notably, it was observed that the intensities stabilize when the particle size becomes sufficiently small [241].

The most direct approach to mitigate the impact of particle size effects on the emitted spectrum intensity and enhance the accuracy of concentration measurements is to construct calibration curves using standard specimens of known composition [241].

The variance in attenuation lengths of nickel (Ni) and copper (Cu) fluorescence photons, coupled with the outlined morphology, could influence the volume ratio of Ni/Cu and result in a shift in the measured concentrations. Since the analysis was done using a powder and pieces of the catalysts, the surface and volumetric irregularities may elucidate the observed behavior in the analysis.

Indeed, the complexity of the sample, inherent to its natural composition, introduces an additional source of potential error in the analysis. The presence of diverse chemical elements, especially those with similar and low-energy photon emissions, such as in the case of copper and nickel, can contribute to these errors. The intricate nature of the material underscores the importance of considering and addressing the diverse elemental composition for accurate and reliable analytical results.

An additional potential source of error arises from the incomplete homogeneity of the samples, resulting in localized regions with a higher concentration of metal. This is particularly evident when examining the samples prepared using the impregnation method, as indicated in Table 5. The uneven distribution of metal within the samples can introduce variability in the analysis and should be considered when interpreting the results.

However, it is noteworthy that the analysis yielded satisfactory results, qualitatively affirming the presence of metals in the catalysts and providing a reasonable approximation to the theoretically expected outcomes. Therefore, a

calibration curve would be necessary to obtain a better response from the equipment and a more reliable analysis of the samples.

Complementary techniques such as scanning electron microscopy (SEM) can provide additional information to support the accurate chemical composition in geopolymeric systems.

One of the key advantages of chemical analysis using Scanning Electron Microscopy (SEM) is its ability to provide high-resolution imaging combined with elemental analysis. SEM allows for the visualization of sample surfaces at magnifications ranging, providing detailed morphological information. Simultaneously, the incorporation of energy-dispersive X-ray spectroscopy (EDS) within the SEM setup enables the identification of composition, elemental distribution and identify specific phases.

Microscopy images were acquired at different magnifications to examine the catalyst morphology and the interaction between active phase and the support. The primary objective was to identify the location of metals within the geopolymer mass after its incorporation, providing insights into its distribution and behavior.

Figure 11 Scanning Electron Microscope (SEM) Images of geopolymeric support samples (GEO) at various magnifications (x30, x300, and x1000).

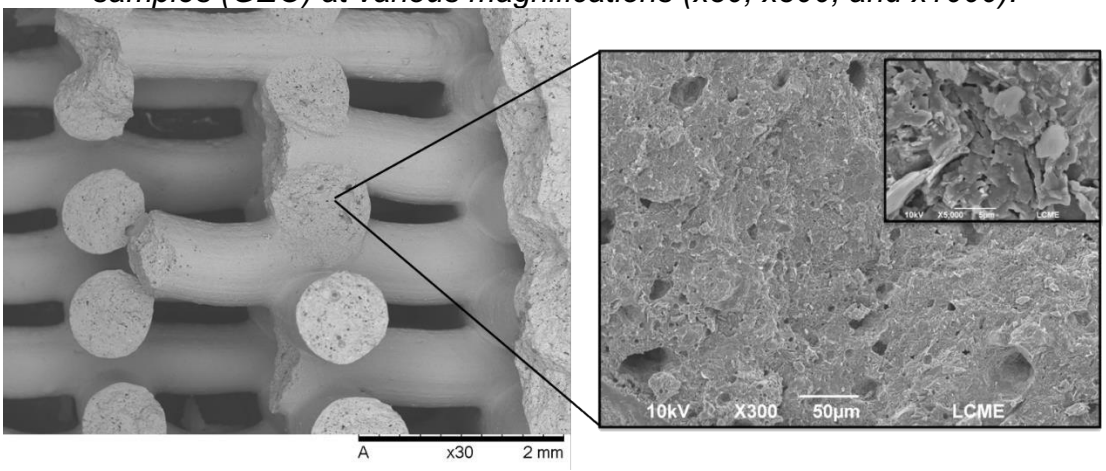

Source: author (2023).

From the SEM images, the metakaolin particles appeared as plates forming a layer-like structure as seen in Figure 13, considering the solid-liquid reaction system as a gel system with relatively low water content, it is reasonable to hypothesize that the solid raw material maintains its primary shape with minimal changes throughout the geopolymerization process.

The geopolymer exhibits a compact microstructure, which becomes evident when examining an image taken from a section of the sample that underwent pressure during the extrusion process. The application of pressure during extrusion can result in a rearrangement of particles and a reduction in pore size, leading to a denser microstructure.

Figure 13 illustrates that the geopolymer samples predominantly exhibit glassy microstructures, which align with their X-ray amorphous XRD patterns. The amorphous nature of the material is evident in the absence of distinct diffraction peaks in the XRD patterns, indicating a disordered atomic arrangement. This observation is in line with the glassy appearance observed in the microstructures of the geopolymer samples.

SEM images of geopolymer samples contain zeolites revealing the presence of distinct crystalline structures with spherical particles and size around 5 μm. The zeolites often appear as individual particles or aggregates dispersed within the geopolymer matrix, which can be attributed to the presence of various impurities in the raw material. These impurities promote rapid nucleation, resulting in limited crystal growth during geopolymerization [243].

For a more comprehensive chemical analysis and to compare the results obtained from the peaks observed in X-ray diffraction (XRD) analysis, an Energy Dispersive X-ray Spectroscopy (EDS) analysis was conducted. EDS is a technique that is coupled with a Scanning Electron Microscope (SEM), allowing for both quantitative and qualitative chemical characterization of the samples. By utilizing EDS, it becomes possible to obtain elemental composition information and further complement the findings from the XRD analysis.

Figure 12 Energy dispersion spectrum of the geopolymeric support without the presence of active phase.

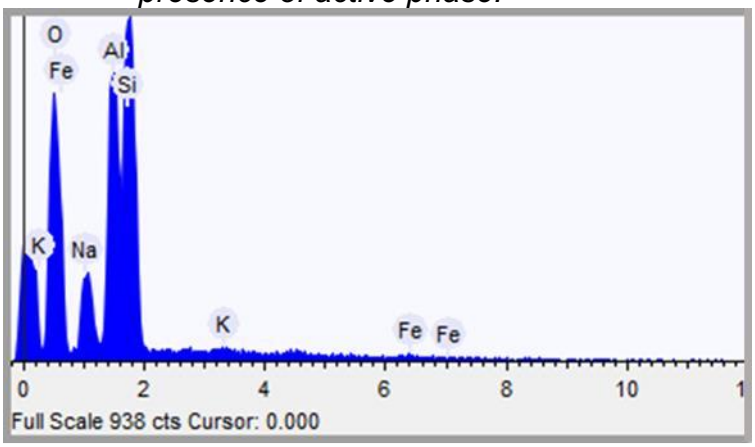

Source: author (2023).

The EDS analyses of the supports, as depicted in Figure 14 and Table 6, reveal a chemical composition that closely aligns with the findings reported in the X-ray fluorescence analysis (Table 3) of metakaolin and the other reagents added to the mixture for the preparation of the geopolymer.

Table 6 Theoretical and Experimental weight of the chemical elements present in the geopolymer sample.

Geopolymer sample (GEO)	Theoretical weight (w.t%)	Experimental weight (w.t%)
Oxygen (O)	58%	64.9%
Silicon (Si)	16%	16.8%
Aluminium (Al)	12%	12.0%
Sodium (Na)	7%	5.8%
Iron (Fe)	0.3%	0.3%
Potassium (K)	0.2%	0.2%
Others elementes	6.5%	-

Source: author (2023).

Some differences can be observed, particularly in the oxygen content of the sample, as geopolymer matrices typically contain various chemical elements predominantly in oxide forms. Due to the complex nature of the geopolymer composition, the EDS analysis may not have been able to identify all the chemical elements present. It's important to consider the inherent variability in geopolymeric materials, which can arise from variations in the raw materials used, the synthesis process, and the curing conditions. This variability can lead to differences in the chemical composition of different regions within the sample.

Additionally, the presence of impurities or contaminants in the geopolymer matrix can contribute to variations in the oxygen content. These impurities can arise from the raw materials or may be introduced during the synthesis or handling processes. Contaminants can impact the overall chemical composition, potentially resulting in differences in the oxygen levels between different regions of the sample.

Moreover, variations in sample preparation techniques can also influence the observed differences. Factors such as the homogeneity of mixing, curing conditions, and sample size can affect the distribution and density of the geopolymer matrix.

To analyze the interaction between the active phase and the support, higher magnification microscopies were employed to examine both the internal and external

parts of each sample. This approach aimed to identify the specific locations where the metals with catalytic capacity are situated. By utilizing higher magnifications, detailed observations of the sample structure and the distribution of catalytically active metals could be made, providing insights into the spatial relationship between the active phase and the support material.

Figure 15 illustrates the samples produced using the impregnation method, containing 10% nickel nitrate (Ni10_IMP), magnified up to 10,000x. The internal section of the sample, composed solely of geopolymers, exhibits a structure like that mentioned earlier in Figure 14. This higher magnification provides a clearer view of the pore sizes and shapes, which were not as evident before, revealing diameters of up to 10 μm. Notably, the geopolymeric matrix in the analyzed sample remains unaffected. Another significant observation is the lack of apparent pores on the external surface, suggesting that the impregnation method effectively infiltrated the sample, resulting in a more compact catalyst structure.

Figure 13 Images of the internal and external part of the catalyst produced by impregnation containing 10% nickel nitrate (Ni10_IMP) performed via SEM with 30x, 1,000x and 10,000x magnification.

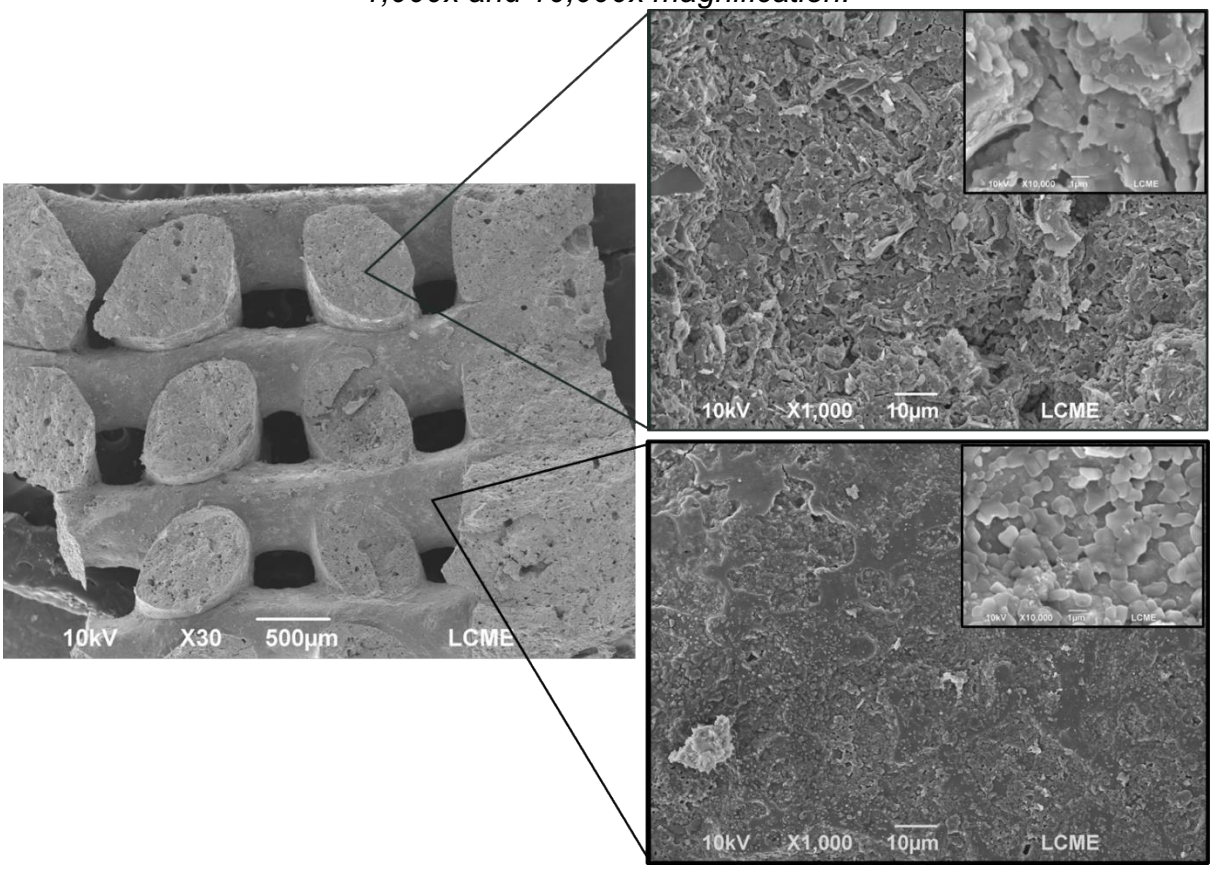

Source: author (2023).

Upon examining the external part of the sample at a magnification of 10,000x, it becomes apparent that the pores were not entirely obstructed by the impregnation process. However, there was a noticeable decrease in pore size, reducing to approximately 1 μm. Interestingly, the impregnated samples exhibit an increased quantity of pores compared to the non-impregnated ones. This observation suggests that the impregnation method has resulted in a greater surface area available for heterogeneous catalysis to take place. The smaller pore size and higher pore density in the impregnated samples contribute to enhanced catalytic activity, as they provide more sites for chemical reactions to occur.

The highly alkaline nature of the geopolymer matrix has a significant impact on the impregnation process. The water and nitrate solution used in the impregnation method typically have a high pH, as a result, a portion of the nitrate compounds undergoes chemical transformations, leading to the formation of smaller particles, primarily nickel oxide. This phenomenon has been demonstrated in the X-ray diffraction (XRD) analysis of the sample, confirming the conversion of nitrate compounds to nickel oxide within the geopolymer matrix.

The surface of the geopolymer particles exhibited the growth of rod-like composed of nickel oxide. These newly formed NiO displayed varying aggregation properties, ranging from individual, separated grains to notable radiated formations composed of several grains. The distinct morphologies observed highlight the potential for diverse surface structures and catalytic behavior in the supported geopolymer system.

In Figure 16, the sample containing 10% copper nitrate (Cu10_IMP), prepared using the impregnation method, is displayed. Like the previous sample prepared using the same method, there is no apparent impairment of the geopolymer matrix. However, upon closer examination at a magnification of 1,000x from the external surface, a reduction in pore size can be observed compared to Figure 10, which depicted the pure support material. The pores in Figure 14 exhibit a range of diameters, indicating the presence of varied pore sizes within the impregnated sample. This observation suggests that the impregnation process has influenced the pore structure of the geopolymer matrix, leading to a decrease in pore size.

A noteworthy observation in Figure 16 is the presence of spicule-like structures alongside the pores. These structures are also abundant in the images obtained from

the external part of the sample. It is important to note that these spicules are, in fact, copper [244]. Their formation can be attributed to the chemical reaction between the impregnated copper nitrate and the geopolymer matrix, as a result, lead to the formation of copper nanowires. They exhibit elongated crystalline structures and are dispersed throughout the sample[245], [246], [247].

Figure 14 Images of the internal and external part of the catalyst produced by impregnation containing 10% copper nitrate (Cu10_IMP) performed via SEM with 30x, 1,000x and 10,000x magnification.

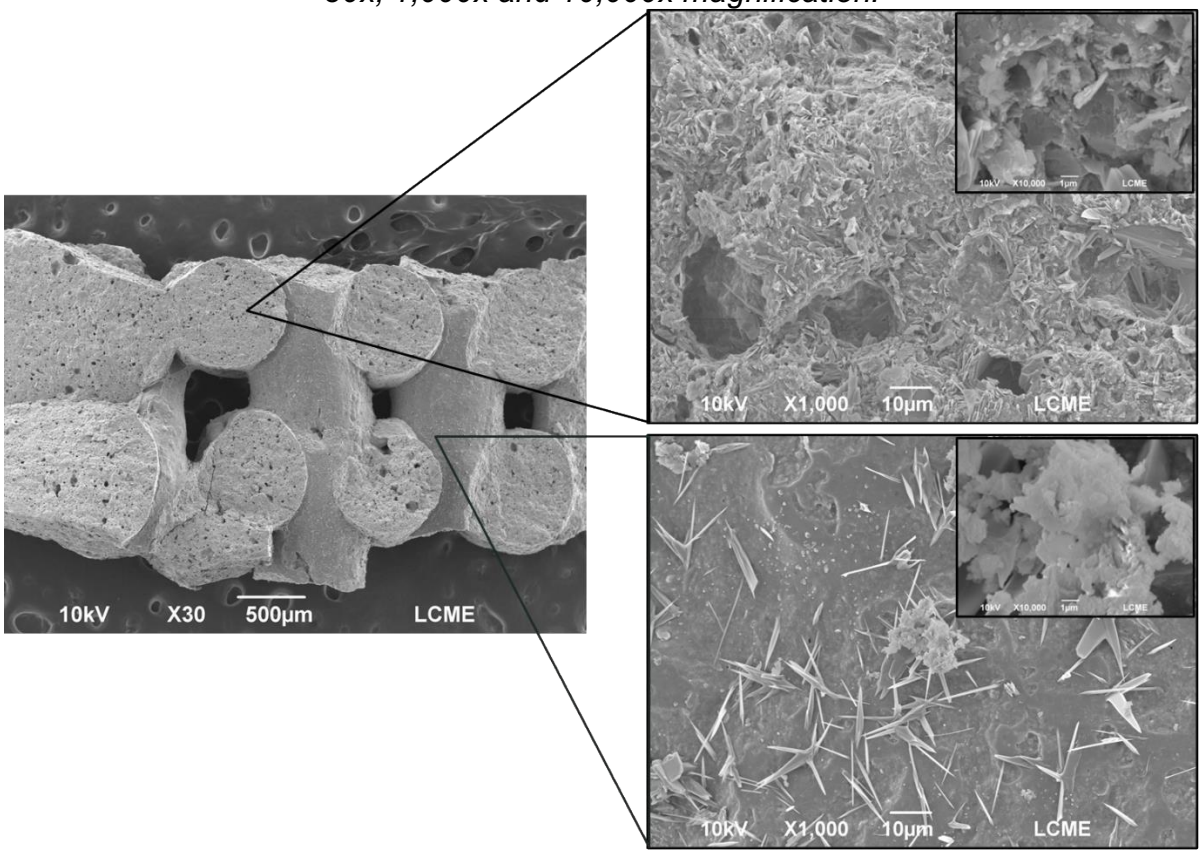

Source: author (2023).

In environments with high pH, such as in the synthesis of geopolymer materials, the formation of copper (Cu) nanowires can occur. This phenomenon is attributed to the unique chemical interactions and conditions present in alkaline solutions[246], [247] . The introduction of sodium hydroxide to a copper nitrate solution resulted in the formation of a precipitate with a light blue or blue color, identified as copper hydroxide, which follows the reaction below, Equation 1 and 2:

$$Cu(No_3)_2 + 2NaOH \rightarrow Cu(OH)_2 + 2\,NaNO_3 \quad (1)$$

$$Cu(OH)_2 \rightarrow CuO + H_2O \quad (2)$$

In high pH environments, copper ions (Cu^{2+}) tend to undergo reduction reactions due to the high concentration of hydroxide ions (OH^-) present. The reduction of Cu^{2+} ions lead to the deposition and growth of metallic copper, which can take on various forms depending on the specific conditions [246]. The growth of Cu nanowires occurs along specific crystallographic directions, resulting in elongated structures with nanoscale dimensions.

These formations exhibit high aspect ratios, large surface areas, and unique electronic and optical properties, making them attractive for various technological applications, including nanoelectronics, sensors, and catalysis. The coexistence of these spicule-like structures and the pores adds complexity to the microstructure of the impregnated geopolymer, potentially influencing its catalytic properties and surface characteristics.

Figure 15 Images of the internal and external part of the bimetallic catalyst produced by impregnation (Ni10Cu2_IMP) performed via SEM with 30x, 1,000x and 10,000x magnification.

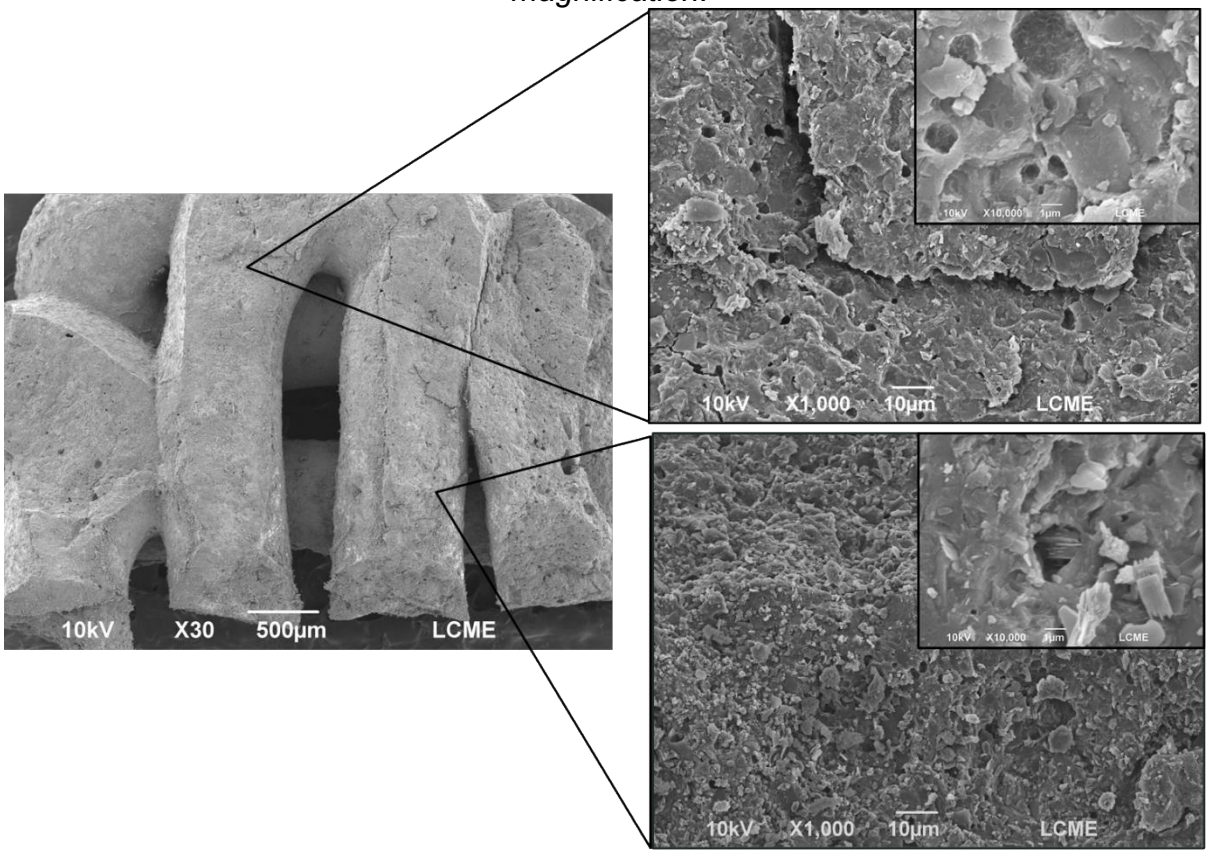

Source: author (2023).

In the bimetallic samples, as show in Figure 17, the formation of Cu nanowires is prominently observed near the pores. This can be attributed to the larger contact surface area available in those regions, leading to a higher local pH. The increased pH promotes the reduction of copper ions and facilitates the growth of Cu nanowires. As a result, the formation of Cu nanowires is enhanced in these specific areas where the contact between the impregnated copper species and the geopolymer matrix is more pronounced.

Figure 16 EDS analysis of the samples made by impregnation method.

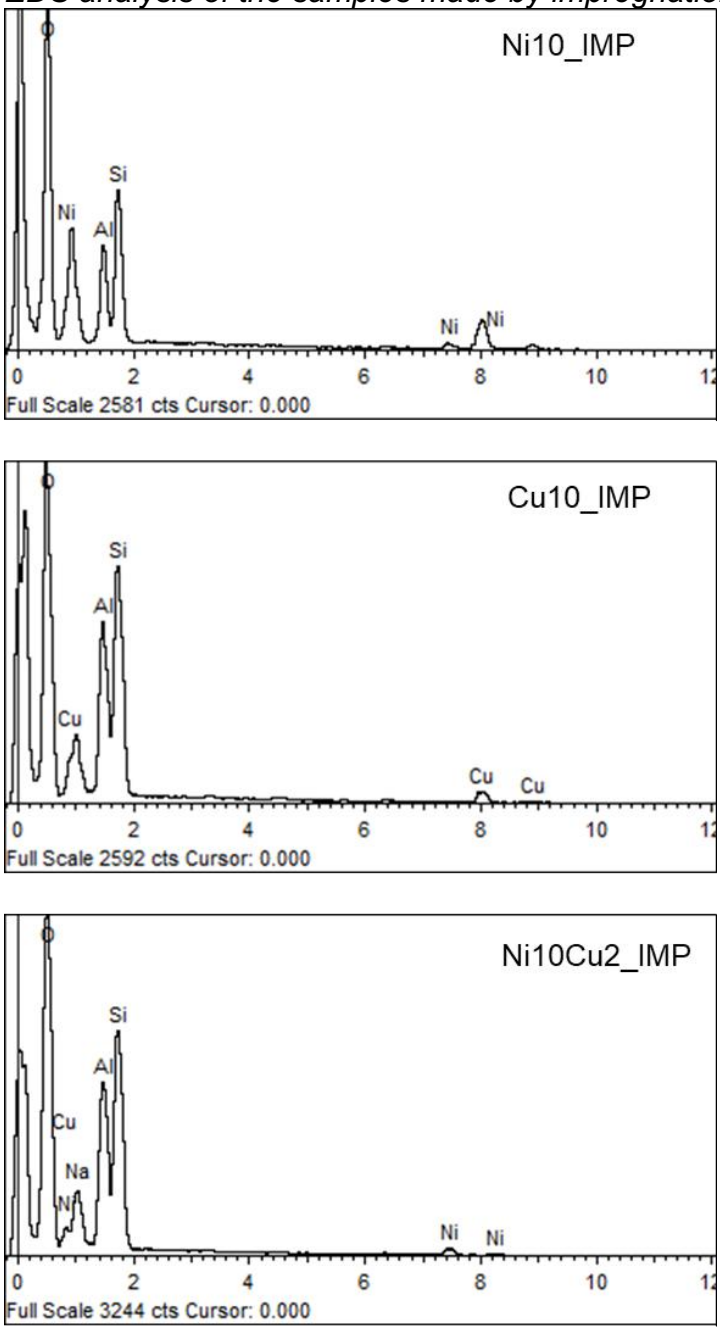

Source: author (2023).

To obtain a chemical analysis of the impregnated samples prepared using the method mentioned, Energy Dispersive X-ray Spectroscopy (EDS) was performed. The results of this analysis can be observed in Figure 16, confirming the presence of the active phase in each respective sample, supports the successful impregnation of the desired catalytic species in the samples and corroborates the results presented via XRD and XRF.

Figure 17 EDS analysis of the samples made by addition method.

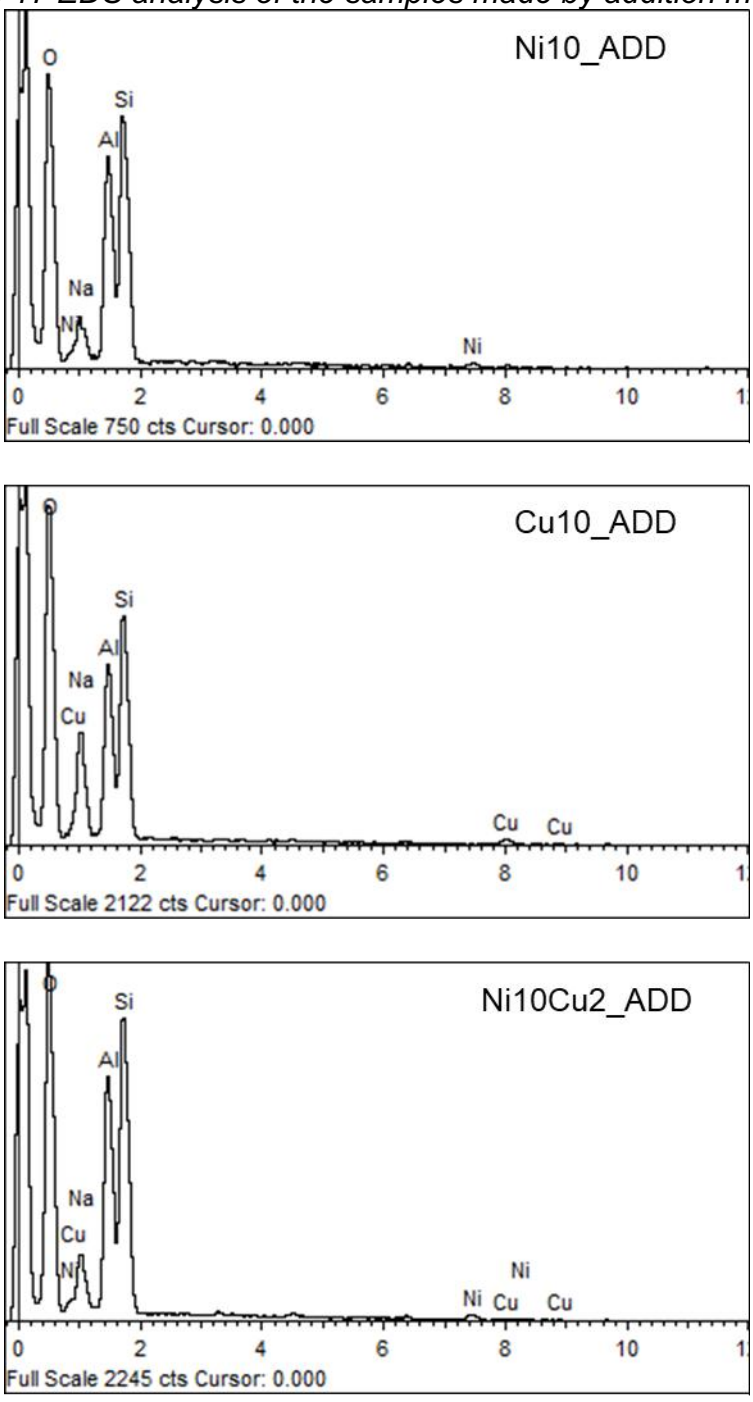

Source: author (2023).

EDS analyses were also conducted on the samples prepared using the addition method, as show in Figure 19. Consistent with the results obtained from X-ray diffraction (XRD) and X-ray fluorescent (XRF) analysis (as shown in Table 4), the presence of the active phase within the geopolymer matrix was confirmed. This alignment between the three analytical techniques further supports the identification and verification of the active phase in the samples.

In contrast to the sample consisting solely of geopolymer, it was not feasible to perform a quantitative analysis of the active phase using Energy Dispersive Spectroscopy (EDS). This analysis provides qualitative information about the elemental composition of a sample, but the quantification of specific phases can be challenging. The difficulty in conducting a quantitative analysis can be attributed to several factors [248], [249], [250]:

i) Elemental Overlap: In the presence of multiple elements, such as in the case of geopolymer and the active phase, there can be spectral overlap between the peaks of different elements.

ii) Matrix Effects: The composition of the geopolymer matrix can influence the X-ray emission and absorption processes during EDS analysis. The presence of other elements in the matrix can lead to spectral interference and affect the accuracy of quantitative analysis for the active phase.

iii) Elemental Concentration: If the concentration of the active phase is relatively low compared to the geopolymer matrix, it may be difficult to detect and accurately quantify the active phase using EDS.

iv) Sample Heterogeneity: If the active phase is not uniformly dispersed or if there are variations in its concentration throughout the sample, it can affect the reliability of the quantitative measurements.

The limitations in conducting quantitative analysis of the active phase via Energy Dispersive X-ray Spectroscopy (EDS), in this context, Scanning Electron Microscopy (SEM) analysis provides valuable insights into the microstructure, morphology, and elemental distribution also in the samples made by the addition method.

Figure 18 Images of the internal and external part of the catalyst produced by addition method, containing 10% nickel nitrate (Ni10_ADD) performed via SEM with 30x, 1,000x and 10,000x magnification.

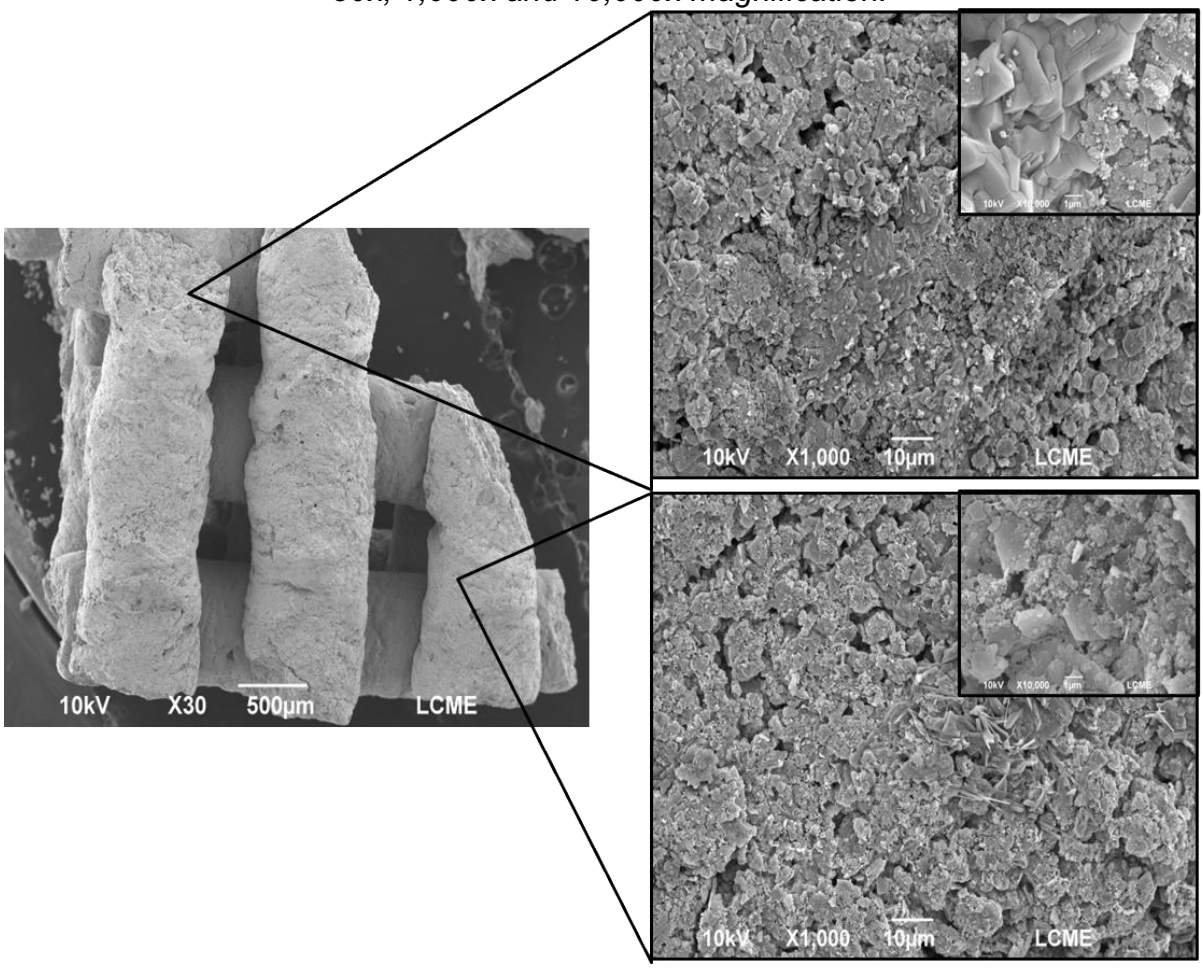

Source: author (2023).

Upon observing Figure 20, which displays SEM images of the sample containing 10% nickel nitrate prepared using the addition method, noticeable differences become apparent when compared to the corresponding sample prepared via the impregnation method. The first notable difference, even at lower magnification, is a sense of fragility and a less robust appearance in the sample made by the addition method. This fragility could be attributed to variations in the distribution and bonding of the active phase within the geopolymer matrix. The different preparation methods can lead to variations in the microstructure and morphology of the samples, ultimately affecting their mechanical properties and overall stability.

When examining the external part of the sample, it becomes evident that the structure is not as compact as the one depicted in Figure 15, which also contains 10% nickel nitrate but was produced using the impregnation method. The observed

difference in compactness suggests that the addition method may result in a less dense arrangement of the geopolymeric catalysts. This could be attributed to the incorporation of the nitrate in the geopolymer matrix. Nitrate, in its hexahydrated form, can interfere with the geopolymerization process. The presence of excess water molecules associated with the nitrate ions can disrupt the formation of strong chemical bonds within the geopolymer matrix.

To delve deeper into the properties of the samples, BET tests were conducted. The findings from these tests will be expounded upon in the following section, furnishing crucial insights into the specific surface area and porosity of the catalysts. This analysis will contribute to a comprehensive understanding of the structural characteristics and potential applications of the materials under investigation.

Similar to the sample produced by the impregnation method, the catalyst prepared using the addition method also exhibits small portions of nickel oxide in the form of rod-like structures. The formation of such structures in the interior of the catalysts can enhance the reactivity and provide active sites for chemical reactions, since these are present both in the internal and external part of the sample.

In the sample containing 10% copper nitrate prepared using the addition method (Figure 21), the nanowires that were observed in the samples made by the impregnation method are not visible. This indicates that the formation of nanowires did not occur or that the concentration of copper nitrate used was not sufficient to produce them with this methodology. It is possible that the copper ions from the copper nitrate were incorporated into the catalyst matrix in a different form or morphology, such as nanoparticles or dispersed species.

Figure 19 Images of the internal and external part of the catalyst produced by addition method, containing 10% copper nitrate (Cu10_ADD) performed via SEM with 30x, 1,000x and 10,000x magnification.

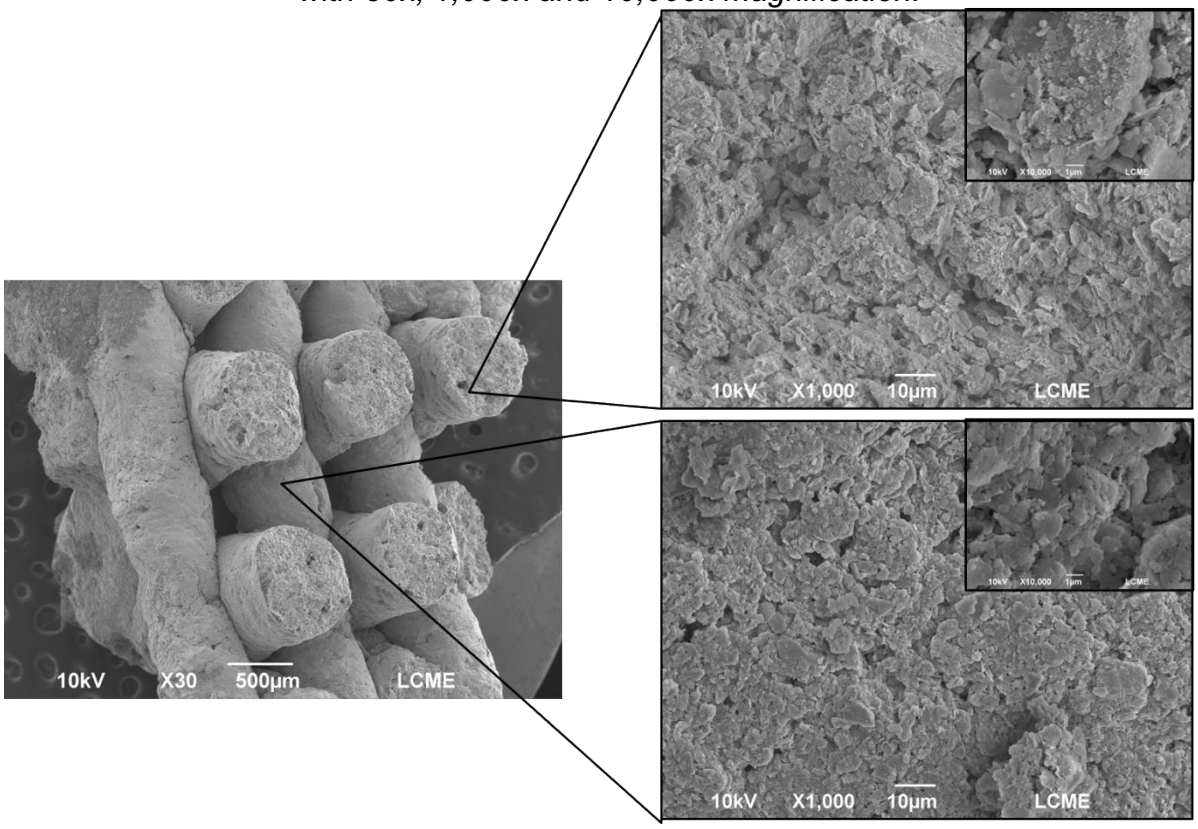

Source: author (2023).

The catalyst exhibits a certain degree of fragility along with the presence of grooves and micro cracks in its structure. These features indicate that the catalyst may possess a porous and interconnected network. Additionally, in the images, the characteristic presence of geopolymerization can be observed.

In the bimetallic sample, shows as Figure 21, prepared using the addition method, a higher level of compaction is evident when compared to other samples produced using the same method. Moreover, the overall structure of the bimetallic sample appears like the sample without the active phase, suggesting that satisfactory geopolymerization has occurred.

Figure 20 Images of the internal and external part of the bimetallic catalyst produced by addition method, containing 10% nickel nitrate and 2% of copper nitrate (Ni10Cu2_ADD) performed via SEM with 30x, 1,000x and 10,000x magnification.

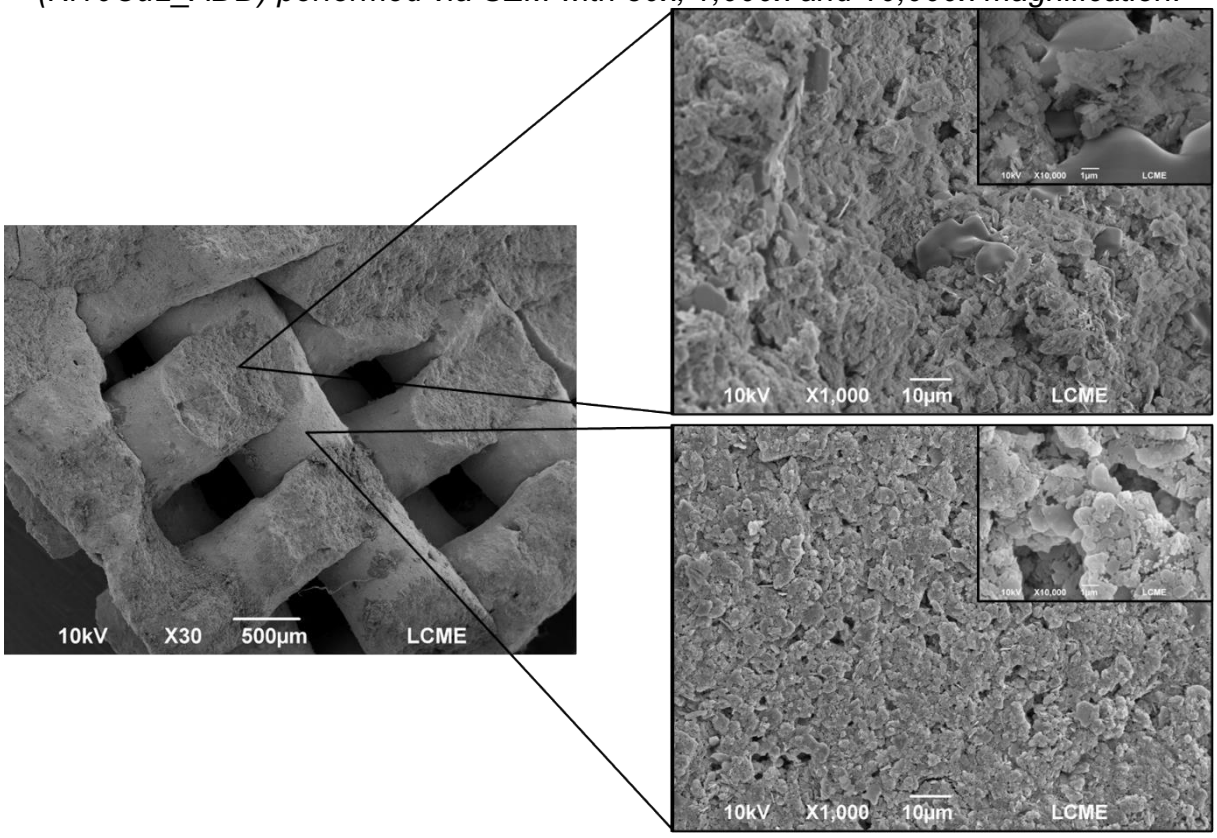

Source: author (2023).

Structures similar to those depicted in Figure 16 can also be observed in the bimetallic sample, particularly the presence of copper spicules. These copper spicules are especially noticeable in proximity to the pores where there is a localized increase in pH. However, it should be noted that these spicules are not as prominent as in the impregnated sample, but they can still be observed in smaller quantities. Additionally, in the sample, nickel rods are predominantly seen on the surface of the material, particularly in the vicinity of the pores and copper spicules.

The presence of copper spicules and nickel rods suggests the successful incorporation of these metallic species into the geopolymer matrix. The observed location of these structures in relation to the pores indicates a potential correlation between the catalyst morphology, pore structure, and the spatial distribution of active species.

The intrinsic porosity is visibly apparent in SEM images of all the samples. As a means of assessing the surface characteristics of the catalysts, BET analyses were conducted on both the powder and portions of the samples, as show in Table 7.

Table 7 Specific surface area and total porosity of the samples.

Sample	Specific surface area (m^2/g)	Total porosity (%)
GEO	29.38	67.21±0.02
Ni10_IMP	36.99	75.48±0.04
Ni10Cu2_IMP	37.70	77.00±0.03
Cu10_IMP	45.98	77.45±0.02
Ni10_ADD	22.39	51.32±0.03
Ni10Cu2_ADD	15.62	35.76±0.02
Cu10_ADD	62.44	78±0.9

Source: author (2023).

The BET theory stands as a pivotal analytical instrument for elucidating the adsorption of gas molecules onto a solid surface, playing a crucial role in measuring the specific surface area of materials. Commonly termed physisorption or adsorption, BET employs an adsorbate, typically Nitrogen, for its assessments. This method finds application in determining the surface area of geopolymers, a factor closely tied to the formation N-A-S-H type gel. An elevated BET surface area signifies an increased this formation within the matrix, establishing a correlation with porosity and exerting an impact on the material's properties.

The rise in specific surface area observed in samples produced through the impregnation method may be attributed to the formation of metal ions (Ni^{2+} and Cu^{2+}). Interestingly, these ions not only failed to seal the active surface of the initial adsorption material but also facilitated the creation of additional adsorption active centers, resulting in the development of new open pores.

Table 7 reveals that samples with enhanced specific surface areas are notably those incorporating copper. In the samples featuring copper through the impregnation method, nanometer-sized spicules form, as evidenced in Figure 15. Another factor contributing to this significant augmentation, in contrast to the pure geopolymer sample, suggests the existence of numerous active adsorption sites of copper. Consequently, it is plausible to speculate that the geopolymer in this study, containing Cu, has the potential to increase the BET surface area.

Even though the samples produced through the addition method, which include nickel, exhibit a more fragile structure, as evidenced in figures 19 and 20, a notable observation emerges when the magnification is increased by a factor of x30. Under these conditions, the samples display a reduction in specific surface area. This observation serves to demonstrate that, the presence of nickel, especially at higher

concentrations, could lead to the blocking or coverage of active adsorption sites on the material's surface and a decrease the porosity. This impediment may restrict the accessibility of gas molecules, used in BET analysis, to the surface, consequently resulting in a decrease in the measured specific surface area. Furthermore, the introduction of nickel particles may facilitate agglomeration, leading to the formation of clusters or larger structures on the material surface. This clustering phenomenon could diminish the effective surface area available for gas adsorption, contributing to the observed decline.

5.2 KINETIC STUDIES

Temperature-Programmed Reduction (TPR) analysis is a powerful technique used to investigate the reducibility and catalytic properties of metallic and bimetallic catalysts. By subjecting the catalysts to a controlled heating and reactive gas environment, TPR analysis allows for the identification of temperature regions associated with the reduction of metallic species and provides quantitative data on their reducibility. This analysis plays a crucial role in understanding the activation and performance of geopolymeric metallic and bimetallic catalysts, contributing to the development of efficient and sustainable catalytic systems.

The TPR profiles, as illustrated in Figure 21, demonstrate distinct reduction peaks for the samples prepared using the impregnation method. Specifically, in the sample impregnated with 10% copper nitrate (Cu10_IMP), two peaks are observed prior to reaching 300°C. The first peak occurs around 210°C, followed by a second peak at approximately 270°C. These findings indicate the presence of different forms of copper oxide on the catalyst surface. It is noteworthy that the reduction maximum of the Cu/GEO system is shifted to lower temperatures compared to pure CuO, suggesting a strong interaction between the copper oxide species and the geopolymeric support [97], [251].

The first two centered peaks in the TPR profile correspond to the reduction of bulk CuO species with varying degrees of interaction with the geopolymer support. The third peak indicates the reduction of bulk crystalline copper oxide that exhibits moderate interactions with the geopolymer support [252]. The high peak intensity observed in the TPR profile can be attributed to significant interactions between CuO

and the geopolymer matrix, which aligns with the SEM analysis in Figure 15, where copper dispersion within the matrix is observed.

Figure 21 TPR of catalysts with impregnated method.

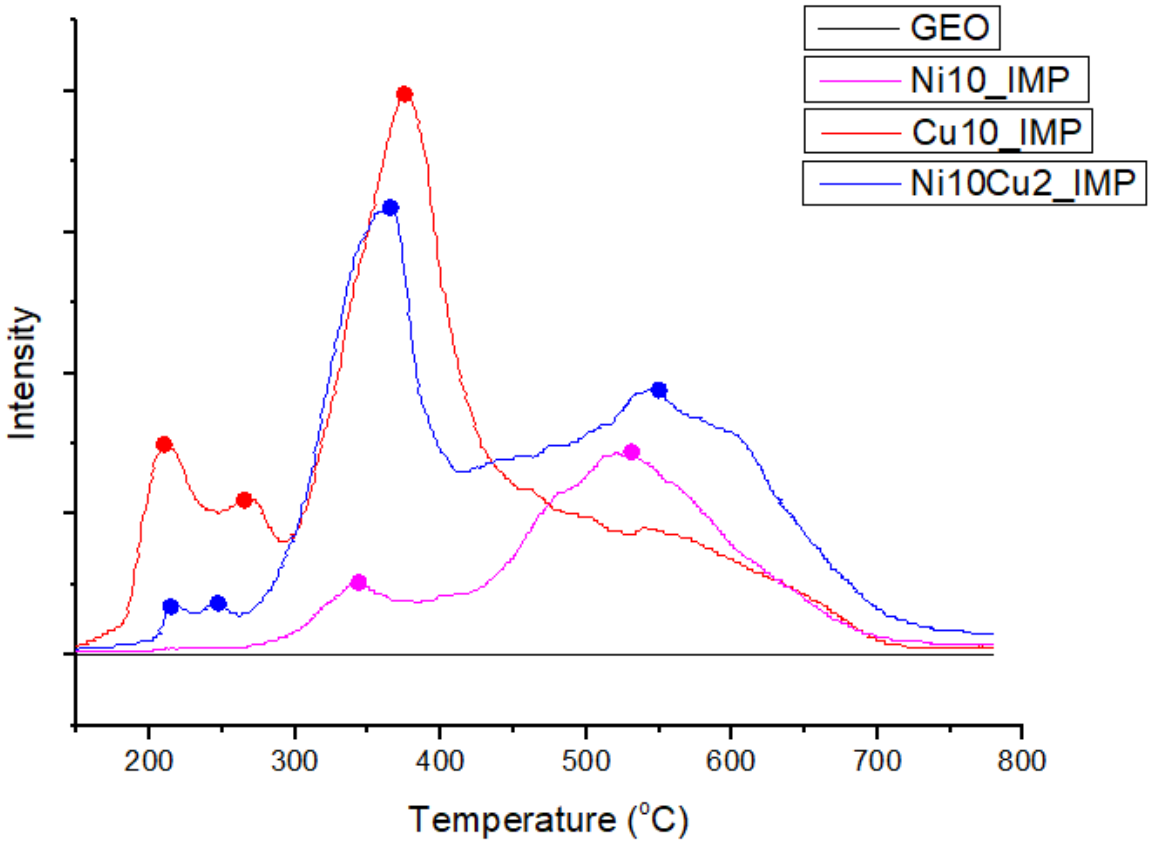

Source: author (2023).

The TPR profile of the bimetallic sample (Ni10Cu2_IMP) exhibits behavior similar to the sample containing only copper, particularly in terms of lower temperatures and a distinct peak observed at approximately 380°C corresponding to the reduction of copper oxide[97]. This sharp peak at 380°C is characteristic of the reduction profile of pure CuO, the presence of this peak suggests the presence of bulk copper oxide within the bimetallic catalyst.

The observed similarity in the reduction behavior between the bimetallic sample and the sample with only copper implies that the copper component in the bimetallic system retains its characteristic reduction properties. These findings indicate that the bimetallic catalyst retains the distinct catalytic behavior associated with the

reduction of copper oxide, while also potentially exhibiting unique catalytic properties arising from the presence of additional active phases.

The samples containing copper display higher peak intensities compared to the pure nickel sample. This disparity in peak intensity suggests a higher concentration or greater dispersion of copper species in the geopolymeric matrix. The enhanced intensity of the peaks associated with copper can be attributed to several factors, including the affinity of copper towards the geopolymeric support, its interaction with the matrix, and the potential formation of active sites that contribute to catalytic activity.

In contrast, the pure nickel sample exhibits lower peak intensities, indicating a lower concentration or less effective dispersion of nickel species within the geopolymer. This discrepancy underscores the different behaviors and catalytic properties exhibited by the copper and nickel components within the geopolymeric catalyst.

According to reports, the reduction temperature of pure NiO typically falls within the range of 360–400 °C [253]. This temperature range represents the thermal decomposition and reduction of nickel oxide to metallic nickel. The specific reduction temperature can vary depending on factors such as the particle size, morphology, and crystalline structure of the NiO particles, as well as the experimental conditions of the analysis. However, it is important to note that the reduction temperature of NiO can be influenced by the presence of other components or interactions with the geopolymeric matrix., such as the presence of metallic nickel and nickel aluminate, already mentioned in XRD analyzes.

The presence of peaks at 596°C in the sample containing only nickel and at 620°C in the bimetallic sample can be indicative of the formation of undesired phases resulting from the interaction of nickel with the support at high temperatures. These peaks can be attributed to the transfer of electrons between the metal and the support, leading to the formation of other compounds or complexes [254]. This electron transfer process suggests the occurrence of reactions or transformations that lead to the generation of new phases, which may not be desirable for the intended catalytic application.

In the analysis of the pure geopolymer (GEO), shows in Figure 22 and 23, no signals or indications of catalytic activity were observed. This is consistent with the fact that the geopolymer matrix, being a support material, does not possess intrinsic catalytic properties.

Figure 22 TPR of catalysts with addition method.

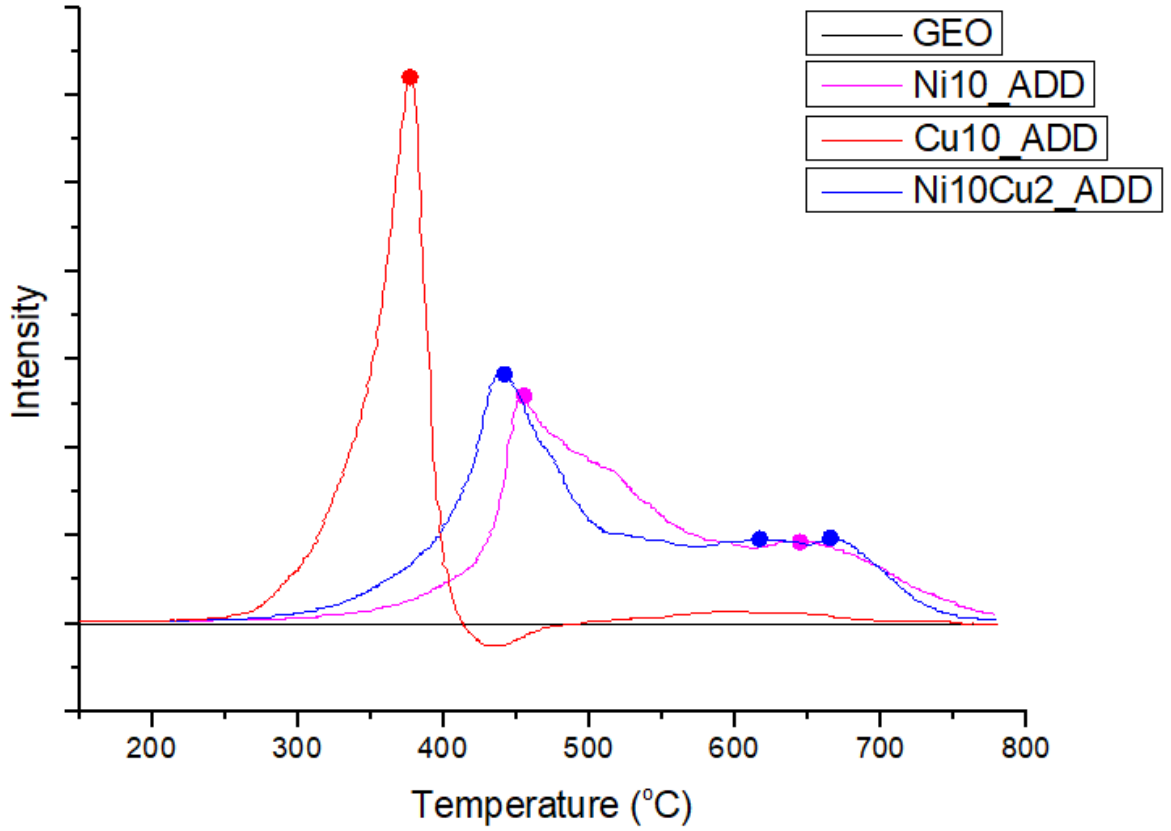

Source: author (2023).

The TPR profiles of the samples obtained by the addition method exhibit significant differences, particularly in the peaks below 350°C, when compared to the samples obtained by the impregnation method. These differences can be attributed to variations in the preparation technique and the distribution of active metal species within the geopolymeric matrix.

In the addition method, where the metal precursors are mixed with the geopolymer precursor during synthesis, the intimate contact between the metal species and the geopolymer matrix leads to a stronger interaction. This can result in distinct reduction behavior, with higher temperature peaks indicating a strongest interaction between the metal species and the support; and the formation of complexes with the geopolymer matrix. The presence of less quantity peaks suggests the formation of specific intermediates or interactions between the metal species and the geopolymer matrix during the reduction process.

The samples containing nickel in both the addition and impregnation methods exhibited similar behavior, particularly above 650°C, in the TPR profiles. This similarity suggests that the reduction of nickel species to the metallic form is predominantly governed by the inherent properties of nickel and its interaction with the geopolymer matrix, rather than being significantly influenced by the specific preparation method.

The impregnation method involves the post-synthesis impregnation of the geopolymer matrix with metal precursors. This method may result in a less uniform distribution of metal species within the geopolymeric matrix, leading to different reduction behaviors. Comparing the TPR behavior of the nickel-based geopolymer support with supports based on other porous materials, it is observed that the geopolymer exhibits better reducibility of the nickel species [179], [181].

The interaction between the geopolymer and nickel can be attributed to several factors. Firstly, the geopolymer matrix can act as a stabilizing agent, preventing the agglomeration or sintering of nickel species, thereby promoting their uniform distribution and accessibility during the reduction process. Secondly, the geopolymer may offer active sites or functional groups that can interact with the nickel species, leading to strong metal-support interactions and facilitating the reduction process. Additionally, the porous nature of the geopolymer allows for efficient diffusion of hydrogen gas, ensuring effective contact with the nickel species for reduction.

Overall, the distinct TPR profiles between the samples obtained by the addition and impregnation methods reflect the influence of the preparation technique on the reduction behavior and the resulting catalytic properties of the geopolymeric metallic catalysts.

5.2.1 Organic Reactions

Modern organic synthesis is built upon the conceptualization of chemical processes that prioritize efficiency, selectivity, and reliability, while concurrently adhering to environmental sustainability. For synthetic methodologies to be deemed acceptable from both environmental and economic standpoints, they should ideally eliminate or significantly minimize the utilization and production of hazardous substances. This paradigm shift enables the execution of setup and work-up steps under operationally straightforward conditions [255], [256], [257].

This section will present the outcomes of various tested organic reactions, highlighting the utilization of non-aggressive reagents in comparison to those conventionally employed, using the catalysts produced.

5.2.1.1 Geopolymers for the Knoevenagel condensation

Ethyl α-cyanocinnamates represent a significant class of organic compounds with diverse applications. For example, ethyl α-cyano-m-nitrocinnamate finds utility in photosensitive compositions and serves as an intermediate in the synthesis of plant growth regulators. Ethyl α-cyanocinnamates featuring alkoxy or hydroxyl substituents in the arenes are employed in ultraviolet filters for safeguarding light-sensitive foods, wood products, paper, dyes, fibers, and plastics [258].

A simple solvent organic synthesis has garnered significant attention in response to global concerns regarding chemical waste and the sustainable use of resources, aligning with the principles of green chemistry. Considering these, a condensation reaction between 3-Methylbenzaldehyde and Ethyl cyanoacetate was undertaken for the synthesis of ethyl-α-cyanocinnamate. This process was facilitated by a reusable geopolymer catalyst under ethanol as the solvent, emphasizing an environmentally conscious and efficient approach to chemical synthesis.

Figure 23 Knoevenagel condensation of 3-Methylbenzaldehyde and Ethyl cyanoacetate.

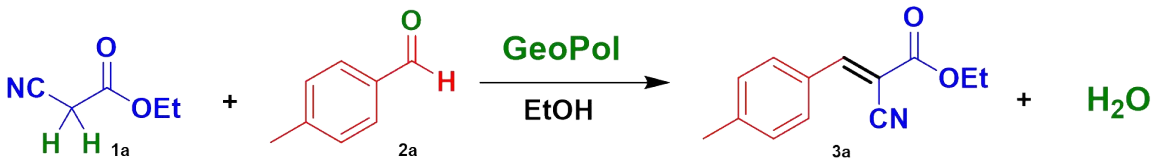

Source: author (2023).

For the Knoevenagel reaction tests, experiments were conducted with varying proportions of Ethyl cyanoacetate (1a) and 3-Methylbenzaldehyde (2a), adjusting reaction times and solvents, as detailed in Table 8. Additionally, a blind test was implemented without the catalyst, to discern whether the reaction would proceed in the absence of the catalyst.

Table 8 Parameters used for the Knoevenagel reaction.

Entrance	1a:2a	GEO (mg/mmol)	GEO (mg)	Solvent (mL/mmol)	Time (h)	Yeld (%)	Recovered (mg)
1	1:1	0	0	EtOH 3 mL	24	<5	0
2	1:1.25	590	590	EtOH 3 mL	24	98	523
3	1:1	200	220	EtOH 3 mL	24	80	195
4	1:1	100	112	EtOH 3 mL	24	90	96
5	1:1	100	139	EtOH 3 mL	24	72	129
6	1:1	100	103	EtOH 3 mL	8	75	89
7	1:1	100	129	EtOH 3 mL	24	70	98
8	1:1	200	195	EtOH 3 mL	24	80	186
9	1:1	100	108	H_2O 3 mL	24	70	51
10	1:1	100	143	EtOH/H2O (1/1) 3 mL	24	56	75

Source: author (2023).

Input reaction 5 was conducted without magnetic stirring, resulting in a reduced yield compared to input reaction 4, which utilized a similar mass of catalyst. The catalyst employed in this reaction was subsequently reused in input reaction 7, indicating that despite the reutilization, the reaction maintained a satisfactory yield. In input reaction 8, the catalyst from reaction 3 was reused, and it is evident that the yield was sustained with minimal loss in catalyst mass. This data holds paramount significance for the research, underscoring the crucial aspects of catalyst integrity and reusability.

Notably, input reaction 6 was carried out within a distinct time frame (only 8 hours) compared to the others, demonstrating that a shorter reaction time resulted in a decrease in yield, although it remained at a high level. This information is pertinent, emphasizing that while reaction duration can impact yield, satisfactory results can still be achieved within a shorter timeframe.

As evident from the results presented in Table 8, reactions employing ethanol as the solvent exhibited higher yields in comparison to those using other solvents (Entries 9 and 10). Notably, the reaction conducted without the utilization of the catalyst yielded less than 5%, signifying either an absence of the reaction or a prolonged reaction time in the absence of geopolymer catalysts. When assessing the weight of

GEO added to the reaction, yields were notably higher with quantities exceeding 200 mg/mmol, except in the case of Entry 4, which achieved a yield of 90%.

The optimization of parameters has not been completed, and once the conditions are optimized, they will be tested on various substrates to assess the methodology's scope.

5.2.1.2 Geopolymers for diazo transfer reaction

One extensively explored method for producing α-diazo carbonyl compounds involves the base-catalyzed diazo transfer reaction to 1,3-dicarbonyl compounds, utilizing sulfonyl azides as diazo transfer reagents [259], [260]. Despite its broad applicability, the selection of an appropriate basic catalyst requires careful consideration due to potential synthetic disadvantages. Drawbacks include the utilization of significant quantities of base and the necessity for intricate aqueous work-up procedures (aimed at removing water-soluble bases from the crude diazo product), often coupled with chromatography stages, resulting in the generation of substantial amounts of waste [261].

Given the contemporary environmental concerns, it becomes imperative to access α-diazo carbonyl compounds through operationally straightforward synthetic protocols. These methods should not only be efficient, selective, and reliable but also environmentally, economically feasible.

In this reaction, pure geopolymers were employed, and 4-Acetamidobenzenesulfonyl azide ($ABSN_3$) was selected as the diazo transfer reagent. ABSN3 was chosen for its moderate reactivity and enhanced safety profile compared to other sulfonyl azides. The formation of the anticipated diazo product was monitored using 1H NMR and thin-layer chromatography. Diazo compound 2b exhibits UV activity, and its formation can be visually observed on the thin-layer.

Figure 24 Reaction of Dibenzoylmethane (1a) and Diethyl malonate (1b) with $ABSN_3$ using a geopolymer as a catalyst.

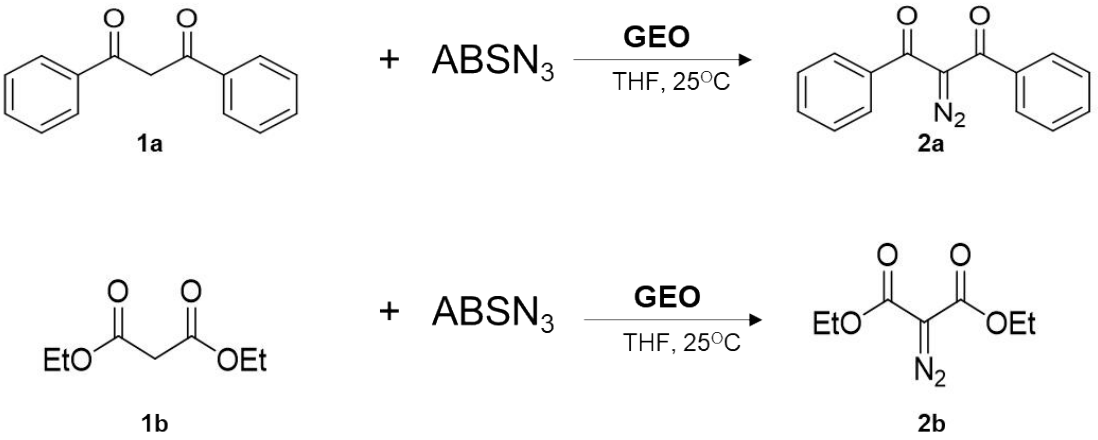

Source: author (2023).

The application of geopolymer-catalyzed diazo transfer reaction was expanded to two substrates: Dibenzoylmethane (1a) and Diethyl malonate (1b). In the first reaction with substrate 1a, 1,3-diketones (2a) were obtained 85% recovered charge within a reaction time of 24 hours. In the second reaction, 1,3-diethyl 2-diazopropanedioate (2b) was obtained in 55% in a 24 hours reaction.

5.2.1.3 Cu-Geopolymers in triazole synthesis

Triazole compounds that feature three nitrogen atoms in the five-membered aromatic azole ring demonstrate a notable ability to bind with a variety of enzymes and receptors in biological systems through diverse non-covalent interactions. As a result, they exhibit versatile biological activities. Research on triazole-based derivatives as medicinal drugs has been an exceedingly active and fruitful area, leading to numerous noteworthy achievements [262], [263], [264].

The most reported methodology in the literature for synthesizing five-membered ring heterocycles is the Huisgen 1,3-dipolar cycloaddition. Specifically, when alkyl or aryl azides react with terminal acetylenes, [1,2,3]-triazoles are formed[265]. In thermally conducted cycloadditions, a 1:1 mixture of the 1,4- and 1,5-regioisomers of triazole is typically obtained. Despite various attempts to control the regioselectivity, with limited success reported, a significant breakthrough occurred with

the discovery of the copper(I)-catalyzed reaction in 2002 [266]. This catalyzed reaction exclusively yields the 1,4-disubstituted-[1,2,3]-triazole.

Copper-containing catalysts (Cu10_IMP and Cu10_ADD) were evaluated in the reaction involving benzyl azide (2a) and phenylacetylene (1a). The protocol employed consisted of using ethanol, maintaining a 1:1 ratio of the reagents, and utilizing the copper catalyst prepared through both impregnation and addition methods. The primary objectives were to achieve the target compounds with high purity and favorable chemical yields using commercially available materials. Remarkably, a mass recovery of 98% was achieved for the impure product, and no post-reaction treatments were conducted, except for filtration, was obtained after a 4-day reaction under optimized ambient temperature conditions. Structural characterization was carried out through NMR analysis.

Figure 25 Reaction involving benzyl azide (2a) and phenylacetylene (1a), with the copper catalyst.

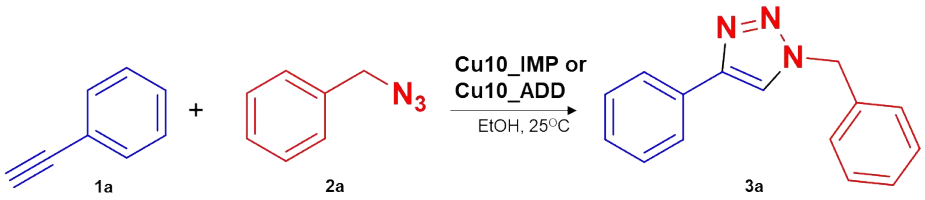

Source: author (2023).

6 CONCLUSION

The catalyst formulations were adjusted to facilitate printing, and the optimization of the quantity of polyethylene glycol (PEG) and other materials ensured the buildability of the material. The goal was to maintain the conformation of the catalyst after drying, avoiding issues such as blockages in the geopolymeric mass and minimizing the presence of bubbles during the printing process.

Two methods were employed for incorporating the active phase metals, preserving the support material's characteristics, stability, and integrity throughout the entire process. Analysis using techniques such as X-ray diffraction (DRX), X-ray fluorescence (FRX), and energy-dispersive X-ray spectroscopy (EDX) confirmed the presence of the active phase in all catalysts produced via impregnation and addition methods. While an exact qualitative analysis of the metal content in each sample proved challenging, the obtained results fell within the expected range, warranting further tests and calibration curves for a more accurate determination.

The bimetallic catalysts successfully met the specified parameters of buildability, conformation, stability, and available material quantity. Both production methods resulted in catalysts with high contact surface and porosity compared to alternative catalyst materials, facilitating greater interaction between the active phase and the reactants.

Temperature-programmed reduction (TPR) tests verified the suitability of all produced samples as catalysts, particularly those with copper in their formulation, which exhibited a predominant presence of metallic species in the reducing form. Nickel catalysts showcased species mainly governed by the inherent properties of nickel and its interaction with the geopolymer matrix.

Successful organic reaction tests demonstrated higher yields than anticipated, even without the optimization of all parameters. To further explore the catalysts' potential, additional tests with diverse reagents and solvents are required. This will expand the scope of substrates and compound formations while maintaining a sustainable reaction environment with environmentally friendly solvents. The experiments highlighted the catalysts' reusability, a pivotal objective in catalysis. The material's capacity for reuse without extensive transformations is crucial for its practical application.

In summary, the development of 3D-printed metallic and bimetallic catalysts supported on geopolymers showcases a sustainable and efficient approach in catalysis, highlighting the potential for advancements in the synthesis of valuable organic compounds with applications across diverse industries.

BIBLIOGRAPHY

[1] B. Török, C. Schäfer, e A. Kokel, *Heterogeneous Catalysis in Sustainable Synthesis*. 2021. doi: 10.1016/C2018-0-01478-4.

[2] J. C. Védrine, “Heterogeneous catalysis on metal oxides”, *Catalysts*, vol. 7, nº 11. 2017. doi: 10.3390/catal7110341.

[3] A. M. Molenbroek, S. Helveg, H. Topsøe, e B. S. Clausen, “Nano-particles in heterogeneous catalysis”, *Top Catal*, vol. 52, nº 10, 2009, doi: 10.1007/s11244-009-9314-1.

[4] D. D. Burduhos Nergis, M. M. A. B. Abdullah, P. Vizureanu, e M. F. Mohd Tahir, “Geopolymers and Their Uses: Review”, *IOP Conf Ser Mater Sci Eng*, vol. 374, nº 1, 2018, doi: 10.1088/1757-899X/374/1/012019.

[5] L. Vieira, L. J. Maschio, E. P. De Araújo, A. M. Da Silva, e R. Vieira, “Development of geopolymers for catalyst support applications”, *Materials Research*, vol. 22, nº 6, 2019, doi: 10.1590/1980-5373-MR-2018-0770.

[6] J. B. Zimmerman, P. T. Anastas, H. C. Erythropel, e W. Leitner, “Designing for a green chemistry future”, *Science*, vol. 367, nº 6476. 2020. doi: 10.1126/science.aay3060.

[7] P. T. Anastas e M. M. Kirchhoff, “Origins, current status, and future challenges of green chemistry”, *Acc Chem Res*, vol. 35, nº 9, 2002, doi: 10.1021/ar010065m.

[8] V. Meille, “Review on methods to deposit catalysts on structured surfaces”, *Appl Catal A Gen*, vol. 315, p. 1–17, 2006, doi: 10.1016/j.apcata.2006.08.031.

[9] N. Pinton, M. V. Vidal, M. Signoretto, A. Martínez-Arias, e V. Cortés Corberán, “Ethanol steam reforming on nanostructured catalysts of Ni, Co and CeO2: Influence of synthesis method on activity, deactivation and regenerability”, *Catal Today*, vol. 296, p. 135–143, nov. 2017, doi: 10.1016/J.CATTOD.2017.06.022.

[10] M. H. Raza, R. Y. Zhong, e M. Khan, “Recent advances and productivity analysis of 3D printed geopolymers”, *Addit Manuf*, vol. 52, p. 102685, abr. 2022, doi: 10.1016/j.addma.2022.102685.

[11] D. T. Pham e R. S. Gault, “A comparison of rapid prototyping technologies”, *Int J Mach Tools Manuf*, vol. 38, nº 10–11, p. 1257–1287, out. 1998, doi: 10.1016/S0890-6955(97)00137-5.

[12] R. M. Cardoso *et al.*, “Additive-manufactured (3D-printed) electrochemical sensors: A critical review”, *Analytica Chimica Acta*, vol. 1118. 2020. doi: 10.1016/j.aca.2020.03.028.

[13] F. Zhang *et al.*, “3D printing technologies for electrochemical energy storage”, *Nano Energy*, vol. 40. 2017. doi: 10.1016/j.nanoen.2017.08.037.

[14] M. Schmitt, R. M. Mehta, e I. Y. Kim, “Additive manufacturing infill optimization for automotive 3D-printed ABS components”, *Rapid Prototyp J*, vol. 26, nº 1, 2020, doi: 10.1108/RPJ-01-2019-0007.

[15] M. R. Nichols, “How does the automotive industry benefit from 3D metal printing?”, *Metal Powder Report*, vol. 74, nº 5, 2019, doi: 10.1016/j.mprp.2019.07.002.

[16] M. Ly, S. Spinelli, S. Hays, e D. Zhu, “3D Printing of Ceramic Biomaterials”, *Engineered Regeneration*, vol. 3, nº 1, 2022, doi: 10.1016/j.engreg.2022.01.006.

[17] A. Bandyopadhyay, S. Bose, e S. Das, “3D printing of biomaterials”, *MRS Bull*, vol. 40, nº 2, 2015, doi: 10.1557/mrs.2015.3.

[18] Y. Qiao *et al.*, “Thermal Shock Synthesis of Nanocatalyst by 3D-Printed Miniaturized Reactors”, *Small*, vol. 16, nº 22, 2020, doi: 10.1002/smll.202000509.

[19] E. G. Gordeev, K. S. Erokhin, A. D. Kobelev, J. V. Burykina, P. V. Novikov, e V. P. Ananikov, “Exploring metallic and plastic 3D printed photochemical reactors for customizing chemical synthesis”, *Sci Rep*, vol. 12, nº 1, 2022, doi: 10.1038/s41598-022-07583-9.

[20] R. Y. Chiou, M. G. Mauk, D. T. Varapula, S. Wang, C. Ruiz, e T. L. Tseng, “Microfluidic systems for studying chemical reactions, mixing, and heat transfer”, em *ASME International Mechanical Engineering Congress and Exposition, Proceedings (IMECE)*, 2017. doi: 10.1115/IMECE2017-72307.

[21] P. J. Kitson, M. H. Rosnes, V. Sans, V. Dragone, e L. Cronin, “Configurable 3D-Printed millifluidic and microfluidic ‘lab on a chip’ reactionware devices”, *Lab Chip*, vol. 12, nº 18, 2012, doi: 10.1039/c2lc40761b.

[22] S. Chunhua e S. Guangqing, “Application and Development of 3D Printing in Medical Field”, *Modern Mechanical Engineering*, vol. 10, nº 03, 2020, doi: 10.4236/mme.2020.103003.

[23] M. C. Maier *et al.*, “3D Printed Reactors for Synthesis of Active Pharmaceutical Ingredients in Continuous Flow”, *Org Process Res Dev*, vol. 24, nº 10, 2020, doi: 10.1021/acs.oprd.0c00228.

[24] H. Chen, L. Guo, W. Zhu, e C. Li, “Recent Advances in Multi-Material 3D Printing of Functional Ceramic Devices”, *Polymers*, vol. 14, nº 21. 2022. doi: 10.3390/polym14214635.

[25] M. J. Mirzaali *et al.*, “Multi-Material 3D Printing of Functionally Graded Hierarchical Soft–Hard Composites”, *Adv Eng Mater*, vol. 22, nº 7, 2020, doi: 10.1002/adem.201901142.

[26] X. Zhou e C. J. Liu, “Three-dimensional Printing for Catalytic Applications: Current Status and Perspectives”, *Adv Funct Mater*, vol. 27, nº 30, 2017, doi: 10.1002/adfm.201701134.

[27] O. A. Alimi, N. Bingwa, e R. Meijboom, “Homemade 3-D printed flow reactors for heterogeneous catalysis”, *Chemical Engineering Research and Design*, vol. 150, 2019, doi: 10.1016/j.cherd.2019.07.024.

[28] C. Parra-Cabrera, C. Achille, S. Kuhn, e R. Ameloot, “3D printing in chemical engineering and catalytic technology: Structured catalysts, mixers and reactors”, *Chemical Society Reviews*, vol. 47, nº 1. 2018. doi: 10.1039/c7cs00631d.

[29] E. Bogdan e P. Michorczyk, “3d printing in heterogeneous catalysis—the state of the art”, *Materials*, vol. 13, nº 20. 2020. doi: 10.3390/ma13204534.

[30] A. S. Díaz-Marta *et al.*, “Three-Dimensional Printing in Catalysis: Combining 3D Heterogeneous Copper and Palladium Catalysts for Multicatalytic Multicomponent Reactions”, *ACS Catal*, vol. 8, nº 1, 2018, doi: 10.1021/acscatal.7b02592.

[31] C. R. Tubío *et al.*, “3D printing of a heterogeneous copper-based catalyst”, *J Catal*, vol. 334, 2016, doi: 10.1016/j.jcat.2015.11.019.

[32] H. Lee, X. Wu, e L. Sun, “Copper-based homogeneous and heterogeneous catalysts for electrochemical water oxidation”, *Nanoscale*, vol. 12, nº 7, 2020, doi: 10.1039/c9nr10437b.

[33] T. Wohlers, “3D Printing and Additive Manufacturing State of the Industry. Annual Worldwide Progress Report.”, *Wohlers Report, Executive summary*, nº Mm. 2017.

[34] I. Gibson, D. W. Rosen, e B. Stucker, *Additive manufacturing technologies: Rapid prototyping to direct digital manufacturing*. 2010. doi: 10.1007/978-1-4419-1120-9.

[35] J. Zhu *et al.*, “Recent advances in 3D printing for catalytic applications”, *Chemical Engineering Journal*, vol. 433, p. 134341, abr. 2022, doi: 10.1016/J.CEJ.2021.134341.

[36] H. Maleki e V. Bertola, “Recent advances and prospects of inkjet printing in heterogeneous catalysis”, *Catalysis Science and Technology*, vol. 10, nº 10. 2020. doi: 10.1039/d0cy00040j.

[37] X. Chu, X. Tang, W. Chen, Y. Yang, W. Zhou, e J. Huang, “Direct-ink-write printing performance of zeolite catalysts with porous structures”, *Ceram Int*, 2023, doi: 10.1016/j.ceramint.2022.12.228.

[38] C. Huo *et al.*, “Hierarchically porous alumina catalyst carrier with biomimetic vein structure prepared by direct ink writing”, *J Eur Ceram Soc*, vol. 41, nº 7, 2021, doi: 10.1016/j.jeurceramsoc.2021.02.016.

[39] S. Rossi, A. Puglisi, L. M. Raimondi, e M. Benaglia, “Stereolithography 3D-printed catalytically active devices in organic synthesis”, *Catalysts*, vol. 10, nº 1, 2020, doi: 10.3390/catal10010109.

[40] I. V. Shishkovsky, A. V. Bulanova, e Y. G. Morozov, “Porous polycarbonate membranes with Ni and Cu nano catalytic additives fabricated by selective laser sintering”, *J. Mater. Sci. Eng. B*, vol. 2, nº Copyright (C) 2013 American Chemical Society (ACS). All Rights Reserved., 2012.

[41] E. Lahtinen, L. Turunen, M. M. Hänninen, K. Kolari, H. M. Tuononen, e M. Haukka, “Fabrication of Porous Hydrogenation Catalysts by a Selective Laser Sintering 3D Printing Technique”, *ACS Omega*, vol. 4, nº 7, 2019, doi: 10.1021/acsomega.9b00711.

[42] T. Shen, H. Xiong, Z. Li, L. Zhang, e K. Zhou, “Fused deposition fabrication of high-quality zirconia ceramics using granular feedstock”, *Ceram Int*, vol. 47, nº 24, 2021, doi: 10.1016/j.ceramint.2021.08.348.

[43] M. Peng *et al.*, “3D Printed Mechanically Robust Graphene/CNT Electrodes for Highly Efficient Overall Water Splitting”, *Advanced Materials*, vol. 32, nº 23, 2020, doi: 10.1002/adma.201908201.

[44] P. Zhang, Z. Wang, J. Li, X. Li, e L. Cheng, “From materials to devices using fused deposition modeling: A state-of-art review”, *Nanotechnology Reviews*, vol. 9, nº 1. 2020. doi: 10.1515/ntrev-2020-0101.

[45] G. Zhu, Y. Hou, J. Xiang, J. Xu, e N. Zhao, “Digital Light Processing 3D Printing of Healable and Recyclable Polymers with Tailorable Mechanical Properties”, *ACS Appl Mater Interfaces*, vol. 13, nº 29, 2021, doi: 10.1021/acsami.1c08872.

[46] Z. X. Khoo, Y. Liu, J. An, C. K. Chua, Y. F. Shen, e C. N. Kuo, “A review of selective laser melted NiTi shape memory alloy”, *Materials*, vol. 11, nº 4. 2018. doi: 10.3390/ma11040519.

[47] S. P. Murray *et al.*, “A defect-resistant Co–Ni superalloy for 3D printing”, *Nat Commun*, vol. 11, nº 1, 2020, doi: 10.1038/s41467-020-18775-0.

[48] Ben Redwood, “Additive Manufacturing Technologies: An Overview ”, *3D Hubs*, vol. 40, nº December 2012, 2020.

[49] S. Jang, S. Park, e · Chang-Jun Bae, “Development of ceramic additive manufacturing: process and materials technology”, *Biomed Eng Lett*, vol. 10, p. 493–503, 2020, doi: 10.1007/s13534-020-00175-4.

[50] G. Lazorenko e A. Kasprzhitskii, “Geopolymer additive manufacturing: A review”, *Addit Manuf*, vol. 55, p. 102782, jul. 2022, doi: 10.1016/J.ADDMA.2022.102782.

[51] S. Muthukrishnan, S. Ramakrishnan, e J. Sanjayan, “Effect of alkali reactions on the rheology of one-part 3D printable geopolymer concrete”, *Cem Concr Compos*, vol. 116, p. 103899, fev. 2021, doi: 10.1016/J.CEMCONCOMP.2020.103899.

[52] J. M. Aguirre-Cortés, A. I. Moral-Rodríguez, E. Bailón-García, A. Davó-Quiñonero, A. F. Pérez-Cadenas, e F. Carrasco-Marín, “3D printing in photocatalysis: Methods and capabilities for the improved performance”, *Appl Mater Today*, vol. 32, p. 101831, jun. 2023, doi: 10.1016/J.APMT.2023.101831.

[53] J. N. Stuecker, J. E. Miller, R. E. Ferrizz, J. E. Mudd, e J. Cesarano, “Advanced Support Structures for Enhanced Catalytic Activity”, *Ind Eng Chem Res*, vol. 43, nº 1, 2004, doi: 10.1021/ie030291v.

[54] I. Lucentini, I. Serrano, L. Soler, N. J. Divins, e J. Llorca, “Ammonia decomposition over 3D-printed CeO2 structures loaded with Ni”, *Appl Catal A Gen*, vol. 591, 2020, doi: 10.1016/j.apcata.2019.117382.

[55] H. Thakkar, S. Eastman, A. Hajari, A. A. Rownaghi, J. C. Knox, e F. Rezaei, “3D-Printed Zeolite Monoliths for CO2 Removal from Enclosed Environments”, *ACS Appl Mater Interfaces*, vol. 8, nº 41, 2016, doi: 10.1021/acsami.6b09647.

[56] M. D. M. Innocentini *et al.*, “Lattice-shaped geopolymer catalyst for biodiesel synthesis fabricated by additive manufacturing”, *Ceram Int*, vol. 45, nº 1, p. 1443–1446, jan. 2019, doi: 10.1016/J.CERAMINT.2018.09.239.

[57] V. Middelkoop *et al.*, “3D printed Ni/Al2O3 based catalysts for CO2 methanation - a comparative and operando XRD-CT study”, *Journal of CO2 Utilization*, vol. 33, p. 478–487, out. 2019, doi: 10.1016/J.JCOU.2019.07.013.

[58] J. Azuaje *et al.*, “An efficient and recyclable 3D printed α-Al2O3 catalyst for the multicomponent assembly of bioactive heterocycles”, *Appl Catal A Gen*, vol. 530, 2017, doi: 10.1016/j.apcata.2016.11.031.

[59] A. D. Salazar-Aguilar *et al.*, “3D-Printed Fe/γ-Al2O3Monoliths from MOF-Based Boehmite Inks for the Catalytic Hydroxylation of Phenol”, *ACS Appl Mater Interfaces*, vol. 14, nº 1, 2022, doi: 10.1021/acsami.1c19755.

[60] F. Agueniou *et al.*, “3D-printing of metallic honeycomb monoliths as a doorway to a new generation of catalytic devices: the Ni-based catalysts in methane dry reforming showcase”, *Catal Commun*, vol. 148, 2021, doi: 10.1016/j.catcom.2020.106181.

[61] S. Kingsland, “ Women in Science: Antiquity Through the Nineteenth Century. A Biographical Dictionary with Annotated Bibliography. Marilyn Bailey Ogilvie ”, *Q Rev Biol*, vol. 62, nº 3, 1987, doi: 10.1086/415520.

[62] M. A. A. Aziz, H. D. Setiabudi, L. P. Teh, N. H. R. Annuar, e A. A. Jalil, “A review of heterogeneous catalysts for syngas production via dry reforming”, *J Taiwan Inst Chem Eng*, vol. 101, p. 139–158, ago. 2019, doi: 10.1016/J.JTICE.2019.04.047.

[63] Y. Gao e Y. Ding, “Nanoporous Metals for Heterogeneous Catalysis: Following the Success of Raney Nickel”, *Chemistry - A European Journal*, vol. 26, nº 41. Wiley-VCH Verlag, p. 8845–8856, 22 de julho de 2020. doi: 10.1002/chem.202000471.

[64] R. Schlögl, *Heterogeneous catalysis*, vol. 54, nº 11. Elsevier B.V., 2015. doi: 10.1002/anie.201410738.

[65] V. Polshettiwar e R. S. Varma, “Green chemistry by nano-catalysis”, *Green Chemistry*, vol. 12, nº 5, 2010, doi: 10.1039/b921171c.

[66] *The IUPAC Compendium of Chemical Terminology*. 2019. doi: 10.1351/goldbook.

[67] M. Filez, Z. Ristanović, e B. M. Weckhuysen, “Micro-spectroscopy to interrogate solid catalysts at work”, em *Encyclopedia of Interfacial Chemistry: Surface Science and Electrochemistry*, 2018. doi: 10.1016/B978-0-12-409547-2.13744-8.

[68] D. Z. Mezalira, “Preparação e caracterização de materiais com propriedades catalíticas para a obtenção de hidrogênio e carbono nanoestruturado a partir da decomposição de etanol e do glicerol”, *Tese de doutorado*, vol. UFSC, 2011.

[69] J. H. Clark, “Catalysis for green chemistry”, em *Pure and Applied Chemistry*, 2001. doi: 10.1351/pac200173010103.

[70] C. S. Ewing, G. Veser, J. J. McCarthy, D. S. Lambrecht, e J. K. Johnson, “Predicting catalyst-support interactions between metal nanoparticles and amorphous silica supports”, *Surf Sci*, vol. 652, p. 278–285, out. 2016, doi: 10.1016/j.susc.2016.03.004.

[71] “A theory of the catalytic surface”, *Proceedings of the Royal Society of London. Series A, Containing Papers of a Mathematical and Physical Character*, vol. 108, nº 745, 1925, doi: 10.1098/rspa.1925.0061.

[72] S. A. Kondrat e J. A. van Bokhoven, “A Perspective on Counting Catalytic Active Sites and Rates of Reaction Using X-Ray Spectroscopy”, *Topics in Catalysis*, vol. 62, nº 17–20. 2019. doi: 10.1007/s11244-018-1057-4.

[73] S. De, J. Zhang, R. Luque, e N. Yan, “Ni-based bimetallic heterogeneous catalysts for energy and environmental applications”, *Energy and Environmental Science*, vol. 9, nº 11. Royal Society of Chemistry, p. 3314–3347, 1º de novembro de 2016. doi: 10.1039/c6ee02002j.

[74] R. Da Paz Fiuza, M. Aurélio Da Silva, e J. S. Boaventura, “Development of Fe–Ni/YSZ–GDC electrocatalysts for application as SOFC anodes: XRD and TPR characterization and evaluation in the ethanol steam reforming reaction”, *Int J Hydrogen Energy*, vol. 35, nº 20, p. 11216–11228, out. 2010, doi: 10.1016/J.IJHYDENE.2010.07.026.

[75] C. Yue, L. Gu, Z. Zhang, X. Wei, e H. Yang, “Nickel- and cobalt-based heterogeneous catalytic systems for selective primary amination of alcohol with ammonia”, *Arabian Journal of Chemistry*, vol. 15, nº 6, p. 103865, jun. 2022, doi: 10.1016/J.ARABJC.2022.103865.

[76] K. Jalama, “Carbon dioxide hydrogenation over nickel-, ruthenium-, and copper-based catalysts: Review of kinetics and mechanism”, *Catal Rev Sci Eng*, vol. 59, nº 2, 2017, doi: 10.1080/01614940.2017.1316172.

[77] Q. Su, S. Yang, Y. He, Z. Qin, e X. Cui, “Prepared self-growing supported nickel catalyst by recovering Ni (Ⅱ) from metal wastewater using geopolymer microspheres”, *J Hazard Mater*, vol. 389, p. 121919, maio 2020, doi: 10.1016/J.JHAZMAT.2019.121919.

[78] T. Pu *et al.*, “Formation and influence of surface hydroxyls on product selectivity during CO2 hydrogenation by Ni/SiO2 catalysts”, *J Catal*, vol. 400, p. 228–233, ago. 2021, doi: 10.1016/J.JCAT.2021.06.008.

[79] T. J. Lin, X. Meng, e L. Shi, “Ni-exchanged Y-zeolite: An efficient heterogeneous catalyst for acetylene hydrocarboxylation”, *Appl Catal A Gen*, vol. 485, p. 163–171, set. 2014, doi: 10.1016/J.APCATA.2014.07.036.

[80] X. Kong, Y. Zhu, H. Zheng, X. Li, Y. Zhu, e Y. W. Li, “Ni Nanoparticles Inlaid Nickel Phyllosilicate as a Metal-Acid Bifunctional Catalyst for Low-Temperature Hydrogenolysis Reactions”, *ACS Catal*, vol. 5, nº 10, 2015, doi: 10.1021/acscatal.5b01080.

[81] E. J. Shin e M. A. Keane, “Gas-phase hydrogenation/hydrogenolysis of phenol over supported nickel catalysts”, *Ind Eng Chem Res*, vol. 39, nº 4, 2000, doi: 10.1021/ie990643r.

[82] Y. Nakagawa, H. Nakazawa, H. Watanabe, e K. Tomishige, “Total Hydrogenation of Furfural over a Silica-Supported Nickel Catalyst Prepared by the Reduction of a Nickel Nitrate Precursor”, *ChemCatChem*, vol. 4, nº 11, 2012, doi: 10.1002/cctc.201200218.

[83] X. Lv, J. F. Chen, Y. Tan, e Y. Zhang, “A highly dispersed nickel supported catalyst for dry reforming of methane”, *Catal Commun*, vol. 20, p. 6–11, abr. 2012, doi: 10.1016/j.catcom.2012.01.002.

[84] S. He *et al.*, “Ni/SiO2 Catalyst Prepared with Nickel Nitrate Precursor for Combination of CO2 Reforming and Partial Oxidation of Methane: Characterization and Deactivation Mechanism Investigation”, *J Nanomater*, vol. 2015, 2015, doi: 10.1155/2015/659402.

[85] L. Zhang, B. Tian, F. Chen, e J. Zhang, “Nickel sulfide as co-catalyst on nanostructured TiO 2 for photocatalytic hydrogen evolution”, *Int J Hydrogen Energy*, vol. 37, nº 22, 2012, doi: 10.1016/j.ijhydene.2012.08.120.

[86] A. H. Braga, E. R. Sodré, J. B. O. Santos, C. M. de Paula Marques, e J. M. C. Bueno, “Steam reforming of acetone over Ni- and Co-based catalysts: Effect of the composition of reactants and catalysts on reaction pathways”, *Appl Catal B*, vol. 195, p. 16–28, 2016, doi: 10.1016/j.apcatb.2016.04.047.

[87] J. L. Ye, Y. Q. Wang, Y. Liu, e H. Wang, “Steam reforming of ethanol over Ni/CexTi1−xO2 catalysts”, *Int J Hydrogen Energy*, vol. 33, nº 22, p. 6602–6611, nov. 2008, doi: 10.1016/J.IJHYDENE.2008.08.036.

[88] J. Comas, F. Marino, M. Laborde, e N. Amadeo, “Bio-ethanol steam reforming on Ni/Al2O3 catalyst”, *Chemical Engineering Journal*, vol. 98, nº 1–2, 2004, doi: 10.1016/S1385-8947(03)00186-4.

[89] J. H. Song, S. J. Han, J. Yoo, S. Park, D. H. Kim, e I. K. Song, “Hydrogen production by steam reforming of ethanol over Ni-Sr-Al2O3-ZrO2 aerogel catalyst”, *J Mol Catal A Chem*, vol. 424, p. 342–350, dez. 2016, doi: 10.1016/J.MOLCATA.2016.09.013.

[90] S. J. Han *et al.*, “Hydrogen production by steam reforming of ethanol over mesoporous Cu-Ni-Al2O3-ZrO2 xerogel catalysts”, *Int J Hydrogen Energy*, vol. 41, nº 4, 2016, doi: 10.1016/j.ijhydene.2015.11.128.

[91] Y. Yang, J. Ma, e F. Wu, “Production of hydrogen by steam reforming of ethanol over a Ni/ZnO catalyst”, *Int J Hydrogen Energy*, vol. 31, nº 7, p. 877–882, jun. 2006, doi: 10.1016/J.IJHYDENE.2005.06.029.

[92] J. Sun, X. P. Qiu, F. Wu, e W. T. Zhu, “H2 from steam reforming of ethanol at low temperature over Ni/Y2O3, Ni/La2O3 and Ni/Al2O3 catalysts for fuel-cell application”, *Int J Hydrogen Energy*, vol. 30, nº 4, p. 437–445, mar. 2005, doi: 10.1016/J.IJHYDENE.2004.11.005.

[93] O. Tursunov, K. Zubek, J. Dobrowolski, G. Czerski, e P. Grzywacz, “Effect of Ni/Al2O3-SiO2 and Ni/Al2O3-SiO2 with K2O Promoter Catalysts on H2, CO and CH4 Concentration by CO2 Gasification of Rosa Multiflora Biomass”, *Oil and Gas Science and Technology*, vol. 72, nº 6, p. 1–16, 2017, doi: 10.2516/ogst/2017037.

[94] A. L. Alberton, M. M. V. M. Souza, e M. Schmal, “Carbon formation and its influence on ethanol steam reforming over Ni/Al2O3 catalysts”, *Catal Today*, vol. 123, nº 1–4, 2007, doi: 10.1016/j.cattod.2007.01.062.

[95] R. Buitrago-Sierra, J. Ruiz-Martínez, J. C. Serrano-Ruiz, F. Rodríguez-Reinoso, e A. Sepúlveda-Escribano, “Ethanol steam reforming on Ni/Al2O3 catalysts:

Effect of the addition of Zn and Pt", *J Colloid Interface Sci*, vol. 383, nº 1, p. 148–154, out. 2012, doi: 10.1016/J.JCIS.2012.06.026.

[96] V. G. Deshmane, S. L. Owen, R. Y. Abrokwah, e D. Kuila, "Mesoporous nanocrystalline TiO2 supported metal (Cu, Co, Ni, Pd, Zn, and Sn) catalysts: Effect of metal-support interactions on steam reforming of methanol", *J Mol Catal A Chem*, vol. 408, p. 202–213, nov. 2015, doi: 10.1016/J.MOLCATA.2015.07.023.

[97] M. Khzouz, E. I. Gkanas, S. Du, e J. Wood, "Catalytic performance of Ni-Cu/Al2O3 for effective syngas production by methanol steam reforming", *Fuel*, vol. 232, 2018, doi: 10.1016/j.fuel.2018.06.025.

[98] Y. K. Chih *et al.*, "Statistical optimization of hydrogen production from bio-methanol steam reforming over Ni-Cu/Al2O3 catalysts", *Fuel*, vol. 331, 2023, doi: 10.1016/j.fuel.2022.125691.

[99] M. Artetxe, J. Alvarez, M. A. Nahil, M. Olazar, e P. T. Williams, "Steam reforming of different biomass tar model compounds over Ni/Al2O3 catalysts", *Energy Convers Manag*, vol. 136, 2017, doi: 10.1016/j.enconman.2016.12.092.

[100] P. Mierczynski *et al.*, "High active and selective Ni/Ceo2 –Al2O3 and Pd–Ni/Ceo2 –Al2O3 catalysts for oxy-steam reforming of methanol", *Catalysts*, vol. 8, nº 9, 2018, doi: 10.3390/catal8090380.

[101] Z. Liu, S. Yao, A. Johnston-Peck, W. Xu, J. A. Rodriguez, e S. D. Senanayake, "Methanol steam reforming over Ni-CeO2 model and powder catalysts: Pathways to high stability and selectivity for H2/CO2 production", *Catal Today*, vol. 311, 2018, doi: 10.1016/j.cattod.2017.08.041.

[102] V. Chiodo, S. Freni, A. Galvagno, N. Mondello, e F. Frusteri, "Catalytic features of Rh and Ni supported catalysts in the steam reforming of glycerol to produce hydrogen", *Applied Catalysis A: General*, vol. 381, nº 1–2. 2010. doi: 10.1016/j.apcata.2010.03.039.

[103] C. K. Cheng, S. Y. Foo, e A. A. Adesina, "Steam reforming of glycerol over Ni/Al2O3 catalyst", *Catal Today*, vol. 178, nº 1, 2011, doi: 10.1016/j.cattod.2011.07.011.

[104] G. Wu *et al.*, "Hydrogen production via glycerol steam reforming over Ni/Al 2O3: Influence of nickel precursors", *ACS Sustain Chem Eng*, vol. 1, nº 8, 2013, doi: 10.1021/sc400123f.

[105] I. N. Buffoni, F. Pompeo, G. F. Santori, e N. N. Nichio, “Nickel catalysts applied in steam reforming of glycerol for hydrogen production”, *Catal Commun*, vol. 10, nº 13, p. 1656–1660, jul. 2009, doi: 10.1016/J.CATCOM.2009.05.003.

[106] R. P. Borges, L. G. Moura, J. J. Spivey, F. B. Noronha, e C. E. Hori, “Hydrogen production by steam reforming of LPG using supported perovskite type precursors”, *Int J Hydrogen Energy*, vol. 45, nº 41, 2020, doi: 10.1016/j.ijhydene.2020.05.183.

[107] A. W. Augustyniak, W. Zawartka, J. A. R. Navarro, e A. M. Trzeciak, “Palladium nanoparticles supported on a nickel pyrazolate metal organic framework as a catalyst for Suzuki and carbonylative Suzuki couplings”, *Dalton Transactions*, vol. 45, nº 34, 2016, doi: 10.1039/c6dt02242a.

[108] K. Fujimoto, T. Shlkada, K. Omata, e H. O. Tomlnaga, “Vapor Phase Carbonylation of Methanol with Supported Nickel Metal Catalysts”, *Industrial and Engineering Chemistry Product Research and Development*, vol. 21, nº 3, 1982, doi: 10.1021/i300007a015.

[109] Q. Zhang, H. Wang, G. Sun, K. Huang, W. Fang, e Y. Yang, “Promoting effect of CeO2 addition to Ni/AC catalyst for vapor phase carbonylation of ethanol to propionic acid”, *Catal Commun*, vol. 10, nº 14, 2009, doi: 10.1016/j.catcom.2009.05.025.

[110] P. P. Nair, R. M. Philip, e G. Anilkumar, “Nickel catalysts in Sonogashira coupling reactions”, *Organic and Biomolecular Chemistry*, vol. 19, nº 19. 2021. doi: 10.1039/d1ob00280e.

[111] S. Chongdar *et al.*, “Nickel Nanoparticles Immobilized over Mesoporous SBA-15 for Efficient Carbonylative Coupling Reactions Utilizing CO2: A Spotlight”, *ACS Applied Materials and Interfaces*, vol. 13, nº 34. 2021. doi: 10.1021/acsami.1c09942.

[112] V. P. Mahajan, Y. A. Kolekar, e B. M. Bhanage, “Ni/Al2O3: Catalyzed Carbonylative Homocoupling of Aryl Iodides for the Synthesis of Symmetrical Diaryl Ketone Using Co2(CO)8 as CO Surrogate”, *Catal Letters*, ago. 2023, doi: 10.1007/s10562-023-04430-y.

[113] V. P. Mahajan, Y. A. Kolekar, e B. M. Bhanage, “Magnetically separable Ni/Fe3O4: An efficient catalyst for phenoxy carbonylation of aryl iodides using bifunctional o-chlorophenyl formate as a CO source”, *Appl Organomet Chem*, vol. 37, nº 4, 2023, doi: 10.1002/aoc.7032.

[114] E. M. Cepollaro, R. Botti, G. Franchin, L. Lisi, P. Colombo, e S. Cimino, “Cu/zsm5-geopolymer 3d-printed monoliths for the nh3-scr of nox”, *Catalysts*, vol. 11, nº 10, 2021, doi: 10.3390/catal11101212.

[115] S. Patel e K. K. Pant, “Influence of preparation method on performance of Cu(Zn)(Zr)-alumina catalysts for the hydrogen production via steam reforming of methanol”, *Journal of Porous Materials*, vol. 13, nº 3, 2006, doi: 10.1007/s10934-006-8033-2.

[116] S. Patel e K. K. Pant, “Production of hydrogen with low carbon monoxide formation via catalytic steam reforming of methanol”, *J Fuel Cell Sci Technol*, vol. 3, nº 4, 2006, doi: 10.1115/1.2349514.

[117] A. Y. Kapran e S. M. Orlyk, “Hydrogen Production in Methanol Reforming on Modified Copper–Zinc Catalysts: A Review”, *Theoretical and Experimental Chemistry*, vol. 53, nº 1. 2017. doi: 10.1007/s11237-017-9495-9.

[118] Y. J. Liu *et al.*, “Sustained release catalysis: Dynamic copper releasing from stoichiometric spinel CuAl2O4 during methanol steam reforming”, *Appl Catal B*, vol. 323, 2023, doi: 10.1016/j.apcatb.2022.122043.

[119] J. Zhao, G. Zhang, H. Liu, Q. Shu, e Q. Zhang, “Improved charge transfer and morphology on Ti-modified Cu/γ-Al2O3/Al catalyst enhance the activity for methanol steam reforming”, *Int J Hydrogen Energy*, vol. 47, nº 42, 2022, doi: 10.1016/j.ijhydene.2022.04.025.

[120] D. Li *et al.*, “Induced activation of the commercial Cu/ZnO/Al2O3 catalyst for the steam reforming of methanol”, *Nat Catal*, vol. 5, nº 2, 2022, doi: 10.1038/s41929-021-00729-4.

[121] T. Y. Amiri e J. Moghaddas, “Cogeled copper–silica aerogel as a catalyst in hydrogen production from methanol steam reforming”, *Int J Hydrogen Energy*, vol. 40, nº 3, p. 1472–1480, jan. 2015, doi: 10.1016/J.IJHYDENE.2014.11.104.

[122] P. Mierczynski, M. Mosinska, W. Maniukiewicz, M. Nowosielska, A. Czylkowska, e M. I. Szynkowska, “Oxy-steam reforming of methanol on copper catalysts”, *Reaction Kinetics, Mechanisms and Catalysis*, vol. 127, nº 2, 2019, doi: 10.1007/s11144-019-01609-6.

[123] O. O. Fasanya, A. Y. Atta, M. T. Z. Myint, J. Dutta, e B. Y. Jibril, “Effects of synthesis methods on performance of CuZn/MCM-41 catalysts in methanol steam reforming”, *Int J Hydrogen Energy*, vol. 46, nº 5, p. 3539–3553, jan. 2021, doi: 10.1016/J.IJHYDENE.2020.10.181.

[124] S. Moogi *et al.*, “Copper promoted Co/MgO: A stable and efficient catalyst for glycerol steam reforming”, *Int J Hydrogen Energy*, vol. 46, nº 34, 2021, doi: 10.1016/j.ijhydene.2020.08.190.

[125] R. B. N. Baig e R. S. Varma, “Copper on chitosan: A recyclable heterogeneous catalyst for azide-alkyne cycloaddition reactions in water”, *Green Chemistry*, vol. 15, nº 7, 2013, doi: 10.1039/c3gc40401c.

[126] M. Emami, R. Bikas, N. Noshiranzadeh, A. Kozakiewicz, e T. Lis, “Cu(II)-Hydrazide Coordination Compound Supported on Silica Gel as an Efficient and Recyclable Heterogeneous Catalyst for Green Click Synthesis of β-Hydroxy-1,2,3-triazoles in Water”, *ACS Omega*, vol. 5, nº 22, 2020, doi: 10.1021/acsomega.0c01491.

[127] N. Aflak *et al.*, “Facile immobilization of copper(I) acetate on silica: A recyclable and reusable heterogeneous catalyst for azide–alkyne clickable cycloaddition reactions”, *Polyhedron*, vol. 170, 2019, doi: 10.1016/j.poly.2019.06.030.

[128] M. Lim, H. Lee, M. Kang, W. Yoo, e H. Rhee, “Azide-alkyne cycloaddition reactions in water: Via recyclable heterogeneous Cu catalysts: Reverse phase silica gel and thermoresponsive hydrogels”, *RSC Adv*, vol. 8, nº 11, 2018, doi: 10.1039/c8ra00306h.

[129] P. Diz *et al.*, “Sol-gel entrapped Cu in a silica matrix: An efficient heterogeneous nanocatalyst for Huisgen and Ullmann intramolecular coupling reactions”, *Appl Catal A Gen*, vol. 502, 2015, doi: 10.1016/j.apcata.2015.05.025.

[130] M. Goswami e A. M. Das, “Synthesis of cellulose impregnated copper nanoparticles as an efficient heterogeneous catalyst for C–N coupling reactions under mild conditions”, *Carbohydr Polym*, vol. 195, 2018, doi: 10.1016/j.carbpol.2018.04.033.

[131] J. F. Kurisingal *et al.*, “Facile Green Synthesis of New Copper-Based Metal-Organic Frameworks: Experimental and Theoretical Study of the CO2Fixation Reaction”, *ACS Sustain Chem Eng*, vol. 8, nº 29, 2020, doi: 10.1021/acssuschemeng.0c02749.

[132] Y. Ni *et al.*, “A green route for methanol carbonylation”, *Catal Sci Technol*, vol. 7, nº 20, 2017, doi: 10.1039/c7cy01621b.

[133] N. Antil, M. Chauhan, N. Akhtar, R. Kalita, e K. Manna, “Selective Methane Oxidation to Acetic Acid Using Molecular Oxygen over a Mono-Copper Hydroxyl Catalyst”, *J Am Chem Soc*, vol. 145, nº 11, 2023, doi: 10.1021/jacs.2c12042.

[134] D. Chakraborty, S. Nandi, D. Mullangi, S. Haldar, C. P. Vinod, e R. Vaidhyanathan, “Cu/Cu 2 O Nanoparticles Supported on a Phenol-Pyridyl COF as a Heterogeneous Catalyst for the Synthesis of Unsymmetrical Diynes via Glaser-Hay Coupling”, *ACS Appl Mater Interfaces*, vol. 11, nº 17, 2019, doi: 10.1021/acsami.9b02860.

[135] J. Cao *et al.*, “Tuning the electronic properties of supported Cu catalysts for efficient epoxidation of long-chain α-olefins”, *Fuel*, vol. 342, 2023, doi: 10.1016/j.fuel.2023.127829.

[136] Z. Wei *et al.*, “Highly crystallized Pd/Cu nanoparticles on activated carbon: An efficient heterogeneous catalyst for sonogashira cross-coupling reaction”, *Catalysts*, vol. 10, nº 2, 2020, doi: 10.3390/catal10020192.

[137] S. Anuma, P. Mishra, e B. R. Bhat, “Copper complex with N-,O- architecture grafted graphene oxide nanosheet as a heterogeneous catalyst for Suzuki cross coupling reaction”, *J Taiwan Inst Chem Eng*, vol. 95, 2019, doi: 10.1016/j.jtice.2018.09.029.

[138] S. Sonei, F. Taghavi, A. Khojastehnezhad, e M. Gholizadeh, “Copper-Functionalized Silica-Coated Magnetic Nanoparticles for an Efficient Suzuki Cross-Coupling Reaction”, *ChemistrySelect*, vol. 6, nº 3, 2021, doi: 10.1002/slct.202004148.

[139] M. Tavassoli, A. Landarani-Isfahani, M. Moghadam, S. Tangestaninejad, V. Mirkhani, e I. Mohammadpoor-Baltork, “Copper Dithiol Complex Supported on Silica Nanoparticles: A Sustainable, Efficient, and Eco-friendly Catalyst for Multicomponent Click Reaction”, *ACS Sustain Chem Eng*, vol. 4, nº 3, 2016, doi: 10.1021/acssuschemeng.5b01432.

[140] S. F. Hamzavi, S. Gerivani, S. Saeedi, K. Naghdipari, e G. Shahverdizadeh, “Preparation and characterization of a novel spherical cellulose–copper(II) oxide composite particles: as a heterogeneous catalyst for the click reaction”, *Mol Divers*, vol. 24, nº 1, 2020, doi: 10.1007/s11030-019-09942-7.

[141] J. H. Sinfelt, “Heterogeneous catalysis: Some recent developments”, *Science*, vol. 195, nº 4279. 1977. doi: 10.1126/science.195.4279.641.

[142] F. Tao, “Synthesis, catalysis, surface chemistry and structure of bimetallic nanocatalysts”, *Chem Soc Rev*, vol. 41, nº 24, 2012, doi: 10.1039/c2cs90093a.

[143] J. H. Sinfelt, D. J. C J Catal, e A. E. J Catal, “Bimetallic Catalysts: Discoveries, Concepts, and Applications”, *Phys. Rev. B: Solid State*, vol. 20, nº 2, 1987.

[144] Z. Bian, S. Das, M. H. Wai, P. Hongmanorom, e S. Kawi, “A Review on Bimetallic Nickel-Based Catalysts for CO2 Reforming of Methane”, *ChemPhysChem*, vol. 18, nº 22. 2017. doi: 10.1002/cphc.201700529.

[145] M. Mosinska *et al.*, “Hydrogen production on Cu-Ni catalysts via the oxy-steam reforming of methanol”, *Catalysts*, vol. 10, nº 3, 2020, doi: 10.3390/catal10030273.

[146] J. L. C. Fajín e M. N. D. S. Cordeiro, “Insights into the Mechanism of Methanol Steam Reforming for Hydrogen Production over Ni–Cu-Based Catalysts”, *ACS Catal*, vol. 12, nº 1, 2022, doi: 10.1021/acscatal.1c03997.

[147] S. Sohrabi e A. Irankhah, “Synthesis, characterization, and catalytic activity of Ni/CeMnO2 catalysts promoted by copper, cobalt, potassium and iron for ethanol steam reforming”, *Int J Hydrogen Energy*, vol. 46, nº 24, 2021, doi: 10.1016/j.ijhydene.2021.01.057.

[148] M. Śliwa e K. Samson, “Steam reforming of ethanol over copper-zirconia based catalysts doped with Mn, Ni, Ga”, *Int J Hydrogen Energy*, vol. 46, nº 1, 2021, doi: 10.1016/j.ijhydene.2020.09.222.

[149] L. C. Chen e S. D. Lin, “The ethanol steam reforming over Cu-Ni/SiO2 catalysts: Effect of Cu/Ni ratio”, *Appl Catal B*, vol. 106, nº 3–4, 2011, doi: 10.1016/j.apcatb.2011.06.028.

[150] B. Dou, C. Wang, Y. Song, H. Chen, e Y. Xu, “Activity of Ni-Cu-Al based catalyst for renewable hydrogen production from steam reforming of glycerol”, *Energy Convers Manag*, vol. 78, 2014, doi: 10.1016/j.enconman.2013.10.067.

[151] N. Hu, C. Yang, L. He, Q. Guan, e R. Miao, “Ni-Cu/Al2O3 catalysts for the selective hydrogenation of acetylene: a study on catalytic performance and reaction mechanism”, *New Journal of Chemistry*, vol. 43, nº 46, 2019, doi: 10.1039/c9nj03956b.

[152] S. Hu *et al.*, “Semi-Hydrogenation of Acetylene to Ethylene Catalyzed by Bimetallic CuNi/ZSM-12 Catalysts”, *Catalysts*, vol. 12, nº 9, 2022, doi: 10.3390/catal12091072.

[153] D. A. Lomelí-Rosales *et al.*, “A General One-Pot Methodology for the Preparation of Mono- and Bimetallic Nanoparticles Supported on Carbon Nanotubes: Application in the Semi-hydrogenation of Alkynes and Acetylene”, *Chemistry - A European Journal*, vol. 25, nº 35, 2019, doi: 10.1002/chem.201901041.

[154] M. K. Gharpurey e P. H. Emmett, “Study of the hydrogenation of ethylene over homogenized copper-nickel alloy films”, *Journal of Physical Chemistry*, vol. 65, nº 7, 1961, doi: 10.1021/j100825a020.

[155] W. K. Hall e P. H. Emmett, “Studies of the hydrogenation of ethylene over copper-nickel alloys”, *Journal of Physical Chemistry*, vol. 63, nº 7, 1959, doi: 10.1021/j150577a016.

[156] Z. Zhang *et al.*, “Efficient and stable Cu-Ni/ZrO2 catalysts for in situ hydrogenation and deoxygenation of oleic acid into heptadecane using methanol as a hydrogen donor”, *Fuel*, vol. 230, 2018, doi: 10.1016/j.fuel.2018.05.018.

[157] A. Aldureid, F. Medina, G. S. Patience, e D. Montané, “Ni-Cu/Al2O3 from Layered Double Hydroxides Hydrogenates Furfural to Alcohols”, *Catalysts*, vol. 12, nº 4, 2022, doi: 10.3390/catal12040390.

[158] M. Kalong *et al.*, “Hydrogen-free hydrogenation of furfural to furfuryl alcohol and 2-methylfuran over Ni and Co-promoted Cu/γ-Al2O3 catalysts”, *Fuel Processing Technology*, vol. 214, 2021, doi: 10.1016/j.fuproc.2020.106721.

[159] Y. Liu e D. Liu, “Study of bimetallic Cu-Ni/γ-Al2O3 catalysts for carbon dioxide hydrogenation”, *Int J Hydrogen Energy*, vol. 24, nº 4, 1999, doi: 10.1016/S0360-3199(98)00038-X.

[160] Q. Tan, Z. Shi, e D. Wu, “CO2 hydrogenation over differently morphological CeO2-supported Cu-Ni catalysts”, *Int J Energy Res*, vol. 43, nº 10, 2019, doi: 10.1002/er.4636.

[161] M. Bakherad, “Recent progress and current applications of Sonogashira coupling reaction in water”, *Applied Organometallic Chemistry*, vol. 27, nº 3. 2013. doi: 10.1002/aoc.2931.

[162] Z. Nasresfahani e M. Z. Kassaee, “Bimetallic Ni/Cu mesoporous silica nanoparticles as an efficient and reusable catalyst for the Sonogashira cross-coupling reactions”, *J Organomet Chem*, vol. 937, 2021, doi: 10.1016/j.jorganchem.2021.121703.

[163] M. A. Nasseri, M. Shahabi, S. A. Alavi G., e A. Allahresani, “A novel, efficient and magnetically recyclable Cu–Ni bimetallic alloy nanoparticle as a highly active bifunctional catalyst for Pd-free Sonogashira and C–N cross-coupling reactions: a combined theoretical and experimental study”, *RSC Adv*, vol. 13, nº 32, p. 22158–22171, 2023, doi: 10.1039/D3RA01965A.

[164] Z. Wang, G. Chen, e K. Ding, “Self-supported catalysts”, *Chemical Reviews*, vol. 109, nº 2. 2009. doi: 10.1021/cr800406u.

[165] Q. Su, Q. Ye, L. Deng, Y. He, e X. Cui, “Prepared self-growth supported copper catalyst by recovering Cu (II) from wastewater using geopolymer microspheres”, *J Clean Prod*, vol. 272, p. 122571, nov. 2020, doi: 10.1016/J.JCLEPRO.2020.122571.

[166] R. J. Davis, “New perspectives on basic zeolites as catalysts and catalyst supports”, em *Journal of Catalysis*, 2003. doi: 10.1016/S0021-9517(02)00034-9.

[167] A. Molnar, “Nafion – Silica Nanocomposites: A New Generation of Water-Tolerant Solid Acids of High Efficiency — An Update”, *Curr Org Chem*, vol. 15, nº 23, 2011, doi: 10.2174/138527211798072449.

[168] H. Zou, S. Wu, e J. Shen, “Polymer/Silica Nanocomposites: Preparation, characterization, propertles, and applications”, *Chemical Reviews*, vol. 108, nº 9. 2008. doi: 10.1021/cr068035q.

[169] N. V. Parizotto *et al.*, “Alumina-supported Ni catalysts modified with silver for the steam reforming of methane: Effect of Ag on the control of coke formation”, *Appl Catal A Gen*, vol. 330, nº 1–2, 2007, doi: 10.1016/j.apcata.2007.06.022.

[170] M. Valden, X. Lai, e D. W. Goodman, “Onset of catalytic activity of gold clusters on titania with the appearance of nonmetallic properties”, *Science (1979)*, vol. 281, nº 5383, 1998, doi: 10.1126/science.281.5383.1647.

[171] B. H. Lipshutz, B. A. Frieman, T. Butler, e V. Kogan, “Heterogeneous catalysis with nickel-on-graphite (Ni/Cg): Reduction of aryl tosylates and mesylates”, *Angewandte Chemie - International Edition*, vol. 45, nº 5, 2006, doi: 10.1002/anie.200502887.

[172] M. Wannaborworn, P. Praserthdam, e B. Jongsomjit, “A comparative study of solvothermal and sol-gel-derived nanocrystalline alumina catalysts for ethanol dehydration”, *J Nanomater*, vol. 2015, 2015, doi: 10.1155/2015/519425.

[173] H. Drobná *et al.*, “Analysis of Ni species formed on zeolites, mesoporous silica and alumina supports and their catalytic behavior in the dry reforming of methane”, vol. 121, p. 255–274, 2017, doi: 10.1007/s11144-017-1149-3.

[174] E. Dahdah, J. Estephane, C. Gennequin, A. Aboukaïs, E. Abi-Aad, e S. Aouad, “Zirconia supported nickel catalysts for glycerol steam reforming: Effect of

zirconia structure on the catalytic performance", *Int J Hydrogen Energy*, vol. 45, nº 7, p. 4457–4467, fev. 2020, doi: 10.1016/J.IJHYDENE.2019.12.019.

[175] M. Rezaei, S. M. Alavi, S. Sahebdelfar, P. Bai, X. Liu, e Z. F. Yan, "CO2 reforming of CH4 over nanocrystalline zirconia-supported nickel catalysts", *Appl Catal B*, vol. 77, nº 3–4, p. 346–354, jan. 2008, doi: 10.1016/J.APCATB.2007.08.004.

[176] M. D. M. V. M. Souza, L. Clavé, V. Dubois, C. A. C. Perez, e M. Schmal, "Activation of supported nickel catalysts for carbon dioxide reforming of methane", *Appl Catal A Gen*, vol. 272, nº 1–2, p. 133–139, 2004, doi: 10.1016/j.apcata.2004.05.026.

[177] P. Leroi, B. Madani, C. Pham-Huu, M. J. Ledoux, S. Savin-Poncet, e J. L. Bousquet, "Ni/SiC: a stable and active catalyst for catalytic partial oxidation of methane", *Catal Today*, vol. 91–92, p. 53–58, jul. 2004, doi: 10.1016/J.CATTOD.2004.03.009.

[178] W. Guo, T. Hu, H. Qin, P. Gao, e H. Xiao, "Preparation and in situ reduction of Ni/SiCxOy catalysts supported on porous SiC ceramic for ethanol steam reforming", *Ceram Int*, vol. 47, nº 10, p. 13738–13744, maio 2021, doi: 10.1016/j.ceramint.2021.01.235.

[179] Z. Hao *et al.*, "Decoupling the effect of Ni particle size and surface oxygen deficiencies in CO2 methanation over ceria supported Ni", *Appl Catal B*, vol. 286, p. 119922, jun. 2021, doi: 10.1016/J.APCATB.2021.119922.

[180] N. Gao, K. Chen, C. Quan, e S. Wu, "Nickel supported over MCM-41 coated ceramic membrane for steam reforming of real tar", *Int J Hydrogen Energy*, vol. 46, nº 40, p. 20882–20892, jun. 2021, doi: 10.1016/J.IJHYDENE.2021.03.213.

[181] Y. J. Zhang, L. C. Liu, Y. Xu, Y. C. Wang, e D. L. Xu, "A new alkali-activated steel slag-based cementitious material for photocatalytic degradation of organic pollutant from waste water", *J Hazard Mater*, vol. 209–210, p. 146–150, mar. 2012, doi: 10.1016/J.JHAZMAT.2012.01.001.

[182] A. De Rossi *et al.*, "Waste-based geopolymeric mortars with very high moisture buffering capacity", *Constr Build Mater*, vol. 191, p. 39–46, 2018, doi: 10.1016/j.conbuildmat.2018.09.201.

[183] J. L. Provis e J. S. J. Van Deventer, *Geopolymers: Structures, processing, properties and industrial applications*. Elsevier Ltd, 2009. doi: 10.1533/9781845696382.

[184] H. Rahier, B. Van Mele, e J. Wastiels, “Low-temperature synthesized aluminosilicate glasses”, *J Mater Sci*, vol. 31, nº 1, 1996, doi: 10.1007/bf00355129.

[185] V. F. F. Barbosa, K. J. D. MacKenzie, e C. Thaumaturgo, “Synthesis and characterisation of materials based on inorganic polymers of alumina and silica: Sodium polysialate polymers”, *International Journal of Inorganic Materials*, vol. 2, nº 4, 2000, doi: 10.1016/S1466-6049(00)00041-6.

[186] H. Rostami e W. Brendley, “Alkali ash material: A novel fly ash-based cement”, *Environ Sci Technol*, vol. 37, nº 15, 2003, doi: 10.1021/es026317b.

[187] C. Shi, P. V Krivenko, e D. Roy, *Alkali-Activated Cements and Concretes*. 2006. doi: 10.4324/9780203390672.

[188] G. S. Ryu, Y. B. Lee, K. T. Koh, e Y. S. Chung, “The mechanical properties of fly ash-based geopolymer concrete with alkaline activators”, *Constr Build Mater*, vol. 47, p. 409–418, 2013, doi: 10.1016/j.conbuildmat.2013.05.069.

[189] M. Zhang, N. A. Deskins, G. Zhang, R. T. Cygan, e M. Tao, “Modeling the Polymerization Process for Geopolymer Synthesis through Reactive Molecular Dynamics Simulations”, 2018, doi: 10.1021/acs.jpcc.8b00697.

[190] L. N. Tchadjie e S. O. Ekolu, “Enhancing the reactivity of aluminosilicate materials toward geopolymer synthesis”, *Journal of Materials Science*, vol. 53, nº 7. 2018. doi: 10.1007/s10853-017-1907-7.

[191] A.M. Mustafa Al Bakri, H. Kamarudin, M. Bnhussain, I. K. Nizar, e W. I. W. Mastura, “Mechanism and Chemical Reaction of Fly Ash Geopolymer Cement-A Review”, *J Chem Inf Model*, vol. 53, nº 5, 2013.

[192] B. Koohestani, P. Mokhtari, E. Yilmaz, F. Mahdipour, e A. K. Darban, “Geopolymerization mechanism of binder-free mine tailings by sodium silicate”, *Constr Build Mater*, vol. 268, p. 121217, jan. 2021, doi: 10.1016/J.CONBUILDMAT.2020.121217.

[193] K. J. D. MacKenzie, “What are these things called geopolymers? A physico-chemical perspective”, em *Ceramic Transactions*, 2004. doi: 10.1002/9781118406892.ch12.

[194] J. Davidovits, “Geopolymers and geopolymeric materials”, *Journal of Thermal Analysis*, vol. 35, nº 2, p. 429–441, mar. 1989, doi: 10.1007/BF01904446.

[195] I. Ozer e S. Soyer-Uzun, “Relations between the structural characteristics and compressive strength in metakaolin based geopolymers with different molar Si/Al ratios”, *Ceram Int*, vol. 41, nº 8, 2015, doi: 10.1016/j.ceramint.2015.04.125.

[196] P. Duxson, J. L. Provis, G. C. Lukey, S. W. Mallicoat, W. M. Kriven, e J. S. J. Van Deventer, “Understanding the relationship between geopolymer composition, microstructure and mechanical properties”, *Colloids Surf A Physicochem Eng Asp*, vol. 269, nº 1–3, 2005, doi: 10.1016/j.colsurfa.2005.06.060.

[197] A. Allahverdi, E. Najafi Kani, e B. Shaverdi, “Carbonation Versus Efflorescence in Alkali-Activated Blast-Furnace Slag in Relation with Chemical Composition of Activator”, *International Journal of Civil Engineering*, vol. 15, nº 4, 2017, doi: 10.1007/s40999-017-0225-4.

[198] J. R. Gasca-Tirado *et al.*, “Ion-exchanged geopolymer for photocatalytic degradation of a volatile organic compound”, *Mater Lett*, vol. 134, 2014, doi: 10.1016/j.matlet.2014.07.090.

[199] S. Wang, “Application of solid ash based catalysts in heterogeneous catalysis”, *Environmental Science and Technology*, vol. 42, nº 19. 2008. doi: 10.1021/es801312m.

[200] X. Zhang *et al.*, “Porous geopolymer composites: A review”, *Compos Part A Appl Sci Manuf*, vol. 150, p. 106629, nov. 2021, doi: 10.1016/J.COMPOSITESA.2021.106629.

[201] C. Reeb, C. Pierlot, C. Davy, e D. Lambertin, “Incorporation of organic liquids into geopolymer materials - A review of processing, properties and applications”, *Ceramics International*, vol. 47, nº 6. 2021. doi: 10.1016/j.ceramint.2020.11.239.

[202] Y. Zhang e L. Liu, “Fly ash-based geopolymer as a novel photocatalyst for degradation of dye from wastewater”, *Particuology*, vol. 11, nº 3, p. 353–358, jun. 2013, doi: 10.1016/J.PARTIC.2012.10.007.

[203] A. Strini *et al.*, “TiO2-based photocatalytic geopolymers for nitric oxide degradation”, *Materials*, vol. 9, nº 7, 2016, doi: 10.3390/ma9070513.

[204] R. Bendoni, F. Miccio, V. Medri, P. Benito, A. Vaccari, e E. Landi, “Geopolymer composites for the catalytic cleaning of tar in biomass-derived gas”, *Renew Energy*, vol. 131, 2019, doi: 10.1016/j.renene.2018.08.067.

[205] R. F. Botti *et al.*, “Additively manufactured geopolymer structured heterogeneous catalysts for biodiesel production”, *Appl Mater Today*, vol. 23, 2021, doi: 10.1016/j.apmt.2021.101022.

[206] R. F. Botti *et al.*, “Biodiesel Processing Using Sodium and Potassium Geopolymer Powders as Heterogeneous Catalysts”, *Molecules*, vol. 25, nº 12, 2020, doi: 10.3390/molecules25122839.

[207] N. Supamathanon *et al.*, “Development of CaO supported on modified geopolymer catalyst for transesterification of soybean oil to biodiesel”, *Mater Today Commun*, vol. 29, 2021, doi: 10.1016/j.mtcomm.2021.102822.

[208] M. I. M. Alzeer, K. J. D. MacKenzie, e R. A. Keyzers, “Erratum: Corrigendum to ‘Porous aluminosilicate inorganic polymers (geopolymers): a new class of environmentally benign heterogeneous solid acid catalysts’ (Appl. Catal. A: Gen. (2016) 524 (173–181))”, *Applied Catalysis A: General*, vol. 526. 2016. doi: 10.1016/j.apcata.2016.08.025.

[209] M. I. M. Alzeer e K. J. D. MacKenzie, “Synthesis and Catalytic Properties of New Sustainable Aluminosilicate Heterogeneous Catalysts Derived from Fly Ash”, *ACS Sustain Chem Eng*, vol. 6, nº 4, 2018, doi: 10.1021/acssuschemeng.7b04923.

[210] H. Alghamdi, S. A. O. Nair, e N. Neithalath, “Insights into material design, extrusion rheology, and properties of 3D-printable alkali-activated fly ash-based binders”, *Mater Des*, vol. 167, abr. 2019, doi: 10.1016/j.matdes.2019.107634.

[211] L. Reig, M. M. Tashima, M. V. Borrachero, J. Monzó, C. R. Cheeseman, e J. Payá, “Properties and microstructure of alkali-activated red clay brick waste”, *Constr Build Mater*, vol. 43, p. 98–106, 2013, doi: 10.1016/j.conbuildmat.2013.01.031.

[212] C. Zhang *et al.*, “Physical properties and microstructure of nickel slag/metakaolin-based geopolymer with different contents of nickel slag”, *Advances in Cement Research*, vol. 32, nº 5, 2020, doi: 10.1680/jadcr.18.00064.

[213] N. Ranjbar *et al.*, “Rheological characterization of 3D printable geopolymers”, *Cem Concr Res*, vol. 147, p. 106498, set. 2021, doi: 10.1016/J.CEMCONRES.2021.106498.

[214] B. Panda, S. C. Paul, L. J. Hui, Y. W. D. Tay, e M. J. Tan, “Additive manufacturing of geopolymer for sustainable built environment”, *J Clean Prod*, vol. 167, p. 281–288, nov. 2017, doi: 10.1016/j.jclepro.2017.08.165.

[215] H. Zhong e M. Zhang, “3D printing geopolymers: A review”, *Cem Concr Compos*, vol. 128, p. 104455, abr. 2022, doi: 10.1016/J.CEMCONCOMP.2022.104455.

[216] M. Xia, B. Nematollahi, e J. Sanjayan, “Printability, accuracy and strength of geopolymer made using powder-based 3D printing for construction applications”, *Autom Constr*, vol. 101, p. 179–189, maio 2019, doi: 10.1016/J.AUTCON.2019.01.013.

[217] G. Franchin *et al.*, “Removal of ammonium from wastewater with geopolymer sorbents fabricated via additive manufacturing”, *Mater Des*, vol. 195, p. 109006, 2020, doi: 10.1016/j.matdes.2020.109006.

[218] S. Ma *et al.*, “3D Printing of Damage-tolerant Martian Regolith Simulant-based Geopolymer Composites”, *Addit Manuf*, vol. 58, 2022, doi: 10.1016/j.addma.2022.103025.

[219] T. Luukkonen *et al.*, “Ag- or Cu-modified geopolymer filters for water treatment manufactured by 3D printing, direct foaming, or granulation”, *Sci Rep*, vol. 10, nº 1, dez. 2020, doi: 10.1038/s41598-020-64228-5.

[220] S. Fu *et al.*, “Monoclinic-celsian ceramics formation: Through thermal treatment of ion-exchanged 3D printing geopolymer precursor”, *J Eur Ceram Soc*, vol. 39, nº 2–3, 2019, doi: 10.1016/j.jeurceramsoc.2018.08.036.

[221] S. H. Bong, M. Xia, B. Nematollahi, e C. Shi, “Ambient temperature cured ‘just-add-water’ geopolymer for 3D concrete printing applications”, *Cem Concr Compos*, vol. 121, 2021, doi: 10.1016/j.cemconcomp.2021.104060.

[222] O. Ly *et al.*, “Optimisation of 3D printed concrete for artificial reefs: Biofouling and mechanical analysis”, *Constr Build Mater*, vol. 272, 2021, doi: 10.1016/j.conbuildmat.2020.121649.

[223] K. G. Oliveira *et al.*, “Geopolymer beads and 3D printed lattices containing activated carbon and hydrotalcite for anionic dye removal”, *Catal Today*, vol. 390–391, p. 57–68, maio 2022, doi: 10.1016/J.CATTOD.2021.12.002.

[224] H. Jin *et al.*, “3D printed geopolymer adsorption sieve for removal of methylene blue and adsorption mechanism”, *Colloids Surf A Physicochem Eng Asp*, vol. 648, 2022, doi: 10.1016/j.colsurfa.2022.129235.

[225] J. William D. Callister e David G. Rethwisch, *Ciência e engenharia de materiais: uma introdução*. 2018.

[226] S.-C. Ho e T.-C. Chou, “The Role of Anion in the Preparation of Nickel Catalyst Detected by TPR and FTIR Spectra”, 1995. [Online]. Disponível em: https://pubs.acs.org/sharingguidelines

[227] M. Nasrollahzadeh, M. Sajadi, M. Atarod, M. Sajjadi, e Z. Isaabadi, “An Introduction to Green Nanotechnology”, *Interface Science and Technology*, vol. 28, nº 1, 2012.

[228] J. C. Lindon, G. E. Tranter, e D. W. Koppenaal, *Encyclopedia of Spectroscopy and Spectrometry*. 2016. doi: 10.5860/choice.48-5433.

[229] M. Rowles e B. O’Connor, “Chemical optimisation of the compressive strength of aluminosilicate geopolymers synthesised by sodium silicate activation of metakaolinite”, *J Mater Chem*, vol. 13, nº 5, p. 1161–1165, abr. 2003, doi: 10.1039/b212629j.

[230] A. Bauer e G. Berger, “Kaolinite and smectite dissolution rate in high molar KOH solutions at 35° and 80°C”, *Applied Geochemistry*, vol. 13, nº 7, p. 905–916, set. 1998, doi: 10.1016/S0883-2927(98)00018-3.

[231] B. Işıkdağ e M. R. Yalghuz, “Strength Development and Durability of Metakaolin Geopolymer Mortars Containing Pozzolans under Different Curing Conditions”, *Minerals*, vol. 13, nº 7, 2023, doi: 10.3390/min13070857.

[232] Z. Li, S. Zhang, Y. Zuo, W. Chen, e G. Ye, “Chemical deformation of metakaolin based geopolymer”, *Cem Concr Res*, vol. 120, p. 108–118, jun. 2019, doi: 10.1016/j.cemconres.2019.03.017.

[233] C. A. Rees, J. L. Provis, G. C. Lukey, e J. S. J. van Deventer, “The mechanism of geopolymer gel formation investigated through seeded nucleation”, *Colloids Surf A Physicochem Eng Asp*, vol. 318, nº 1–3, p. 97–105, abr. 2008, doi: 10.1016/J.COLSURFA.2007.12.019.

[234] R. P. Williams, R. D. Hart, e A. Van Riessen, “Quantification of the extent of reaction of metakaolin-based geopolymers using X-ray diffraction, scanning electron microscopy, and energy-dispersive spectroscopy”, *Journal of the American Ceramic Society*, vol. 94, nº 8, 2011, doi: 10.1111/j.1551-2916.2011.04410.x.

[235] N. Döbelin, “Validation of XRD phase quantification using semi-synthetic data”, *Powder Diffr*, vol. 35, nº 4, 2020, doi: 10.1017/S0885715620000573.

[236] W. A. Dollase, “CORRECTION OF INTENSITIES OF PREFERRED ORIENTATION IN POWDER DIFFRACTOMETRY: APPLICATION OF THE

MARCH MODEL.", *J Appl Crystallogr*, vol. 19, nº pt 4, 1986, doi: 10.1107/S0021889886089458.

[237] A. Yamauchi, M. Iwasaki, K. Hayashi, e K. Tsuji, "Evaluation of full-field energy dispersive X-ray fluorescence imaging apparatus and super resolution analysis with compressed sensing technique", *X-Ray Spectrometry*, vol. 48, nº 6, 2019, doi: 10.1002/xrs.3055.

[238] A. L. Finkel'shtein e T. N. Gunicheva, "Description of the dependence of intensity of x-ray fluorescence on the particle size of powder samples and pulp during x-ray fluorescent analysis", *Inorganic Materials*, vol. 44, nº 14, 2008, doi: 10.1134/S0020168508140136.

[239] A. L. Finkelshtein e N. Brjansky, "Estimating particle size effects in X-ray fluorescence spectrometry", *Nucl Instrum Methods Phys Res B*, vol. 267, nº 14, 2009, doi: 10.1016/j.nimb.2009.05.005.

[240] K. A. Chebakova *et al.*, "X-ray fluorescence spectroscopy features of micro-and nanoscale copper and nickel particle compositions", *Nanomaterials*, vol. 11, nº 9, 2021, doi: 10.3390/nano11092388.

[241] P. Worsfold, A. Townshend, C. Poole, e M. Miró, *Encyclopedia of analytical science*. 2019. doi: 10.5860/choice.43-0032.

[242] C. Villa, E. T. Pecina, R. Torres, e L. Gómez, "Geopolymer synthesis using alkaline activation of natural zeolite", *Constr Build Mater*, vol. 24, nº 11, p. 2084–2090, nov. 2010, doi: 10.1016/J.CONBUILDMAT.2010.04.052.

[243] D. M. Nguyen, H. N. Bich, P. D. Hai Anh, P. H. Ai-Le, e Q. B. Bui, "Vertical copper oxide nanowire arrays attached three-dimensional macroporous framework as a self-supported sensor for sensitive hydrogen peroxide detection", *Arabian Journal of Chemistry*, vol. 13, nº 2, 2020, doi: 10.1016/j.arabjc.2019.04.002.

[244] D. Mardiansyah *et al.*, "Effect of temperature on the oxidation of Cu nanowires and development of an easy to produce, oxidation-resistant transparent conducting electrode using a PEDOT:PSS coating", *Sci Rep*, vol. 8, nº 1, 2018, doi: 10.1038/s41598-018-28744-9.

[245] D. P. Singh, A. K. Ojha, e O. N. Srivastava, "Synthesis of different Cu(OH)2 and CuO (nanowires, rectangles, seed-, belt-, and sheetlike) nanostructures by simple wet chemical route", *Journal of Physical Chemistry C*, vol. 113, nº 9, 2009, doi: 10.1021/jp804832g.

[246] T. Zhang, W. Y. Hsieh, F. Daneshvar, C. Liu, S. P. Rwei, e H. J. Sue, “Copper(i)-alkylamine mediated synthesis of copper nanowires”, *Nanoscale*, vol. 12, nº 33, 2020, doi: 10.1039/d0nr04778c.

[247] T. N. Angelidis e S. A. Sklavounos, “A SEM-EDS study of new and used automotive catalysts”, *Appl Catal A Gen*, vol. 133, nº 1, p. 121–132, dez. 1995, doi: 10.1016/0926-860X(95)00165-4.

[248] P. Jonnard, F. Brisset, F. Robaut, G. Wille, e J. Ruste, “Inter-laboratory comparison of a WDS-EDS quantitative X-ray microanalysis of a metallic glass”, *X-Ray Spectrometry*, vol. 44, nº 1, 2015, doi: 10.1002/xrs.2573.

[249] D. E. Newbury e N. W. M. Ritchie, “Scanning electron microscopy/energy dispersive x-ray spectrometry (sem/eds) elemental microanalysis: Accuracy and precision beyond my wildest dreams”, em *Materials Science and Technology Conference and Exhibition 2016, MS and T 2016*, 2016.

[250] P. M. Sreekanth e P. G. Smirniotis, “Selective reduction of NO with CO over titania supported transition metal oxide catalysts”, *Catal Letters*, vol. 122, nº 1–2, 2008, doi: 10.1007/s10562-007-9365-5.

[251] E. M. Cepollaro, R. Botti, G. Franchin, L. Lisi, P. Colombo, e S. Cimino, “Cu/zsm5-geopolymer 3d-printed monoliths for the nh3-scr of nox”, *Catalysts*, vol. 11, nº 10, out. 2021, doi: 10.3390/catal11101212.

[252] Z. Niazi, A. Irankhah, Y. Wang, e H. Arandiyan, “Cu, Mg and Co effect on nickel-ceria supported catalysts for ethanol steam reforming reaction”, *Int J Hydrogen Energy*, vol. 45, nº 41, p. 21512–21522, ago. 2020, doi: 10.1016/J.IJHYDENE.2020.06.001.

[253] S.-C. Ho e T.-C. Chou, “The Role of Anion in the Preparation of Nickel Catalyst Detected by TPR and FTIR Spectra”, 1995. [Online]. Disponível em: https://pubs.acs.org/sharingguidelines

[254] T. A. Costin, L. G. Dutra, A. J. Bortoluzzi, e M. M. Sá, “Amine-mediated synthesis of amides from 1,3-dicarbonyl compounds through a domino diazo transfer/aminolysis process”, *Tetrahedron*, vol. 73, nº 31, 2017, doi: 10.1016/j.tet.2017.06.013.

[255] P. T. Anastas, “Perspective on Green Chemistry: The most challenging synthetic transformation”, *Tetrahedron*, vol. 66, nº 5. 2010. doi: 10.1016/j.tet.2009.11.019.

[256] J. L. Tucker, “Green chemistry: Cresting a summit toward sustainability”, *Org Process Res Dev*, vol. 14, nº 2, 2010, doi: 10.1021/op9000548.

[257] M. B. Gawande e R. V. Jayaram, “A novel catalyst for the Knoevenagel condensation of aldehydes with malononitrile and ethyl cyanoacetate under solvent free conditions”, *Catal Commun*, vol. 7, nº 12, 2006, doi: 10.1016/j.catcom.2006.03.008.

[258] G. Maas, “New syntheses of diazo compounds”, *Angewandte Chemie - International Edition*, vol. 48, nº 44. 2009. doi: 10.1002/anie.200902785.

[259] A. C. B. Burtoloso, P. B. Momo, e G. L. Novais, “Traditional and new methods for the preparation of diazocarbonyl compounds”, *An Acad Bras Cienc*, vol. 90, nº 1, 2018, doi: 10.1590/0001-3765201820170768.

[260] G. M. Diogo, P. A. M. Moro, T. A. Costin, M. Fantinel, e M. M. Sá, “Chitosan as a sustainable heterogeneous catalyst for the preparation of functionalized α-diazo carbonyl compounds”, *Tetrahedron Green Chem*, vol. 1, 2023, doi: 10.1016/j.tgchem.2023.100006.

[261] L. R. Peyton, S. Gallagher, e M. Hashemzadeh, “Triazole antifungals: A review”, *Drugs of Today*, vol. 51, nº 12. 2015. doi: 10.1358/dot.2015.51.12.2421058.

[262] Z. Kazeminejad, M. Marzi, A. Shiroudi, S. A. Kouhpayeh, M. Farjam, e E. Zarenezhad, “Novel 1, 2, 4-Triazoles as Antifungal Agents”, *BioMed Research International*, vol. 2022. 2022. doi: 10.1155/2022/4584846.

[263] C. -H. Zhou e Y. Wang, “Recent Researches in Triazole Compounds as Medicinal Drugs”, *Curr Med Chem*, vol. 19, nº 2, 2012, doi: 10.2174/092986712803414213.

[264] H. Gallardo, G. Conte, F. Bryk, M. C. S. Lourenço, M. S. Costac, e V. F. Ferreira, “Synthesis and evaluation of 1-alkyl-4-phenyl-[1,2,3]-triazole derivatives as antimycobacterial agent”, *J Braz Chem Soc*, vol. 18, nº 6, 2007, doi: 10.1590/S0103-50532007000600027.

[265] K. Sonogashira, “Development of Pd-Cu catalyzed cross-coupling of terminal acetylenes with sp2-carbon halides”, *J Organomet Chem*, vol. 653, nº 1–2, 2002, doi: 10.1016/S0022-328X(02)01158-0.